UNIVERSITY OF CALIFORNIA SAN DIEGO

Using Fluorescence Microscopy to Study Antibiotics and Factors that Influence Bacterial Susceptibility

A dissertation submitted in partial satisfaction of the
requirements for the degree Doctor of Philosophy

in

Biology

by

Hannah Y. Tsunemoto

Committee in charge:

Professor Joseph Pogliano, Chair
Professor Eric Allen, Co-Chair
Professor Matthew Daugherty
Professor Victor Nizet
Professor Bernhard Palsson

2020

The Dissertation of Hannah Y. Tsunemoto is approved, and it is acceptable in quality and form for publication on microfilm and electronically:

_____

_____

_____

_____
Co-Chair

_____
Chair

University of California San Diego

2020

TABLE OF CONTENTS

LIST OF FIGURES

Chapter 2

Chapter 3

Chapter 4

LIST OF TABLES

Chapter 2

Chapter 3

ACKNOWLEDGEMENTS

First and foremost, I would like to thank my PhD advisor Joe Pogliano for giving me the opportunity to be a part of your lab and for being so supportive over the past five years. I always knew that you had my back, even when I kept bothering you about emails and experiments. I appreciate the trust you had in my scientific ability, your guidance when I had questions or problems, and the encouragement you gave me whenever I needed it.

I would like to thank all the members of the Pogliano Labs, past and present, for being the best lab family anyone could ask for. Thank you Joe, Kit, Javi, Marcy, Penny, Krithika, Diana, Ranmali, Eammon, Katrina, Kanika, Erica, Eray, Amy, Emily, Jelani, Mac, Christine, Gaya, Andrew, Jason, John Paul, and my wonderful former and current undergraduate students, Lauren, Caroline, Helen, and Kevin. I would like to specifically thank Alan for his friendship and his seemingly never-ending knowledge of facts, both useful and not so useful; Anne for her attention for detail, her support during long experiments, and her ability to effortlessly keep the labs running smoothly; Mike for pioneering bacterial cytological profiling and for being an amazing mentor during my rotation; Arthur and Elizabeth for being the best office mates and friends and having the best inside jokes; and finally Joe Sugie for his expertise in all things analytical and his patience with me when I ask stupid questions. I would also like to thank Ria for her supply of food to our lab and her friendship.

I would like to thank my cohort (which is and always will be the best) and the friends that I made in graduate school. I would like to thank my D&D crew Andy, Amy, Brian, Tim, and Wendy, my fried chicken and cartoons friend Nina, and my fried shrimp and brunch friend Myan. I would also like to specifically thank Roland for choosing me to be his best friend ever since we realized that we share the same favorite color and the same type of sunscreen during boot camp.

I would like to thank my committee members, Eric Allen, Matt Daugherty, Victor Nizet, and Bernhard Palsson for all their guidance and suggestions throughout the years. While committee meetings were always nerve-wracking, you all were very supportive and made me want to do better each year. I also would like to thank all my collaborators, especially the members of the iARME team and the Nizet Lab. I am very lucky to have had the opportunity to be a part of a wide variety of projects and work with such awesome people. Additionally, I would like to thank the wonderful administrators of the Division of Biological Sciences, Suzi, Marifel, and Melody. I would not have gotten this far without you all.

I would like to thank my family for their unconditional love and support. Thank you to my parents Steve and Mary for being patient and understanding, even when I decided to become the kind of doctor that doesn't make oodles of money. Thank you to my sister, Rachel, for her attempts at warning me about how difficult graduate school is and her guidance in both science and in life. I always like to blame you for my interest in science, and you continue to inspire me to be a better person. Thank you to my brother-in-law Yarin for his wisdom in buying a car, his advice in thinking about my future, and his obvious puns. Thank you to my fur-nephew Juneau, my fur-brother Butters, and my fur-baby Humboldt Fog. Finally, I would like to thank my boyfriend Sam for supporting me when I was stressed, for making silly jokes when I needed cheering up, and for loving food adventures just as much as I do. I look forward to many more years of exploring the world and eating everything with you. Thank you also to Sam's family for accepting me as one of your own and showering me with love.

Last, but certainly not least, I would like to thank bacteria for their sacrifice for these experiments and their ability to be finnicky jerks.

Chapter 2, in large part, is being formulated into a manuscript in preparation for the publication of the material. Hannah Tsunemoto, Joseph Sugie, Joe Pogliano, 2020. The dissertation author was the primary investigator and author of this material.

Chapter 3, in large part, is being formulated into a manuscript in preparation for the publication of the material. Hannah Tsunemoto, Joseph Sugie, Joe Pogliano, 2020. The dissertation author was the primary investigator and author of this material.

Chapter 4, in part, is a reprint of the material as it appears in Ulloa, ER., Dillon, N., Tsunemoto, H., Pogliano, J., Sakoulas, G., & Nizet, V., 2019, Avibactam sensitizes carbapenem-resistant NDM-1-producing *Klebsiella pneumoniae* to innate immune clearance in The Journal of Infectious Disease, and in Dillon, N., Holland, M., Tsunemoto, H., Hancock, B., Cornax, I., Pogliano, J., Sakoulas, G., & Nizet, V., 2019, Surprising synergy of dual translation inhibition vs *Acinetobacter baumannii* and other multidrug-resistant bacterial pathogens in EBioMedicine. The dissertation author was a co-author of these papers.

VITA

2013 Bachelor of Science, Hawaii Pacific University

2020 Doctor of Philosophy, University of California San Diego

PUBLICATIONS

Poudel, S., **Tsunemoto, H.**, Seif, Y., Sastry, A.V., Szubin, R., Xu, S., Machado, H., Olson, C.A., Anand, A., Pogliano, J., Nizet, V., & Palsson, B.O. Revealing 29 sets of independently modulated genes in *Staphylococcus aureus*, their regulators, and role in key physiological response. *PNAS*. 202008413. (2020).

Salazar, M., Machado, H., Dillon, N., **Tsunemoto, H.**, Szubin, R., Dahesh, S., Pogliano, J., Sakoulas, G., Palsson, B.O., Nizet, V., & Feist, A.M. Genetic determinants enabling media-dependent adaptation to nafcillin in methicillin-resistant *Staphylococcus aureus*. *mSystems*. 5(2):e00828-19. (2020).

Ulloa, ER., Kousha, A., **Tsunemoto, H**., Pogliano, J., Licitra, C., LiPuma, J., Sakoulas, G., Nizet, V., & Kumaraswamy, M.. Azithromycin exerts bactericidal activity and enhances innate immune-mediated killing of MDR *Achromobacter xylosoxidans*. *Infect. Microb. Dis.* 2:10-17. (2020).

Rajput, A., Poudel, S., **Tsunemoto, H**., Meehan, M., Szubin, R., Olson, C.A., Lamsa, A., Seif, Y., Dillon, N., Vrbanac, A., Sugie, J., Dahesh, S., Monk, J.M., Dorrestein, P.C., Knight, R., Nizet, V., Palsson, B.O., Feist, A.M., & Pogliano, J. Profiling the effect of nafcillin on HA-MRSA D712 using bacteriological and physiological media. *Sci. Data*. 6(1):322. (2019).

Dillon, N., Holland, M., **Tsunemoto, H.**, Hancock, B., Cornax, I., Pogliano, J., Sakoulas, G., & Nizet, V. Surprising synergy of dual translation inhibition vs *Acinetobacter baumannii* and other multidrug-resistant bacterial pathogens. *EBioMedicine*. 46:193-201. (2019).

Poudel, S., **Tsunemoto, H.**, Meehan, M., Szubin, R., Olson, C.A., Lamsa, A., Seif, Y., Dillon, N., Vrbanac, A., Sugie, J., Dahesh, S., Monk, J.M., Dorrestein, P.C., Pogliano, J., Knight, R., Nizet, V., Palsson, B.O., & Feist, A.M. Characterization of CA-MRSA TCH1516 exposed to nafcillin in bacteriological and physiological media. *Sci Data*. 6(1):43. (2019)

Ulloa, ER., Dillon, N., **Tsunemoto, H.**, Pogliano, J., Sakoulas, G., & Nizet, V. Avibactam sensitizes carbapenem-resistant NDM-1-producing *Klebsiella pneumoniae* to innate immune clearance. *J. Infect. Dis*. 220:484-93. (2019).

Htoo, HH., Brumage, L, Chaikeeratisak, V., **Tsunemoto, H.**, Sugie, J., Tribuddharat, C., Pogliano, J., & Nonejuie, P. Bacterial cytological profiling as a tool to study mechanisms of action of

antibiotics that are active against *Acinetobacter baumannii*. *Antimicrob. Agents Chemother*. 63(4): e02310-18. (2019).

Seif, Y., Monk, JM., Mih, N., **Tsunemoto, H**., Poudel, S., Zuniga, C., Broddrick, J., Zengler, K., & Palsson, B.O. A computational knowledge-base elucidates the response of *Staphylococcus aureus* to different media types. *PLoS Comput. Biol.* 15(1): e1006644. (2019).

Munguia, J., LaRock, DL., **Tsunemoto, H.**, Olson, J. Cornax, I., Pogliano, J., & Nizet, V. The Mla pathway is critical for *Pseudomonas aeruginosa* resistance to outer membrane permeabilization and host innate immune clearance. *J. Mol. Med. (Berl)*. 95(10): 1127-1136. (2017).

ABSTRACT OF THE DISSERTATION

Using Fluorescence Microscopy to Study Antibiotics and Factors that Influence Bacterial Susceptibility

by

Hannah Tsunemoto

Doctor of Philosophy in Biology

University of California San Diego, 2020

Professor Joseph Pogliano, Chair
Associate Professor Eric Allen, Co-Chair

This dissertation looks at the overall theme of antibiotics and factors that influence bacterial susceptibility through the application of the fluorescence microscopy tool Bacterial Cytological Profiling (BCP). The first chapter is a brief history of antibiotics and the rise of bacterial resistance, the use of bacteriophages as an alternative therapy, and an overview of current fluorescence microscopy techniques used in the field to study antibiotic mechanism of action (MOA) and susceptibility.

Chapter 2 describes the integration of microfluidics and fluorescence microscopy to investigate antibiotic transport kinetics in *Escherichia coli*. Uptake of fluorescently-tagged azithromycin and roxithromycin were observed in different genetic backgrounds to characterize the extent to which the outer and inner membranes, and efflux, function as barriers to antimicrobial

activity. Different growth media was used to further characterize antibiotic uptake by cells under different microenvironments, specifically the impact of bicarbonate on transport kinetics.

Chapter 3 focuses on the application of BCP to probe the molecular interactions between antibiotic treatment and the jumbo phage φKZ during infection of *Pseudomonas aeruginosa*. A diverse set of antibiotic classes were assayed, including those commonly used to treat *P. aeruginosa* infections. Further investigation into cell-wall active antibiotics were completed to explore mechanistic explanations for observed increases in relative phage infection and phage nucleus localization.

Chapter 4 is an overview of several collaborations with Victor Nizet's lab at UCSD to examine antimicrobial synergies active against multi-drug resistant bacteria using BCP. This work included studies examining binding of the antimicrobial peptide LL-37 to *Klebsiella pneumoniae* during treatment with non-β-lactam β-lactamase inhibitors and the synergy between two protein synthesis inhibitors against *Acinetobacter baumannii*.

CHAPTER 1:

Using antimicrobial compounds and bacteriophages against pathogenic bacteria

1.1 Discovery of antibiotics and the development of antibiotic resistance

It has been famously estimated that there are approximately 6 x 10^{30} microbial cells on earth [1], and within each ecological niche, communities of bacteria compete or cooperate with each other for nutrients and space. From these interactions, some species have evolved the ability to generate and secrete specialized metabolites that can negatively impact surrounding cells. One genus of bacteria that is particularly prolific in producing antimicrobial compounds is the soil inhabiting *Streptomyces* [2]. Humans have since taken advantage of these environmental antagonisms and utilized bacteria-derived weaponry against pathogenic microbes to benefit public health.

Bacteria-vs-bacteria competition is not the only source of antimicrobial molecules. Plants and animals also face attack from microbes and have evolved their own methods of defense. While the people of ancient history may not have understood the underlying mechanisms, it has been shown that the traditional cures of many cultures contain a myriad of active therapeutic compounds. Traditional Chinese Medicine (TCM), for example, relies on natural sources such as the leaves, bark, or roots of plants to provide varying bioactivities and these herbs are often used in concert with one another. Recent probing of the numerous TCM repertoire led to the characterization of artemisinin, a group of potent anti-malarial compounds [3].

Despite the long history of treatments with TCM and other alternative medicines, the classic example for the founding of the "antibiotic era" is Alexander Fleming's serendipitous discovery of penicillin, a specialized metabolite biosynthesized by a *Penicillium* mold [3, 4]. The introduction of penicillin into clinical use more than a decade later marked the beginning of the modern arms race of humans against pathogenic bacteria.

Over the last century, researchers have dedicated themselves to identifying novel antibiotics either by mining natural products from diverse origins, such as plants and the Actinobacteria, which encompasses *Streptomyces sp.* Studying the biosynthetically rich *Streptomyces* alone resulted in the identification of a wide range of antimicrobial compounds, including streptomycin, the first active molecule against *Mycobacterium tuberculosis* [5]. In fact, it is estimated that 80% of all known antibiotics were derived from a *Streptomyces* source [6]. Advancements in scientific methods have allowed for the chemical alteration of known scaffolds, for example modifications of the β-lactam backbone, to increase efficacy or bioavailability, and broaden our clinical arsenal against infectious disease [7, 8].

An important property of antibiotics is their mechanism of action (MOA) and the identification of their molecular target. It is important to be able to differentiate between inhibition of the main biosynthetic pathways as well as identify those that broadly impact cell viability through non-specific mechanisms, e.g. bleach. Before the application of microscopy techniques, discussed later in this dissertation, identifying the MOA for a specific antimicrobial compound required a variety of time-consuming and relatively non-specific assays [9].

Historically, understanding an antibiotic's MOA was limited to the biosynthetic pathway. Using radioactive precursors, macromolecular synthesis assays could identify if a particular treatment blocked one or more of the five essential processes of bacterial cell growth: DNA, RNA, protein, cell wall, or fatty acid [10]. To identify the specific molecular target of antibiotic required the generation, isolation, and sequencing of resistant mutants. This methodology has its limitations since it often requires large amounts of the antibiotic, which in cases of natural product work may not be feasible, or if the resistance mechanism is not related to the target itself, e.g. efflux pumps or degradation [11]. The advancements in sequencing technology is a benefit to this approach since

the time and cost to sequencing the whole genome of a bacteria has decreased while the accuracy has increased [12].

Another way to identify the molecular target of an antibiotic is to screening gene-knockout collections under antibiotic conditions. The Keio Collection, a library of single-gene knockout mutants in *Escherichia coli* [13], has been used in a variety of studies to test the effects of small molecules, bacteriophages, and even media components such as bicarbonate of bacterial viability [14-16]. The development of transposon libraries and random barcode TnSeq provides a similar platform as gene-knockout collections and simplifies antibiotic screening since pooled screens can be performed and sequenced [11, 17]. Other methods for characterizing an antibiotic's target and MOA include transcriptional or proteomic profiling in response to a given treatment [18, 19]. These techniques can provide a greater picture into how an antibiotic is affecting the physiology of a given bacteria, although proteomics tends to be more costly when compared to sequencing [19].

While humans have only been exploiting these natural compounds as therapeutics for less than a century, environmental interspecies competition has been occurring since the beginning of their existence. *Streptomyces* are inherently resistant to many of the bioactive metabolites they synthesize, and stress is an ideal driver of evolution in the species that are in competition with these producers. Many studies have shown that bacteria isolated from caves and permafrost, previously untouched by human influence, contained functional resistance genes to several antibiotics, including macrolides and tetracyclines. Monitoring the evolution of resistance in these environmental microbes is difficult due to confounding factors such as horizontal gene transfer (HGT) [20]. While these bacteria may not impact human health directly, they represent a potential reservoir of resistance for pathogenic organisms.

Despite early excitement about the possibility of a "magic bullet" against infectious bacteria, a term coined by Paul Ehrlich, another early innovator of antibiotics, the microbes fought back [7]. Resistance to pharmaceutical antibiotics was observed very shortly after being added to the market [21]. In the case of penicillin, less than a year after its first clinical application, several instances of *Staphylococcus aureus* resistance were documented, and within 20 years, over 80% of *S. aureus* isolates were impervious to penicillin activity [22]. A similar observation was made for *M. tuberculosis* and streptomycin, where resistance occurred within the first year of clinical use [21].

The rapid evolution of antibiotic resistant pathogens has been attributed to increased selective pressure accompanied by lax prescription practices by both doctors and patients. Horizontal gene transfer between the gut microbiome, which can be affected by administered antibiotics, and infectious microbes is an additional contribution to antibiotic resistance. A 2019 report from the Centers for Disease Control (CDC) and Prevention classified 18 strains of bacterial pathogens as urgent, serious, or concerning threats to human health, many of which are multi-drug resistant (MDR). The CDC estimated that almost 2.8 million infections by antibiotic resistant pathogens occur each year [23]. The rise of these antibiotic resistant "superbugs," including *S. aureus* and *M. tuberculosis*, complicates effective treatment and forces physicians to turn to toxic drugs of last resort [7, 21, 22].

Gram-negative bacteria make up the majority of these MDR pathogenic strains. While some portions of the bacterial cell envelope are shared between Gram-positive and Gram-negative bacteria, the outer membrane (OM) of Gram-negative species plays the largest role in their intrinsic resistance to a wide array of antibiotics. Much research has been dedicated to understanding the complex nature of the OM. The OM is an asymmetrical lipid bilayer composed of phospholipids

in the inner leaflet and lipopolysaccharides (LPS) in the outer leaflet. The LPS of the OM are attracted to one another and thus form a tight biophysical barrier to hydrophobic molecules that could pass easily through the simpler cytoplasmic membrane [24, 25]. While some antibiotics can pass through the OM via outer membrane channels known as porins [26], the presence of efflux pumps can lower intracellular concentration of antibiotics to levels that are non-effective against the bacteria. Several Gram-negative bacteria have multiple types of efflux pumps which provide resistance to multiple types of antibiotics [25, 27].

Other mechanisms of antibiotic resistance fall under three broad categories: antimicrobial modifications/degradation, alteration or bypass of target, and global cell changes. The best-known example for antibiotic degradation is the evolution of modified cell wall enzymes to become β-lactamases, which cut the active site of β-lactam containing drugs such as the penicillins. In contrast, bacteria like methicillin-resistant *S. aureus* evolved alternate penicillin-binding proteins, like PBP2A which have an altered protein structure that occludes binding of β-lactam antibiotics [28]. Bacteria can also alter their metabolomic activity and enter a transient state of resistance termed persistence [29].

Additionally, some bacterial species can form biofilms. True biofilms have an extracellular matrix composed of exopolysaccharides, DNA, and lipids, and bacteria existing in a biofilm experience variable access to nutrients as you move through the three-dimensional space, resulting in transcriptionally distinct sub-populations within genetically identical cells. Biofilms have significant resistance to many antimicrobial agents compared to their planktonic counterparts, which is attributed to decreased penetration through the extracellular matrix [30]. Biofilm growth on surgical equipment and implanted devices can cause severe healthcare associated infections [31].

In efforts to forestall the inevitable decline of antibiotic use as successful treatments, recent research has been dedicated to identifying potential synergies between antibiotics and/or molecules that subvert bacterial resistance mechanisms, e.g. β-lactamase inhibitors, for the development of adjuvant anti-infective therapies [32]. Another approach is identifying immune boosting compounds that enhance innate and adaptive immune responses to infection rather than targeting the pathogen itself [33]. Antimicrobial peptides (AMPs) are produced in almost all organisms, including bacteria and humans, and have become of interest as alternatives to antibiotics treatment [34]. Several studies have demonstrated that host AMPs, such as the human cathelicidin LL-37, can synergize with antibiotics *in vitro* to kill MDR bacteria [35-39].

One particularly promising alternative is the use of viruses that infect bacteria, known as bacteriophages, implementing a "the enemy of my enemy is my friend" strategy. The application of bacteriophages against infectious bacteria will be discussed further in the following section.

1.2 Application of bacteriophages as alternatives to antibiotic treatment

The previously mentioned estimate of 6×10^{30} microbial cells on earth is dwarfed by the predicted 10^{31} bacteriophage particles. Within ecological niches, phages impose selective pressure for evolution of their bacterial hosts like that of bacterial-produced specialized metabolites. Similarly, interspecies interactions force modifications on the side of the virus, encouraging adaptations of phage and host in step with one another. Despite their abundance, characterization of these phages and our understanding of their lifecycles, host specificity, and co-evolution is limited [40].

The best studied bacteriophage is phage λ, discovered in the early 1950s by Esther Lederberg and who also identified *E. coli* as its host. Subsequent research using phage λ provided detailed viral infection models (lytic and lysogenic cycles) and paved the way for major

breakthroughs in molecular biology, including methods for genetic recombination and gene expression control [41]. In 1982, Frederick Sanger sequenced the whole ~48.5 kb genome of phage λ, further contributing to its position as a powerful genetic tool even into the modern age [42].

At the microscopic level, phage λ is orders of magnitude smaller than its bacterial host. This is not the case for every bacteriophage; jumbo phages are defined as having a >200 kb genome. Phage G is the largest known jumbo phage and host, its *Bacillus megaterium*, is about three- to four-times larger than *E. coli*. The increased genome of these large phages can lead to increased molecular complexity [43]. Research by Kraemer et al. demonstrated that the *Pseudomonas* jumbo phage 201φ2-1 encodes a tubulin-like spindle capable of centering the viral DNA during infection [44]. It is important to note that some of these jumbo phages infect pathogenic bacteria, such as *P. aeruginosa, Klebsiella pneumoniae,* and *Acinetobacter baumannii* [43].

Early instances of using viruses to target infectious bacteria can be traced back to Felix d'Herelle in 1917, about a decade before the discovery of penicillin [45]. The recent rise of MDR bacteria has renewed interest in pursuing phage therapy as alternatives to antibiotics [46, 47]. Although phage therapy has not been approved for widespread use in the United States, there have been several significant uses of bacteriophages against MDR infections under the principles of compassionate use [48]. Famously, in 2016, Tom Patterson was successfully treated with a cocktail of phages, identified through a joint effort of the US Navy, UCSD, and Texas A&M, to clear an infection caused by an MDR strain of *A. baumannii* [49]. This case brought greater widespread attention to the revival of phage therapy.

Since then, several other success stories of phage therapy have been documented against other MDR bacteria. Chan et al. described the use of a jumbo phage known as OMKO1 to treat a

recurrent *P. aeruginosa* infection within an aortic graft after ineffective control with antibiotic treatment. The researchers noted that *in vitro* treatment of *P. aeruginosa* biofilms with OMKO1 alone and or in combination with one of two antibiotics, ceftazidime and ciprofloxacin, led to significant decrease in biofilm density over antibiotic treatment alone [50].

Another example of was the treatment of a *M. abscessus* infection in a young girl who had cystic fibrosis using a cocktail of three phages identified as part of the SEA-PHAGES program run by the Howard Hughes Medical Institute. This case is of particular interest because the researchers genetically edited two phages to become more effective at killing bacteria by forcing them to be constitutively lytic [51]. Despite a surge in research, much is still unknown about phages and how their use may indirectly impact human health, specifically their interactions with the host immune system and microbiome [45].

Several traits that need to be considered prior to the utilization of a phage for patient therapy are as follows: clearance of the target bacteria, the lack of toxin-producing genes, lack of a lysogenic phase, its ability for transduction, and its host range [52]. One important characteristic of bacteriophages that defines their host specificity is how they recognize, bind, and enter their host cell, also known as absorption. The process of absorption has been highly studied from as far back as Delbruck in 1940 [53] when random collisions were thought to be the main means for attachment of phage to host cell. Since then, studies have demonstrated that tailed phage can increase the likelihood for successful infection by using their tail fibers to "walk" along the bacterial cell surface to find its appropriate receptor [54]. The receptors for several of these tailed phages have been identified as OM porins (OMPs), including phage λ and its receptor, the maltoporin LamB [55, 56].

It has been suggested that phage therapy might face similar downfalls as antibiotics. Just as environmental and human-driven pressures forced selection of antibiotic-resistant microbes, so can phage therapy force selection of phage-resistance to infection. Bacteria have evolved an adaptive immune response against bacteriophage infection, the CRISPR-Cas system (clustered regularly interspaced short palindromic repeats), that functions by targeting foreign nucleic acids complementary to acquired spacers for degradation. To date, it is estimated that about 50% of all bacteria contain one or more types of the CRISPR-Cas system [57]. Other mechanisms of phage resistance include modifications of surface phage receptors either at the protein structure or the protein expression levels [58]. It is important to note several studies have demonstrated that bacteria that evolve resistance against phages that utilize OMPs as their receptors often experience a trade-off resulting in increased antibiotic sensitivity [59, 60].

Antibiotics and phages can be used in combination with each other in an effort to subvert bacterial resistance mechanisms to either antibiotic individually. It has been shown that co-treatment with certain antibiotics at sub-inhibitory levels can promote phage infectivity [61]. The term phage-antibiotic synergy (PAS) was first described by Comeau et al. during treatment of *E. coli* with cefotaxime and a lytic phage [62]. Preliminary research resulted in promising activity against many MDR pathogens, including *P. aeruginosa* and *A. baumannii* [61, 63]. While many of the underlying mechanisms of PAS are currently unclear, advances in scientific techniques, such as fluorescence microscopy, can help broaden our understanding of these interactions at the molecular level.

1.3 Use of fluorescence microscopy to study antibiotic action and bacteriophage infection

Microscopy was utilized by the “father of microbiology” Anton van Leeuwenhoek with lenses that had a resolution power of almost one micron [64]. The technology has come a long way

since then, and with it, the understanding that bacteria can be similarly complex as eukaryotic cells with both temporal and spatial localization of proteins and, by extension, functions [65, 66]. Fluorescence microscopy is one of the most widely available and, arguably, one of the most broadly applicable forms of microscopic tools. It is especially versatile in studying antibiotics and their effects on bacteria.

Utilizing a set of fluorescent dyes that stain various components of the bacterial cell, Lamsa et al. characterized the MOA of a secreted metabolite of *Bacillus subtilis*, showing that it collapsed the proton motive force of both Gram-positive and Gram-negative bacteria [67]. Following that study, Nonejuie et al. demonstrated the ability to use a fluorescent microscopy tool dubbed Bacterial Cytological Profiling (BCP) to differentiate between antibiotics that target different biosynthetic pathways by taking advantage of the distinct morphological changes in bacterial cells upon treatment with those antibiotics. BCP was shown to be relatively rapid, in the timescale of hours, compared to previous MOA assays [9]. More recently, Zahir et al. described a high-throughput morphology-based screening platform incorporating glass-bottom 96-well plates and the Keio collection of *E. coli* single-gene deletion mutants to monitor phenotypic changes in cell shape in response to a cell wall active compound, cefsulodin [68].

Other applications of fluorescence microscopy to study effects of antimicrobial compounds on bacteria include the utilization of the voltage sensitive dyes $DiSC_3(5)$ and $DiBAC_4(3)$ to identify antibiotics that cause membrane depolarization as demonstrated by Winkel et al. Concentrating within the cell, the voltage sensitive dyes self-quench, and upon depolarization of the membrane, there is rapid release of the dye into the supernatant and an increase in fluorescence signal [69]. Lee et al. also used membrane potential dynamics and the fluorescent dye thioflavin-T to observe differences in stress response to antibiotic treatment that were mediated by magnesium flux [70].

It is relatively easy and inexpensive to design and generate functional fluorescent proteins to answer a broad range of questions related to cell biology, including how an antibiotic affects a bacterial cell. Pogliano et al. combined multiple fluorescent techniques, including GFP-tagging of the essential cell division protein of *B. subtilis* DivIVA, to show that daptomycin treatment led to incorrect localization of cell division machinery and thus disruption of proper cell growth [71]. Muller et al. later used various GFP-tagged proteins within different biosynthetic processes to show that daptomycin interferes with membrane fluidity [72].

With the increasing availability of fluorescently tagged antibiotics, it is possible to expand the study of protein-antibiotic interactions beyond the MOA. Previous methods of studying the binding of an antibiotic to its target or uptake into a cell required radioactive labeling [73, 74]. Several fluorescent conjugates of antibiotics have been developed and utilized to study localization of infection or toxicity within a host, protein target localization or antibiotic accumulation within a bacterial cell, and resistance mechanisms by bacteria [75-78]. Researchers have also taken advantage of certain antibiotics that fluoresce on their own without the need for conjugation to an additional probe. Cinquin et al. demonstrated the use of a fluoroquinolone antibiotic that excites under UV to study accumulation within *Enterobacter aerogenes* [79].

Fluorescence microscopy is not limited to the realm of the foundational science laboratory; it has implications for the clinical environment as well. Quach et al. used BCP to rapidly classify sensitive and resistant strains of methicillin-resistant *S. aureus* based on the lysis patterns under antibiotic treatment [80]. Sabhachandani et al. combined bead-based isolation, droplet microfluidics, and fluorescence microscopy to identify susceptibility breakpoints of pathogenic *E. coli* from patient urine samples for two different antibiotics [81]. These techniques are of interest

due to their ability to bypass the long culturing times required by other antibiotic susceptibility testing methods commonly used in the clinic to determine treatment options for infected patients.

Fluorescence microscopy can also be used to study the lifecycle of bacteriophages. Chatterjee & Rothenberg monitored the movement of fluorescently labeled phage λ to track its interaction dynamics with its bacterial receptor LamB [82]. Following the footsteps of Kraemer et al. [44], Chaikeeratisak et al. used fluorescently conjugated proteins to show the phage-encoded spindle is conserved across related *Pseudomonas* phages φKZ and φPA3. Chaikeeratisak et al. also discovered that these jumbo phages produce a proteinaceous shell around their DNA, mimicking the nucleus of eukaryotic organisms [83, 84]. This level of molecular complexity was previously uncharacterized and leads to interesting hypotheses regarding eukaryogenesis.

This dissertation contributes to the current field by describing the application of fluorescence microscopy to study the effect of antibiotics on pathogenic bacteria in a variety of ways. These include the application of fluorescent antibiotics to characterizing antibiotic uptake kinetics in *E. coli*, probing the effect of media conditions that mimic the human host environment on bacterial susceptibility, and observing phenotypic profiles of multi-drug resistant strains in response to drug combination treatment [85, 86]. This dissertation also describes the use of fluorescence microscopy to observe interactions between jumbo phage infection with different antibiotics from a variety of classes and their dual effects on host cell and viral cytology.

1.4 References

1. Whitman, W.B., Coleman, D.C., and Wiebe, W.J., *Prokaryotes: the unseen majority.* Proc Natl Acad Sci U S A, 1998. **95**(12): p. 6578-83.
2. Hibbing, M.E., Fuqua, C., Parsek, M.R., and Peterson, S.B., *Bacterial competition: surviving and thriving in the microbial jungle.* Nat Rev Microbiol, 2010. **8**(1): p. 15-25.
3. White, N.J., Hien, T.T., and Nosten, F.H., *A Brief History of Qinghaosu.* Trends Parasitol, 2015. **31**(12): p. 607-610.
4. Waksman, S.A., Schatz, A., and Reynolds, D.M., *Production of antibiotic substances by actinomycetes.* Ann N Y Acad Sci, 2010. **1213**: p. 112-24.
5. Waksman, S.A., *Tenth anniversary of the discovery of streptomycin, the first chemotherapeutic agent found to be effective against tuberculosis in humans.* Am Rev Tuberc, 1954. **70**(1): p. 1-8.
6. Procopio, R.E., Silva, I.R., Martins, M.K., Azevedo, J.L., and Araujo, J.M., *Antibiotics produced by Streptomyces.* Braz J Infect Dis, 2012. **16**(5): p. 466-71.
7. Aminov, R.I., *A brief history of the antibiotic era: lessons learned and challenges for the future.* Front Microbiol, 2010. **1**: p. 134.
8. Lewis, K., *Platforms for antibiotic discovery.* Nat Rev Drug Discov, 2013. **12**(5): p. 371-87.
9. Nonejuie, P., Burkart, M., Pogliano, K., and Pogliano, J., *Bacterial cytological profiling rapidly identifies the cellular pathways targeted by antibacterial molecules.* Proc Natl Acad Sci U S A, 2013. **110**(40): p. 16169-74.
10. Cotsonas King, A. and Wu, L., *Macromolecular synthesis and membrane perturbation assays for mechanisms of action studies of antimicrobial agents.* Curr Protoc Pharmacol, 2009. **Chapter 13**: p. Unit 13A 7.
11. Santiago, M., Lee, W., Fayad, A.A., Coe, K.A., Rajagopal, M., Do, T., Hennessen, F., Srisuknimit, V., Müller, R., Meredith, T.C., and Walker, S., *Genome-wide mutant profiling predicts the mechanism of a Lipid II binding antibiotic.* Nature chemical biology, 2018. **14**(6): p. 601-608.
12. Donkor, E.S., *Sequencing of bacterial genomes: principles and insights into pathogenesis and development of antibiotics.* Genes, 2013. **4**(4): p. 556-572.
13. Baba, T., Ara, T., Hasegawa, M., Takai, Y., Okumura, Y., Baba, M., Datsenko, K.A., Tomita, M., Wanner, B.L., and Mori, H., *Construction of Escherichia coli K-12 in-frame, single-gene knockout mutants: the Keio collection.* Molecular systems biology, 2006. **2**: p. 2006.0008-2006.0008.
14. Farha, M.A., French, S., Stokes, J.M., and Brown, E.D., *Bicarbonate Alters Bacterial Susceptibility to Antibiotics by Targeting the Proton Motive Force.* ACS Infectious Diseases, 2018. **4**(3): p. 382-390.

15. Heo, J., Cho, K., Kim, U., Cho, D.-H., Ko, S., Tran, Q.-G., Lee, Y.J., Ryu, C.-M., and Kim, H.-S., *Genome-wide high-throughput screening of interactive bacterial metabolite in the algal population using Escherichia coli K-12 Keio collection.* Scientific reports, 2020. **10**(1): p. 10647-10647.

16. Piya, D., Lessor, L., Koehler, B., Stonecipher, A., Cahill, J., and Gill, J.J., *Genome-wide screens reveal Escherichia coli genes required for growth of T1-like phage LL5 and V5-like phage LL12.* Scientific reports, 2020. **10**(1): p. 8058-8058.

17. Wetmore, K.M., Price, M.N., Waters, R.J., Lamson, J.S., He, J., Hoover, C.A., Blow, M.J., Bristow, J., Butland, G., Arkin, A.P., and Deutschbauer, A., *Rapid Quantification of Mutant Fitness in Diverse Bacteria by Sequencing Randomly Bar-Coded Transposons.* mBio, 2015. **6**(3): p. e00306-15.

18. Bandow, J.E., Brötz, H., Leichert, L.I.O., Labischinski, H., and Hecker, M., *Proteomic approach to understanding antibiotic action.* Antimicrobial agents and chemotherapy, 2003. **47**(3): p. 948-955.

19. O'Rourke, A., Beyhan, S., Choi, Y., Morales, P., Chan, A.P., Espinoza, J.L., Dupont, C.L., Meyer, K.J., Spoering, A., Lewis, K., Nierman, W.C., and Nelson, K.E., *Mechanism-of-Action Classification of Antibiotics by Global Transcriptome Profiling.* Antimicrobial agents and chemotherapy, 2020. **64**(3): p. e01207-19.

20. Perry, J., Waglechner, N., and Wright, G., *The Prehistory of Antibiotic Resistance.* Cold Spring Harb Perspect Med, 2016. **6**(6).

21. Davies, J. and Davies, D., *Origins and evolution of antibiotic resistance.* Microbiol Mol Biol Rev, 2010. **74**(3): p. 417-33.

22. Lobanovska, M. and Pilla, G., *Penicillin's Discovery and Antibiotic Resistance: Lessons for the Future?* Yale J Biol Med, 2017. **90**(1): p. 135-145.

23. CDC, *Antibiotic Resistance Threats in the United States*, C. U.S. Department of Health and Human Services, Editor. 2019.

24. Silhavy, T.J., Kahne, D., and Walker, S., *The bacterial cell envelope.* Cold Spring Harbor perspectives in biology, 2010. **2**(5): p. a000414-a000414.

25. Silver, L.L., *Challenges of antibacterial discovery.* Clinical microbiology reviews, 2011. **24**(1): p. 71-109.

26. Nikaido, H., *Molecular basis of bacterial outer membrane permeability revisited.* Microbiology and molecular biology reviews : MMBR, 2003. **67**(4): p. 593-656.

27. Li, X.-Z., Plésiat, P., and Nikaido, H., *The challenge of efflux-mediated antibiotic resistance in Gram-negative bacteria.* Clinical microbiology reviews, 2015. **28**(2): p. 337-418.

28. Munita, J.M. and Arias, C.A., *Mechanisms of Antibiotic Resistance.* Microbiology spectrum, 2016. **4**(2): p. 10.1128/microbiolspec.VMBF-0016-2015.

29. Barrett, T.C., Mok, W.W.K., Murawski, A.M., and Brynildsen, M.P., *Enhanced antibiotic resistance development from fluoroquinolone persisters after a single exposure to antibiotic.* Nature Communications, 2019. **10**(1): p. 1177.

30. Hall, C.W. and Mah, T.-F., *Molecular mechanisms of biofilm-based antibiotic resistance and tolerance in pathogenic bacteria.* FEMS Microbiology Reviews, 2017. **41**(3): p. 276-301.

31. Kathju, S., Nistico, L., Tower, I., Lasko, L.-A., and Stoodley, P., *Bacterial biofilms on implanted suture material are a cause of surgical site infection.* Surgical infections, 2014. **15**(5): p. 592-600.

32. Wambaugh, M.A., Shakya, V.P.S., Lewis, A.J., Mulvey, M.A., and Brown, J.C.S., *High-throughput identification and rational design of synergistic small-molecule pairs for combating and bypassing antibiotic resistance.* PLoS Biol, 2017. **15**(6): p. e2001644.

33. Paik, S., Kim, J.K., Chung, C., and Jo, E.K., *Autophagy: A new strategy for host-directed therapy of tuberculosis.* Virulence, 2019. **10**(1): p. 448-459.

34. Rončević, T., Puizina, J., and Tossi, A., *Antimicrobial Peptides as Anti-Infective Agents in Pre-Post-Antibiotic Era?* International journal of molecular sciences, 2019. **20**(22): p. 5713.

35. Kumaraswamy, M., Lin, L., Olson, J., Sun, C.F., Nonejuie, P., Corriden, R., Dohrmann, S., Ali, S.R., Amaro, D., Rohde, M., Pogliano, J., Sakoulas, G., and Nizet, V., *Standard susceptibility testing overlooks potent azithromycin activity and cationic peptide synergy against MDR Stenotrophomonas maltophilia.* J Antimicrob Chemother, 2016. **71**(5): p. 1264-9.

36. Lin, L., Nonejuie, P., Munguia, J., Hollands, A., Olson, J., Dam, Q., Kumaraswamy, M., Rivera, H., Jr., Corriden, R., Rohde, M., Hensler, M.E., Burkart, M.D., Pogliano, J., Sakoulas, G., and Nizet, V., *Azithromycin Synergizes with Cationic Antimicrobial Peptides to Exert Bactericidal and Therapeutic Activity Against Highly Multidrug-Resistant Gram-Negative Bacterial Pathogens.* EBioMedicine, 2015. **2**(7): p. 690-8.

37. Ulloa, E.R., Kousha, A., Tsunemoto, H., Pogliano, J., Licitra, C., LiPuma, J.J., Sakoulas, G., Nizet, V., and Kumaraswamy, M., *Azithromycin Exerts Bactericidal Activity and Enhances Innate Immune Mediated Killing of MDR Achromobacter xylosoxidans.* Infectious Microbes & Diseases, 2020. **2**(1).

38. Sakoulas, G., Bayer, A.S., Pogliano, J., Tsuji, B.T., Yang, S.-J., Mishra, N.N., Nizet, V., Yeaman, M.R., and Moise, P.A., *Ampicillin enhances daptomycin- and cationic host defense peptide-mediated killing of ampicillin- and vancomycin-resistant Enterococcus faecium.* Antimicrobial agents and chemotherapy, 2012. **56**(2): p. 838-844.

39. Sakoulas, G., Rose, W., Berti, A., Olson, J., Munguia, J., Nonejuie, P., Sakoulas, E., Rybak, M.J., Pogliano, J., and Nizet, V., *Classical beta-Lactamase Inhibitors Potentiate the Activity of Daptomycin against Methicillin-Resistant Staphylococcus aureus and Colistin against Acinetobacter baumannii.* Antimicrob Agents Chemother, 2017. **61**(2).

40. Hatfull, G.F. and Hendrix, R.W., *Bacteriophages and their genomes.* Curr Opin Virol, 2011. **1**(4): p. 298-303.

41. Casjens, S.R. and Hendrix, R.W., *Bacteriophage lambda: Early pioneer and still relevant.* Virology, 2015. **479-480**: p. 310-30.

42. Sanger, F., Coulson, A.R., Hong, G.F., Hill, D.F., and Petersen, G.B., *Nucleotide sequence of bacteriophage lambda DNA.* J Mol Biol, 1982. **162**(4): p. 729-73.

43. Yuan, Y. and Gao, M., *Jumbo Bacteriophages: An Overview.* Front Microbiol, 2017. **8**: p. 403.

44. Kraemer, J.A., Erb, M.L., Waddling, C.A., Montabana, E.A., Zehr, E.A., Wang, H., Nguyen, K., Pham, D.S., Agard, D.A., and Pogliano, J., *A phage tubulin assembles dynamic filaments by an atypical mechanism to center viral DNA within the host cell.* Cell, 2012. **149**(7): p. 1488-99.

45. Cisek, A.A., Dabrowska, I., Gregorczyk, K.P., and Wyzewski, Z., *Phage Therapy in Bacterial Infections Treatment: One Hundred Years After the Discovery of Bacteriophages.* Curr Microbiol, 2017. **74**(2): p. 277-283.

46. Lin, D.M., Koskella, B., and Lin, H.C., *Phage therapy: An alternative to antibiotics in the age of multi-drug resistance.* World journal of gastrointestinal pharmacology and therapeutics, 2017. **8**(3): p. 162-173.

47. Gordillo Altamirano, F.L. and Barr, J.J., *Phage Therapy in the Postantibiotic Era.* Clin Microbiol Rev, 2019. **32**(2).

48. McCallin, S., Sacher, J.C., Zheng, J., and Chan, B.K., *Current State of Compassionate Phage Therapy.* Viruses, 2019. **11**(4): p. 343.

49. Schooley, R.T., Biswas, B., Gill, J.J., Hernandez-Morales, A., Lancaster, J., Lessor, L., Barr, J.J., Reed, S.L., Rohwer, F., Benler, S., Segall, A.M., Taplitz, R., Smith, D.M., Kerr, K., Kumaraswamy, M., Nizet, V., Lin, L., McCauley, M.D., Strathdee, S.A., Benson, C.A., Pope, R.K., Leroux, B.M., Picel, A.C., Mateczun, A.J., Cilwa, K.E., Regeimbal, J.M., Estrella, L.A., Wolfe, D.M., Henry, M.S., Quinones, J., Salka, S., Bishop-Lilly, K.A., Young, R., and Hamilton, T., *Development and Use of Personalized Bacteriophage-Based Therapeutic Cocktails To Treat a Patient with a Disseminated Resistant Acinetobacter baumannii Infection.* Antimicrob Agents Chemother, 2017. **61**(10).

50. Chan, B.K., Turner, P.E., Kim, S., Mojibian, H.R., Elefteriades, J.A., and Narayan, D., *Phage treatment of an aortic graft infected with Pseudomonas aeruginosa.* Evolution, medicine, and public health, 2018. **2018**(1): p. 60-66.

51. Dedrick, R.M., Guerrero-Bustamante, C.A., Garlena, R.A., Russell, D.A., Ford, K., Harris, K., Gilmour, K.C., Soothill, J., Jacobs-Sera, D., Schooley, R.T., Hatfull, G.F., and Spencer, H., *Engineered bacteriophages for treatment of a patient with a disseminated drug-resistant Mycobacterium abscessus.* Nature Medicine, 2019. **25**(5): p. 730-733.

52. Hyman, P., *Phages for Phage Therapy: Isolation, Characterization, and Host Range Breadth.* Pharmaceuticals (Basel, Switzerland), 2019. **12**(1): p. 35.

53. Delbrück, M., *ADSORPTION OF BACTERIOPHAGE UNDER VARIOUS PHYSIOLOGICAL CONDITIONS OF THE HOST.* The Journal of general physiology, 1940. **23**(5): p. 631-642.

54. Storms, Z.J. and Sauvageau, D., *Modeling tailed bacteriophage adsorption: Insight into mechanisms.* Virology, 2015. **485**: p. 355-62.

55. Rakhuba, D.V., Kolomiets, E.I., Dey, E.S., and Novik, G.I., *Bacteriophage receptors, mechanisms of phage adsorption and penetration into host cell.* Pol J Microbiol, 2010. **59**(3): p. 145-55.

56. Berkane, E., Orlik, F., Stegmeier, J.F., Charbit, A., Winterhalter, M., and Benz, R., *Interaction of bacteriophage lambda with its cell surface receptor: an in vitro study of binding of the viral tail protein gpJ to LamB (Maltoporin).* Biochemistry, 2006. **45**(8): p. 2708-20.

57. Westra, E.R., van Houte, S., Gandon, S., and Whitaker, R., *The ecology and evolution of microbial CRISPR-Cas adaptive immune systems.* Philos Trans R Soc Lond B Biol Sci, 2019. **374**(1772): p. 20190101.

58. Oechslin, F., *Resistance Development to Bacteriophages Occurring during Bacteriophage Therapy.* Viruses, 2018. **10**(7).

59. Burmeister, A.R., Fortier, A., Roush, C., Lessing, A.J., Bender, R.G., Barahman, R., Grant, R., Chan, B.K., and Turner, P.E., *Pleiotropy complicates a trade-off between phage resistance and antibiotic resistance.* Proc Natl Acad Sci U S A, 2020. **117**(21): p. 11207-11216.

60. Chan, B.K., Sistrom, M., Wertz, J.E., Kortright, K.E., Narayan, D., and Turner, P.E., *Phage selection restores antibiotic sensitivity in MDR Pseudomonas aeruginosa.* Sci Rep, 2016. **6**: p. 26717.

61. Tagliaferri, T.L., Jansen, M., and Horz, H.P., *Fighting Pathogenic Bacteria on Two Fronts: Phages and Antibiotics as Combined Strategy.* Front Cell Infect Microbiol, 2019. **9**: p. 22.

62. Comeau, A.M., Tetart, F., Trojet, S.N., Prere, M.F., and Krisch, H.M., *Phage-Antibiotic Synergy (PAS): beta-lactam and quinolone antibiotics stimulate virulent phage growth.* PLoS One, 2007. **2**(8): p. e799.

63. Uchiyama, J., Shigehisa, R., Nasukawa, T., Mizukami, K., Takemura-Uchiyama, I., Ujihara, T., Murakami, H., Imanishi, I., Nishifuji, K., Sakaguchi, M., and Matsuzaki, S., *Piperacillin and ceftazidime produce the strongest synergistic phage–antibiotic effect in Pseudomonas aeruginosa.* Archives of Virology, 2018. **163**(7): p. 1941-1948.

64. Amos, B., *Lessons from the history of light microscopy.* Nat Cell Biol, 2000. **2**(8): p. E151-2.

65. Kentner, D. and Sourjik, V., *Use of fluorescence microscopy to study intracellular signaling in bacteria.* Annu Rev Microbiol, 2010. **64**: p. 373-90.

66. Yao, Z. and Carballido-Lopez, R., *Fluorescence imaging for bacterial cell biology: from localization to dynamics, from ensembles to single molecules.* Annu Rev Microbiol, 2014. **68**: p. 459-76.

67. Lamsa, A., Liu, W.T., Dorrestein, P.C., and Pogliano, K., *The Bacillus subtilis cannibalism toxin SDP collapses the proton motive force and induces autolysis.* Mol Microbiol, 2012. **84**(3): p. 486-500.

68. Zahir, T., Camacho, R., Vitale, R., Ruckebusch, C., Hofkens, J., Fauvart, M., and Michiels, J., *High-throughput time-resolved morphology screening in bacteria reveals phenotypic responses to antibiotics.* Commun Biol, 2019. **2**: p. 269.

69. Te Winkel, J.D., Gray, D.A., Seistrup, K.H., Hamoen, L.W., and Strahl, H., *Analysis of Antimicrobial-Triggered Membrane Depolarization Using Voltage Sensitive Dyes.* Front Cell Dev Biol, 2016. **4**: p. 29.

70. Lee, D.D., Galera-Laporta, L., Bialecka-Fornal, M., Moon, E.C., Shen, Z., Briggs, S.P., Garcia-Ojalvo, J., and Suel, G.M., *Magnesium Flux Modulates Ribosomes to Increase Bacterial Survival.* Cell, 2019. **177**(2): p. 352-360 e13.

71. Pogliano, J., Pogliano, N., and Silverman, J.A., *Daptomycin-mediated reorganization of membrane architecture causes mislocalization of essential cell division proteins.* J Bacteriol, 2012. **194**(17): p. 4494-504.

72. Muller, A., Wenzel, M., Strahl, H., Grein, F., Saaki, T.N.V., Kohl, B., Siersma, T., Bandow, J.E., Sahl, H.G., Schneider, T., and Hamoen, L.W., *Daptomycin inhibits cell envelope synthesis by interfering with fluid membrane microdomains.* Proc Natl Acad Sci U S A, 2016. **113**(45): p. E7077-E7086.

73. Zhao, G., Meier, T.I., Kahl, S.D., Gee, K.R., and Blaszczak, L.C., *BOCILLIN FL, a sensitive and commercially available reagent for detection of penicillin-binding proteins.* Antimicrob Agents Chemother, 1999. **43**(5): p. 1124-8.

74. Bryan, L.E. and Van den Elzen, H.M., *Streptomycin accumulation in susceptible and resistant strains of Escherichia coli and Pseudomonas aeruginosa.* Antimicrob Agents Chemother, 1976. **9**(6): p. 928-38.

75. Matijasic, M., Munic Kos, V., Nujic, K., Cuzic, S., Padovan, J., Kragol, G., Alihodzic, S., Mildner, B., Verbanac, D., and Erakovic Haber, V., *Fluorescently labeled macrolides as a tool for monitoring cellular and tissue distribution of azithromycin.* Pharmacol Res, 2012. **66**(4): p. 332-42.

76. Phetsang, W., Pelingon, R., Butler, M.S., Kc, S., Pitt, M.E., Kaeslin, G., Cooper, M.A., and Blaskovich, M.A., *Fluorescent Trimethoprim Conjugate Probes To Assess Drug Accumulation in Wild Type and Mutant Escherichia coli.* ACS Infect Dis, 2016. **2**(10): p. 688-701.

77. Stone, M.R.L., Butler, M.S., Phetsang, W., Cooper, M.A., and Blaskovich, M.A.T., *Fluorescent Antibiotics: New Research Tools to Fight Antibiotic Resistance.* Trends Biotechnol, 2018. **36**(5): p. 523-536.

78. Stone, M.R.L., Masi, M., Phetsang, W., Pages, J.M., Cooper, M.A., and Blaskovich, M.A.T., *Fluoroquinolone-derived fluorescent probes for studies of bacterial penetration and efflux.* Medchemcomm, 2019. **10**(6): p. 901-906.

79. Cinquin, B., Maigre, L., Pinet, E., Chevalier, J., Stavenger, R.A., Mills, S., Refregiers, M., and Pages, J.M., *Microspectrometric insights on the uptake of antibiotics at the single bacterial cell level.* Sci Rep, 2015. **5**: p. 17968.

80. Quach, D.T., Sakoulas, G., Nizet, V., Pogliano, J., and Pogliano, K., *Bacterial Cytological Profiling (BCP) as a Rapid and Accurate Antimicrobial Susceptibility Testing Method for Staphylococcus aureus.* EBioMedicine, 2016. **4**: p. 95-103.

81. Sabhachandani, P., Sarkar, S., Zucchi, P.C., Whitfield, B.A., Kirby, J.E., Hirsch, E.B., and Konry, T., *Integrated microfluidic platform for rapid antimicrobial susceptibility testing and bacterial growth analysis using bead-based biosensor via fluorescence imaging.* Microchimica Acta, 2017. **184**(12): p. 4619-4628.

82. Chatterjee, S. and Rothenberg, E., *Interaction of bacteriophage l with its E. coli receptor, LamB.* Viruses, 2012. **4**(11): p. 3162-78.

83. Chaikeeratisak, V., Nguyen, K., Egan, M.E., Erb, M.L., Vavilina, A., and Pogliano, J., *The Phage Nucleus and Tubulin Spindle Are Conserved among Large Pseudomonas Phages.* Cell Rep, 2017. **20**(7): p. 1563-1571.

84. Chaikeeratisak, V., Nguyen, K., Khanna, K., Brilot, A.F., Erb, M.L., Coker, J.K., Vavilina, A., Newton, G.L., Buschauer, R., Pogliano, K., Villa, E., Agard, D.A., and Pogliano, J., *Assembly of a nucleus-like structure during viral replication in bacteria.* Science, 2017. **355**(6321): p. 194-197.

85. Dillon, N., Holland, M., Tsunemoto, H., Hancock, B., Cornax, I., Pogliano, J., Sakoulas, G., and Nizet, V., *Surprising synergy of dual translation inhibition vs. Acinetobacter baumannii and other multidrug-resistant bacterial pathogens.* EBioMedicine, 2019. **46**: p. 193-201.

86. Ulloa, E.R., Dillon, N., Tsunemoto, H., Pogliano, J., Sakoulas, G., and Nizet, V., *Avibactam Sensitizes Carbapenem-Resistant NDM-1-Producing Klebsiella pneumoniae to Innate Immune Clearance.* J Infect Dis, 2019. **220**(3): p. 484-493.

CHAPTER 2:

Using microfluidics and fluorescence microscopy to monitor antibiotic uptake kinetics in *Escherichia coli*

2.1 Abstract

The effectiveness of an antimicrobial compound is tightly linked to its ability to reach its intended target. In the case of many antibiotics, that means passing through the bacterial cell envelope and into the cytoplasm, the mechanisms by which are poorly understood. Previous research in monitoring antibiotic uptake often used indirect methods or required the use of radioactive labeling. By incorporating microfluidics and the fluorescence microscopy technique known as bacterial cytological profiling together, in this study we observe the uptake of two fluorescently tagged macrolides, azithromycin and roxithromycin, at the single cell level with greater temporal resolution. Using these tools, we have quantitatively assessed the capacity of individual components of the Gram-negative bacteria *Escherichia coli* cell envelope, e.g. outer membrane vs inner membrane, in preventing the accumulation of antibiotics. Additionally, we show that cells grown in bicarbonate-containing media such as the eukaryotic cell culture media RPMI 1640 have increased uptake rates compared to growth in standard bacteriologic medias and this kinetic difference suggests that bicarbonate alters outer membrane permeability. Together, these results provide insight into how various conditions or mutants affect the kinetics of antibiotic uptake and therefore influence antibiotic susceptibility.

2.2 Introduction

Antibiotics are inarguably a pillar of modern medicine, but our dependency on these compounds generates artificial selective pressure on rapidly changing infectious bacteria. Introduction of a new antibiotic into clinical use is quickly followed by the occurrence of resistant bacteria. Indeed, some pathogenic strains have evolved resistance to multiple classes of antibiotics leading to treatment complications or necessitating the use of toxic last-line drugs [1]. The ESKAPEE group of pathogens (*Enterococcus faecium, Staphylococcus aureus, Klebsiella*

pneumoniae, *Pseudomonas aeruginosa*, *Enterobacter* spp., and *Escherichia coli*) are the leading cause of healthcare-associated infections, and often present multi-drug resistance [2, 3]. The majority of these species are Gram-negative bacteria whose physiology itself creates several innate defenses to antimicrobial action [3].

A major barrier to antibiotic susceptibility in Gram-negative bacteria, is the presence of the outer membrane. The outer membrane is an asymmetrical lipid bilayer with lipopolysaccharides in the outer leaflet and phospholipids in the inner leaflet [4]. This composition makes the outer membrane highly hydrophobic, preventing the diffusion of hydrophilic molecules. The outer membrane also has several channels known as porins that can restrict the passage of molecules from the external environment based on their size [5]. Decreased expression of certain outer membrane porins (OMPs) has been associated with resistance to several classes of antibiotics, including β-lactams and aminoglycosides, in several species of Gram-negative bacteria [6].

Compounds that can make it past the outer membrane have to traverse the peptidoglycan cell wall and vicious periplasm before reaching the inner membrane [4]. Upon entering the bacterial cytoplasm, antibiotics are subject to export by powerful efflux pumps. These efflux pumps use either ATP hydrolysis or the electrochemical gradient of the proton motive force (PMF) to extrude toxic molecules from the cell, thus lowering an antibiotic's intracellular concentration below that of its effective concentration [7]. The first description of efflux pump-mediated resistance to antibiotic was described by Ball et al. in 1980 regarding acquired tetracycline resistance in *E. coli* [8]. Since then, several classes of efflux pumps have been identified in both Gram-negative and Gram-positive bacteria [9, 10].

Co-evolution with bacteria has provided ways of over-coming some of the intrinsic resistances of Gram-negative species. Cationic antimicrobial peptides (AMPs) have been

identified from a variety of biological sources from bacteria to the fruit fly *Drosophila* to humans [11]. In general, these positively charged AMPs function by readily inserting themselves into the negatively charged bacterial membranes, forming non-specific pores thereby disrupting the barrier-nature of the membrane [12, 13]. The bacterial polymyxins, first described in 1947 [14], and its derivatives have been well studied and are even used clinically (e.g. colistin) [15]. Polymyxin B nonapeptide (PMBN) has decreased bactericidal action relative to its original form, but has been shown to greatly sensitive *Salmonella typhimurium, E. coli,* and *Pseudomonas aeruginosa* to other antibiotics [16, 17]. The human cathelicidin LL-37 has also been shown to help to clear infections through the disruption of the bacterial membrane [18, 19]. Several studies have demonstrated the ability of LL-37 to affect bacterial survival on its own [20, 21], as well as synergize with commonly used antibiotics to clear infections [22, 23].

While there has been a great deal of research into the mechanism of action of antibiotics [24], relatively little research has been done on the kinetics of antibiotic uptake. Early research in quantifying uptake often used indirect methods such as correlating changes in susceptibility to a given antibiotic in mutants lacking OMPs or with altered outer membranes [25, 26]. Other foundational studies used radioactive antibiotics to demonstrate the diffusion of macrolide antibiotics across membranes or the energy-dependent uptake of aminoglycosides [27-29]. One recent study used liquid chromatography-mass spectrometry tools to quantify uptake of a variety of antibiotics in *E. coli* [30]. With the advancement in microscopy techniques, the increasing availability of fluorescent antibiotics [31-33], and the development of microfluidics, we are in the unique position to monitor uptake at the single-cell level.

Bacterial Cytological Profiling (BCP), a fluorescence microscopy method to profile morphological changes in bacteria treated with antibiotics, can accurately classify antibiotics based

on their target at the biosynthetic pathway level [34, 35], and has been used in a variety of bacterial species [36, 37]. The implementation of microfluidics, a specialized platform for controlling nutrient and antibiotic availability, with BCP provides a unique way to study the kinetics of antibiotic uptake.

Recent research has suggested that the standard medium for susceptibility testing, cation-adjusted Mueller-Hinton broth (CAMHB), may mask an antibiotic's true potency when used in an infected patient, and that eukaryotic cell culture media, such as RPMI 1640, is a better mimic for the host environment [22, 38-40]. Bicarbonate is the primary buffering in the human body and is thought to contribute to these observed differences in antibiotic susceptibility, although the exact mechanism is still unclear. In 2006, Dorschner et al. showed that growth of MRSA and *E.coli* in bicarbonate containing media lead to increased membrane permeability, global gene expression changes, and thinning of the cell wall in *S. aureus* [41]. In 2018, Farha et al. suggested that the presence of bicarbonate affects antibiotic uptake and subsequent susceptibility by altering bacterial PMF [42]. Using BCP and microfluidics, we can test this hypothesis by observing uptake in media with or without bicarbonate, like RPMI 1640 supplemented with 10% LB (R10LB) and CAMHB, respectively.

In this study, we sought to address questions related to the ability of antibiotics to penetrate the outer membrane of Gram-negative bacteria, a key step that determines the efficacy of many novel antibiotics. Macrolide antibiotics, such as azithromycin and roxithromycin, have been shown to cross the outer membrane through diffusion rather than using OMPs [43], which makes them ideal for probing the specific effect of the outer membrane. Using microfluidics and BCP, we quantified the uptake of azithromycin and roxithromycin tagged with the fluorescent probe

nitrobenzofurazan (NBD) under different conditions including genetic backgrounds, synergy with membrane permeabilizing agents, and media type.

2.3 Materials and Methods

Bacterial strains, growth, and antibiotics

Escherichia coli strains MC4100, MC4100Δ*tolC*, and MC4100*lptD4213* and MRSA LAC were used in this study. The bacteria were plated on LB agar inoculated in various media for assay at 30°C, for MICs, or 37°C, for microfluidics. The media used in this study was LB, LB + 25 mM HCO_3 (LB+HCO3), RPMI 1640 + 10% LB (R10LB), or cation-adjusted Mueller Hinton Broth (CA-MHB). Preparations of antibiotics were performed according to manufacturer's or, in the case of the fluorescent labeled conjugates, the provider's recommendations. NBD-azithromycin (NBD-Azm) and NBD-roxithromycin (NBD-Rox) were provided by the Nizet Lab at University of California, San Diego and the Blaskovich Lab at the University of Queensland, respectively.

Minimal Inhibitory Concentration (MICs) Assays

MICs of NBD-Azm, NBD-Rox, and PMBN, shown in **Table 2.1**, were determined using the broth microdilution method (6). In brief, overnight cultures of bacterial strains were diluted 1:100 in the appropriate media type and allowed to grow at 30°C with rolling until an optical density at 600 (OD_{600}) of ~0.15 – 0.2, or early exponential phase. The bacterial culture was diluted 1:100 into each well of a 96-well plate containing antibiotics at appropriate concentrations serially diluted. MICs were determined by OD_{600} readings after 18-24 hours of incubation at 30°C with shaking.

Microfluidics and fluorescence microscopy

Overnight cultures of bacterial strains were diluted 1:100 and 1:1000 into fresh media and incubated at 37°C without shaking until OD_{600} ~0.1. Microfluidics plates (B04A-03, EMD

Millipore) were prepared, and run through the manufacturer's liquid priming protocol. Cells were diluted to OD_{600} ~0.01 and added to the flow cell via manufacturer's cell loading protocol. Cells were acclimated to flow cell for 30 minutes with media containing no antibiotics, followed by 90 – 120 minutes antibiotic treatment. For synergy experiments, PMBN was added at selected concentrations during the acclimation period for 30 or 60 minutes, for the NBD-Rox and NBD-Azm experiments, respectively.

Microfluidics flow parameters were set at 37ºC with 10 kPa pressure and ambient air flow. An inert red dye, ATTO 655, was used at 1 ug/mL to ensure proper flow through cell chamber. DAPI, at 1 ug/mL, was used to confirm cytology after post-antibiotic treatment (data not shown). Microscopy images were taken on a Deltavision Deconvolution Microscope (GE Healthcare) using phase contrast, and fluorescence at 475 and 632 nm excitations every 5 minutes for 1 hour. Exposure parameters were kept consistent throughout all experiments for a given fluorescent antibiotic.

Quantitation of Fluorescence Microscopy

Microscopy images were taken on a Deltavision Deconvolution Microscope (GE Healthcare) using phase contrast, and fluorescence at 475 and 632 nm excitations every 5 minutes for 1 hour. Images were loaded into FIJI [44] using default settings for hyperstacks and stabilized using the HyperStackReg plugin created by Ved Sharma. The resulting stabilized images were channel-separated and saved as individual tiff files for further processing by a custom MATLAB 2017b (The MathWorks, Inc., Natick, Massachusetts) script. In brief, files are loaded into MATLAB in batches and the largest non-blank rectangle remaining in the stabilized image is found cropped to that size. Each channel associated with that image is cropped as well. The phase contrast channel associated with each image is used in conjunction with the red channel (632 nm

excitation) to perform image segmentation and obtain cell outlines. Cell properties including green channel (475 nm excitation) fluorescence, cell width and cell length were measured from these outlines. This processing is applied across all time points to obtain measurements over time for each experimental condition. Image processing and quantification was performed by Joseph Sugie, a Postdoc in the J. Pogliano lab.

2.4 Results

Role of outer membrane and efflux on antibiotic accumulation

We first sought to probe the extent to which the outer membrane and active efflux prevents antibiotic accumulation in bacteria. To address this question, we utilized three different strains of *E. coli*, wild-type MC4100, efflux-pump deficient MC4100Δ*tolC*, and outer membrane impaired MC4100*lptD4213*. These strains were first acclimated to growth in LB media in the microfluidics plate for 30 minutes, and then exposed to a fluorescent antibiotic with phase contrast and fluorescence images collected over time. This allowed us to visualize antibiotic accumulation at the single cell level.

In the absence of an intact outer membrane (**Figure 2.1**, *lptD4213*) accumulation of NBD-azithromycin (NBD-Azm) and NBD-roxithromycin (NBD-Rox) within the cell was observed to occur rapidly, level off within the first 20 minutes of treatment. In comparison, in the absence of efflux (**Figure 2.1**, Δ*tolC*), there was steady accumulation of both fluorescent antibiotics over 60 minutes of treatment without leveling off. The antibiotics did not accumulate to the same level in the efflux pump mutant compared to the outer membrane mutant. No uptake of either antibiotic was observed under wild-type conditions, which has both an intact outer membrane and efflux (**Figure 2.1**). These results show that the rate of uptake is substantially different between the three strains, as expected, and that the extent of accumulation also varies significantly between the Δ*tolC*

mutant and the *lptD4213* mutant. In addition, examining the entry of antibiotics into the *lptD4213* mutant, whose outer membrane is severely compromised, suggests that the inner membrane forms a barrier that slows the diffusion of NBD-Azm and NBD-Rox into the cell, but does not prevent it from accumulating to high intracellular levels within 20 minutes of exposure.

Effect of membrane permeabilization on antibiotic accumulation

We next studied the disruption of the outer membrane using a cationic AMP, polymyxin B nonapeptide (PBMN), to see if it affected antibiotic uptake in a similar fashion to that of the *lptD4213* mutant. We grew wild-type MC4100 with PMBN, known to target the outer membrane and thus affect antibiotic efficacy [13, 15-17, 45], for 30-60 minutes before treatment with fluorescent antibiotics at the respective concentrations and microscopy imaging to monitor increase in fluorescence signal within the cells over time. Treatment of wild type *E.coli* with sub-MIC levels of PMBN (32 μg/ml) (**Table 2.1**), led to increased accumulation of both NBD-Azm and NBD-Rox compared to untreated cells (**Figure 2.2A, B**). It is interesting to note during time-lapse imaging of antibiotic uptake, the fluorescence signal appears to accumulate in the periplasmic space during treatment with PMBN (**Figure 2.2E, F**). Periplasmic accumulation suggests that while PMBN is capable of permeabilizing the outer membrane, the inner membrane may be playing a role in slowing the accumulation of the antibiotic in the cytoplasm, which we also observed in the *lptD4213* mutant.

Since treatment of wild type cells with PMBN and the *lptD4213* mutant showed increased antibiotic uptake compared to the wild-type, we tested if there were synergy between the two. PMBN acts by disrupting the outer membrane but in the *lptD4213* mutant the outer membrane is already compromised, raising the question of whether PMBN is capable of further disrupting the outer membrane of the *lptD4213* mutant. However, in checkerboard experiments examining MICs,

we found no synergy between PMBN and the *lptD4213* mutant with NBD-Azm (**Table 2.1**). These results imply that the outer membrane in the *lptD4213* mutant is so weakened that PMBN does not provide any additional disruption to it. Therefore, our studies examining antibiotic uptake in the *lptD4213* mutant most likely report the barrier the inner membrane presents to antibiotic accumulation.

Effect of media condition on antibiotic accumulation

A key focus of my studies has been investigating the response of bacteria in different media which alters antibiotic susceptibility, such as the eukaryotic cell culture media RPMI 1640. Bicarbonate has been proposed to be an important component of RPMI 1640 because it has been shown that the supplementation of bicarbonate in standard bacteriologic media alone is capable of altering antibiotic susceptibility [46]. In order to assay the effect of media type on antibiotic uptake, we treated wild-type MC4100 and Gram-positive methicillin-resistant *S. aureus* LAC strains with the same relative concentrations of NBD-Azm in media without bicarbonate (CAMHB and LB) or with bicarbonate (R10LB and LB + 25 mM HCO_3 (LB+HCO3)). For both *E.coli* and MRSA, the strains were grown in the microfluidic plate in the four different media for 30 minutes before the addition of the fluorescent antibiotics at the concentrations indicated.

In the two media containing bicarbonate, (**Figure 2.3A, B**, LB+HCO3 or R10LB), the fluorescence antibiotic accumulated within cells rapidly and plateaued within the first 20 minutes of treatment in both strains. In comparison, in media without bicarbonate (**Figure 2.3A, B**, LB or CAMHB), relatively low uptake of the fluorescent antibiotic was observed. This demonstrates bicarbonate alone added to LB causes the accumulation of the fluorescent antibiotics to similar levels as cells grown in RPMI 1640 supplemented with 10% LB (R10LB). These results suggest

that in both *E.coli* and *S. aureus*, bicarbonate is sufficient and likely the major contributor to the differences in antibiotic susceptibility.

We also observed in these experiments the accumulation of fluorescently labeled antibiotics in the periplasmic space during growth in bicarbonate-containing media as we previously observed during growth of the *E.coli lptD* mutant or with PMBN (**Figure 2.3E, F**) for wild type *E. coli*. This suggests, that similar to treatment with the known-outer membrane permeabilizer PMBN, bicarbonate may also be affecting the integrity of the outer membrane to increase antibiotic uptake in wild-type cells.

2.5 Discussion

Using BCP and microfluidics in conjunction with each other allows us to answer some general questions regarding antibiotic transport into cell, including how rapidly does uptake occur, how does co-treatment with membrane permeabilizers affect the rate of uptake, and how do media conditions, specifically the presence of bicarbonate, alter antibiotic uptake kinetics. Azm and Rox are both second-generation macrolide antibiotics, sharing the same lactone-ring backbone, with slight modifications [47]. Rox contains an N-oxime side chain at the C9 position of the lactone-ring. Rox compared to Azm has a higher MIC, except in cases where the outer membrane has been compromised (**Table 2.1**), and there are several reports of differences in clinical efficacy between Azm and Rox [48, 49].

Early research in 1990 by Capobianoco & Goldman demonstrated that the accumulation of radioactive-labeled erythromycin and Azm into the Gram-negative *Haemophilus influenzae* was independent of active transport by disrupting the PMF using known inhibitors valinomycin and CCCP, which they concluded to indicate that these macrolides passively diffused across the cell envelope [28]. Additionally, macrolide antibiotics are relatively large and lipophilic, which

prevent them from crossing the outer membrane through porins [6]. This raises the questions of what is the underlying mechanism behind the transport of macrolides into the bacterial cell and what roles do the inner and outer membranes play in preventing antibiotic accumulation.

Examining the slopes of the curves during treatment with NBD-Azm or NBD-Rox (**Figure 2.1, 2.4**), we can see that in both cases there is a similar pattern in the effect that mutations in *tolC* or *lptD4213* have on the uptake of these two antibiotics. The biophysical properties of the outer membrane are good at repelling most antibiotics [5], and in the presence of an intact outer membrane, the transport of the macrolides into the cell is reduced [43]. Both antibiotics are effectively excluded in wild-type cells (**Figure 2.1, 2.2, 2.4**). In the absence of an intact outer membrane, such as in the *lpD4213* mutant, the inner membrane alone is not sufficient to prevent the accumulation of the fluorescence antibiotics (**Figure 2.1**) and suggests that the antibiotics are capable of diffusing through this lipid bilayer. The efflux pump TolC has been previously shown to confer resistance to macrolide treatment in *E. coli* [50]. In the absence of TolC, NBD-Azm and NBD-Rox both accumulate at a low, but steady, rate over the course of 60 minutes (**Figure 2.1**). This demonstrates that TolC is necessary to prevent accumulation of these macrolides.

The efflux capacity of the *lptD4213* mutant is unclear. Since it is unlikely that the outer membrane channel TolC can be properly anchored in the outer membrane of the *lptD4213* mutant, the probability that effective efflux is functional in this strain is low. It is possible that a small amount of the accumulated antibiotic is removed from the cytoplasm via efflux pumps despite the destabilization of the outer membrane, however our data demonstrates that the quick movement of the fluorescent macrolides across the disrupted outer membrane overwhelms the bacterial cell. Therefore, any low level efflux the *lptD4213* mutant is capable of is negligible compared to the rapid increase in intracellular concentration.

How growth in the presence of bicarbonate lowers the MIC of azithromycin has remained unclear. One study suggested that bicarbonate affects the PMF and thereby disables TolC dependent efflux [42]. The fact that the Azm MIC of the MC4100Δ*tolC* mutant (2 μg/ml) is approximately similar to the MIC (4 μg/ml) of wild type *E.coli* cells grown in bicarbonate-containing media is consistent with this model. However, if the only effect of bicarbonate was on disabling TolC dependent efflux, then we might expect that the rates of Azm uptake in MC4100Δ*tolC* and wild type in bicarbonate to be similar. Instead, we found that during growth in media containing bicarbonate, the uptake curves of fluorescent Azm in wild-type *E. coli* are very similar to conditions that have a disrupted outer membrane, either through genetic means or with co-treatment with PMBN, rather than being similar to the Δ*tolC* mutant (**Figures 2.1 – 2.4**). The similarities in uptake curves suggests that the presence of bicarbonate affects the integrity of the outer membrane rather than preventing efflux of the antibiotic through disruption of the PMF. Alternatively, it remains possible that bicarbonate primarily sensitizes cells by reducing the PMF, while also having additional effects on the structure or integrity of the LPS outer membrane barrier. Future studies will be necessary to measure the effect of the bicarbonate on the PMF in these strains.

In these conditions, we observed sequestering of the fluorescent antibiotic within the periplasmic space, which may also indicate the effect of PMBN and bicarbonate is specific to the outer membrane. Additionally, we can see that growth of the Gram-positive MRSA LAC in LB+HCO_3 or RPMI+10%LB has higher fluorescence signal than in non-bicarbonate containing media. As mentioned previously, Dorschner et al. described the thinning of the staphylococcal cell wall during growth in media containing bicarbonate [41], which may explain this observation.

In future studies, we can model the accumulation of the fluorescent antibiotics using the general equation:

$$\frac{dC}{dt} = k_{diffusion}(C_{outside} - C_{inside}) - k_{pump}(C_{inside}) + k_{active\ transport}(C_{outside})$$

Previous work demonstrated that the macrolide antibiotics do not enter the cell via active transport, but rather are capable of diffusing across the outer membrane barrier [43]. This means that the value for $k_{active\ transport}$ is zero. Additionally, we can assume that the value of $k_{diffusion}$ is higher in the outer membrane mutant MC4100 *lptD4213* and that the value of k_{pump} is zero in the efflux mutant MC4100Δ*tolC*. By fitting the measured rates of uptake to the simple model, we will be able to estimate values for these parameters and identify the relative importance of diffusion vs efflux pump in the accumulation of macrolide antibiotics. antibiotics which would enable us to predict intracellular steady-state concentrations in other conditions. Though not explored in this work, the steady-state concentration that is ultimately reached inside the cell has an interesting relation to MIC. It would be of interest to see if there is either a threshold of intracellular concentration or if the area under the curve is more predictive of the point at which the antibiotic overwhelms the cell and how the kinetics of slow versus fast uptake affects this.

In conclusion, this work demonstrates the power of integrating microfluidics and BCP together. By visualizing the uptake of antibiotics in the outer membrane and efflux mutants, we can isolate the contributions of the innate systems that Gram-negative bacteria such as *E.coli* utilize to resist antimicrobial actions. The application of this technique also provided data to understand the mechanistic function of bicarbonate in the sensitization of bacteria to antibiotics at the single cell level. This tool can be applied in the future to study the uptake of other fluorescent antibiotics, such as trimethoprim or ciprofloxacin [31-33, 51], that bypass the outer membrane via OMPs and other active transport mechanisms.

2.6 Acknowledgements

The authors would like to thank Victor Nizet at UCSD and Mark Blaskovich at the University of Queensland for providing the fluorescent antibiotics used in this study. This work was supported by the National Institutes of Health (NIH) National Institute of Allergy and Infectious Disease (NIAID) grant 1-U01-AI124316.

Chapter 2, in large part, is being formulated into a manuscript in preparation for the publication of the material. Hannah Tsunemoto, Joseph Sugie, Joe Pogliano, 2020. The dissertation author was the primary investigator and author of this material.

2.7 Figures

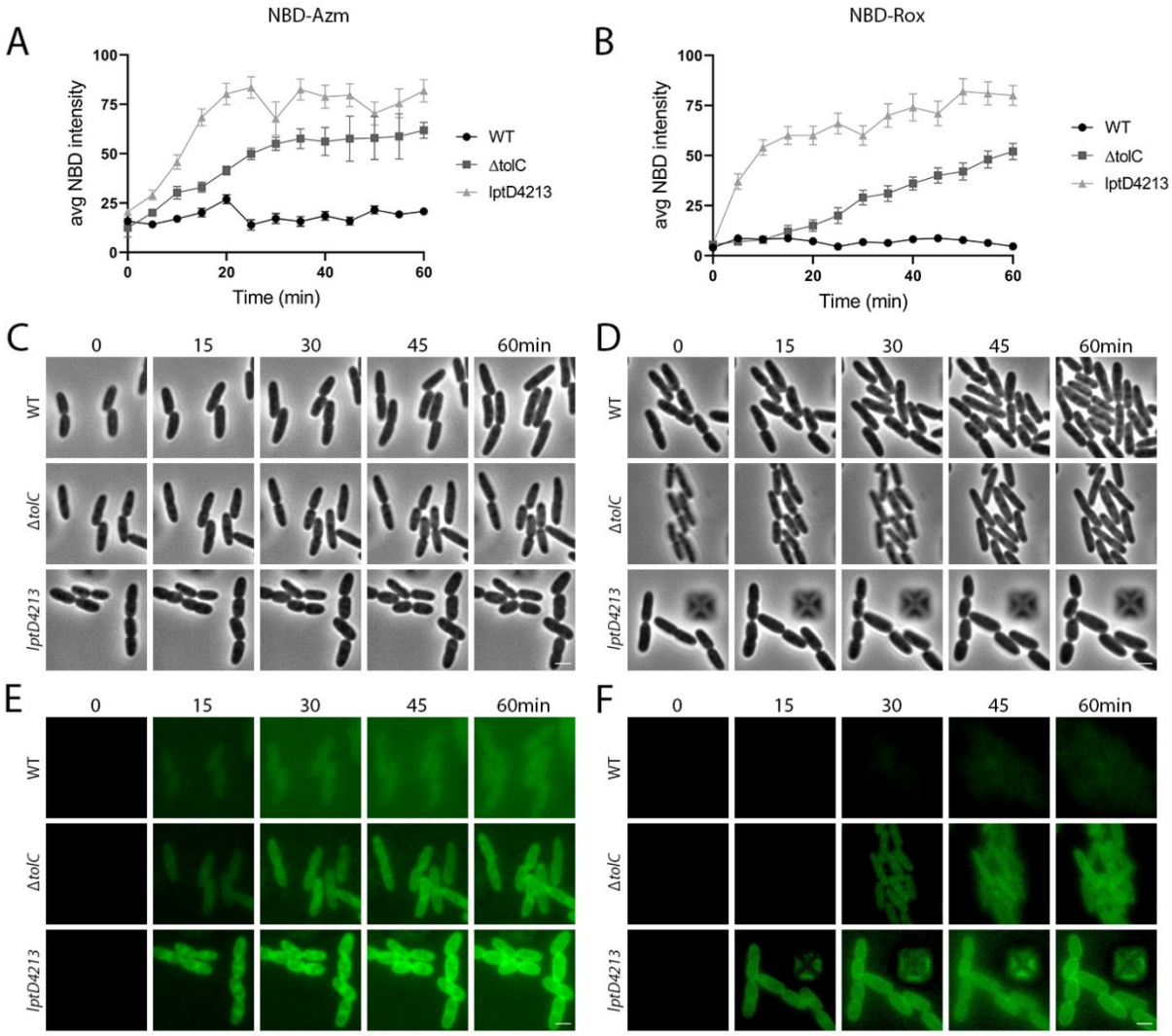

Figure 2.1 Different *E. coli* strains treated with fluorescently labeled antibiotics show differences in their accumulation rate. Wild-type = MC4100, Δ*tolC* = efflux mutant, *lptD4213* = OM mutant. (A, B) Quantification of NBD intensity over time during treatment at 2X MIC of the AD3643 strain for each antibiotic, NBD-Azm (4 ug/mL) and NBD-Rox (16 ug/mL), respectively. Error bars represent standard error of mean (SEM). (C,D) Phase and (E,F) fluorescence microscopy images of cells at different timepoints during treatment with antibiotics. Scale bar represents 2 μm.

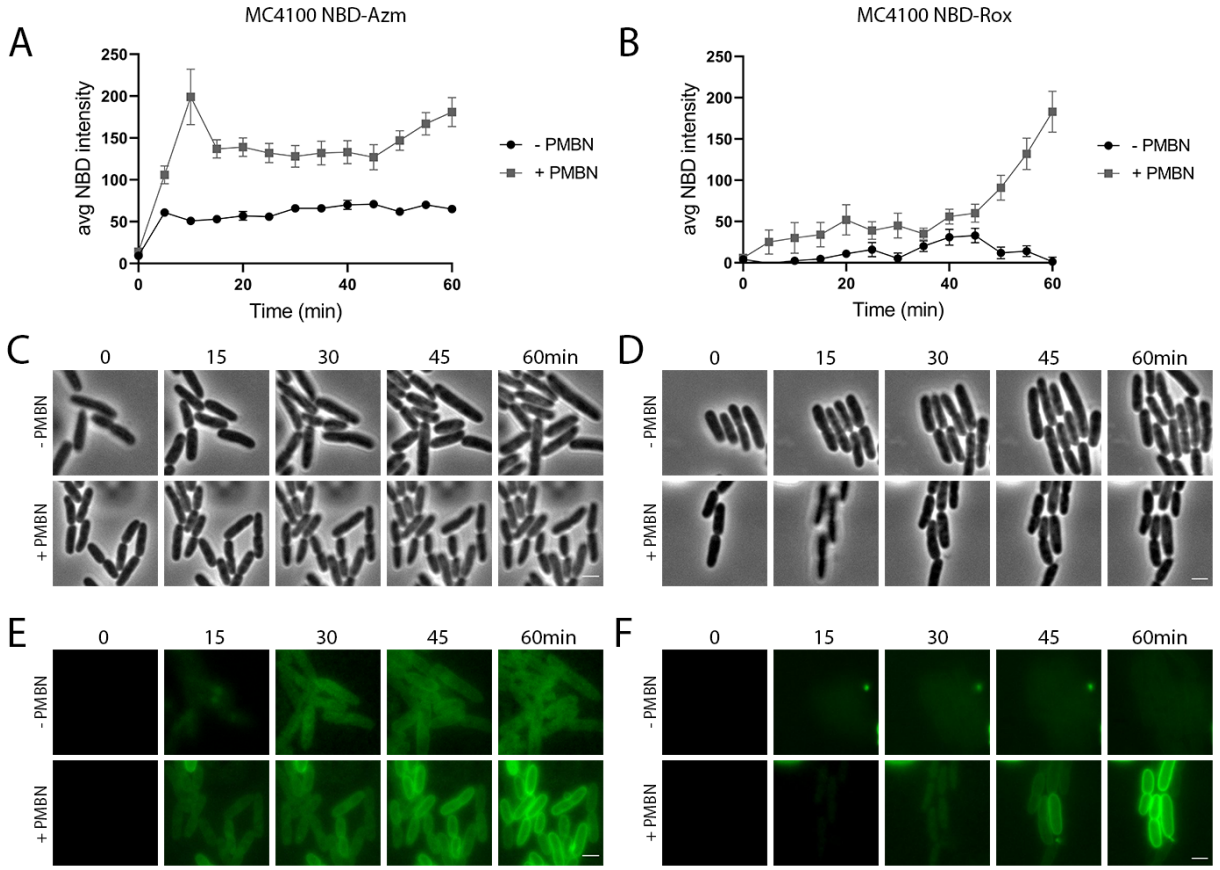

Figure 2.2 The membrane-active peptide PMBN alters accumulation of fluorescent macrolides at sub-MIC levels in *E. coli* WT MC4100. Conditions were as follows: (A, C, E) WT MC4100: NBD-Azm = 8 ug/mL with 32 ug/mL PMBN, (C, B, F) NBD-Rox = 32 ug/mL with 8 ug/mL PMBN. (A, B) Quantification of NBD intensity over time. (C, D) Phase and (E, F) fluorescent microscopy images of cells at different timepoints during treatment with antibiotics. Scale bar represents 2 μm.

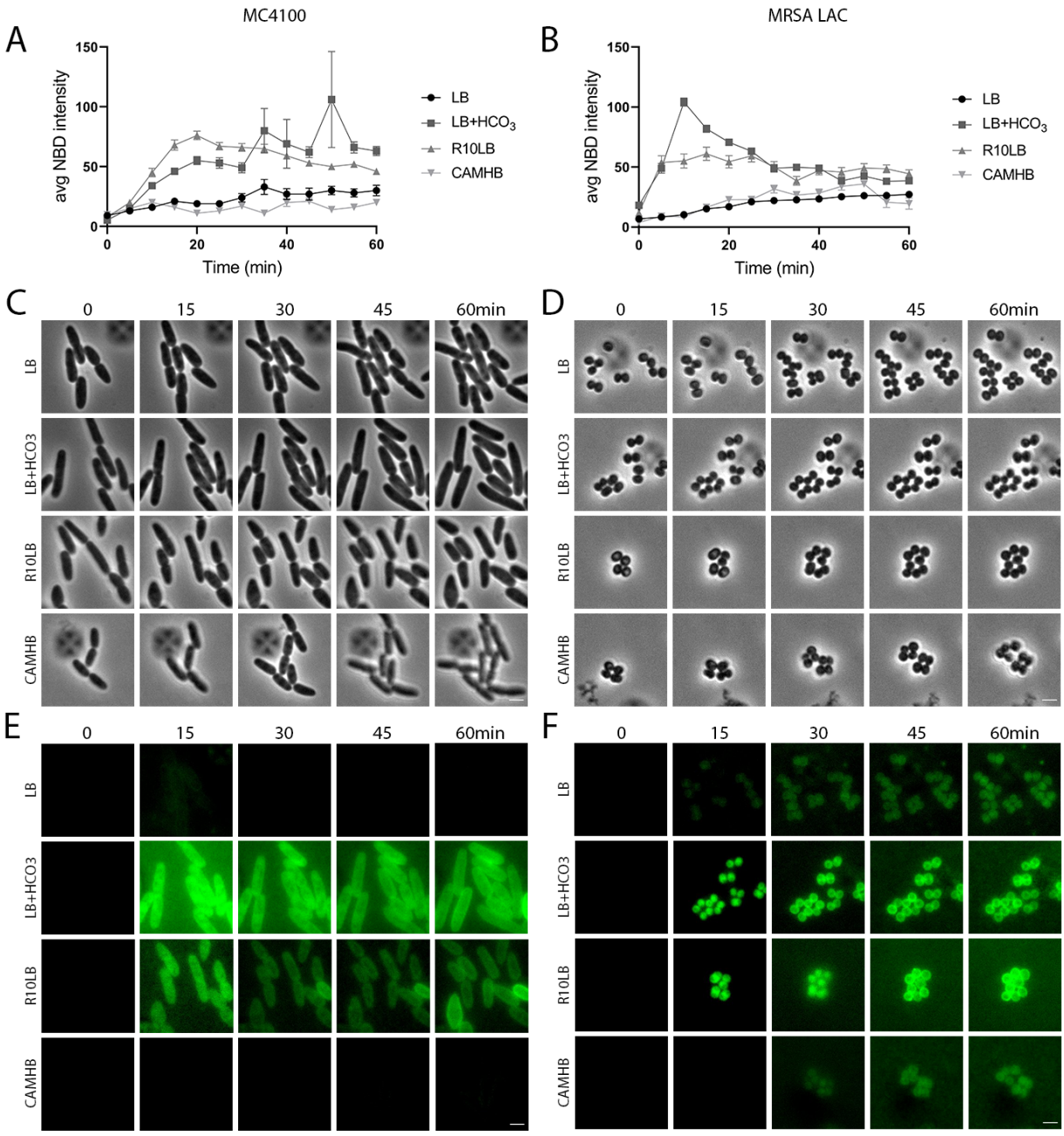

Figure 2.3 Growth in bicarbonate containing media increases fluorescent azithromycin accumulation in *E. coli* MC4100 or MRSA LAC compared to non-bicarbonate containing media. MC4100 treated with 32 ug/mL NBD-Azm and LAC treated with 3.2 ug/mL NBD-Azm, 1X relative MICs in LB. (A, B) Quantification of NBD intensity over time. Error bars represent SEM. (C, D) Phase and (E, F) fluorescent microscopy images of cells at different timepoints during treatment with antibiotics. Scale bar represents 2 μm.

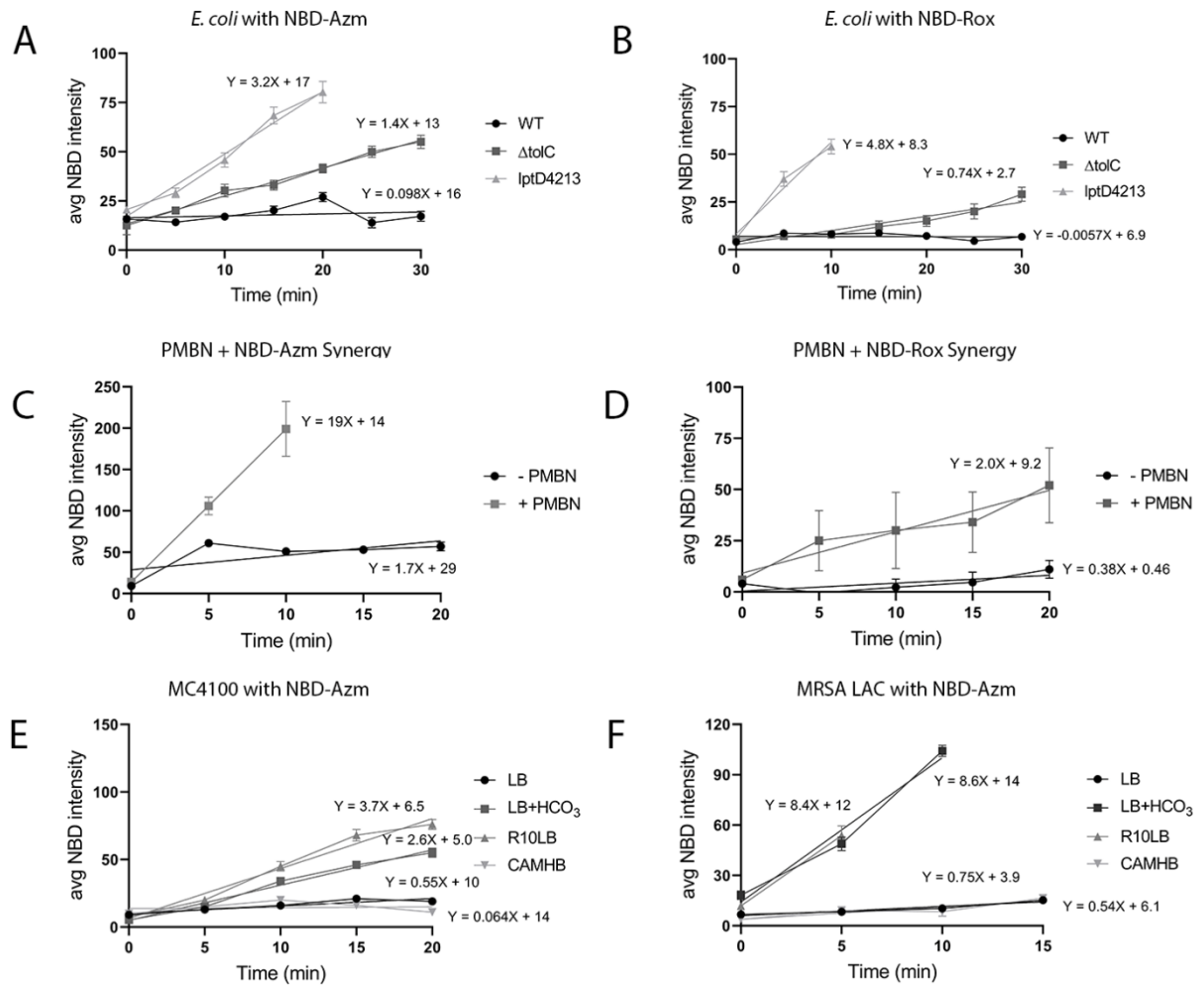

Figure 2.4 Trend lines of linear portions of uptake curves for all experimental conditions. (A, B) Wild-type compared to genetic mutants with respective fluorescent antibiotics, NBD-azithromycin (NBD-Azm) and NBD-roxithromycin (NBD-Rox), (C, D) Synergy with polymyxin B nonapeptide PMBN, (E, F) MC4100 and MRSA LAC with NBD-Azm in different media conditions.

2.8 Tables

Table 2.1 Minimum inhibitory concentration (MIC) of fluorescent antibiotics in experimental conditions. Concentrations of all compounds are in μg/mL and represent biological replicates.

***E. coli* MC4100 - genetic backgrounds**			
	wild-type	**Δ*tolC***	***lptD4213***
NBD-Azm	32	2	0.5
NBD-Rox	>64	8	1
PMBN	>64	>64	>64
***E. coli* MC4100 - AMP**			
	- PMBN	**(+ PMBN)**	***lptD4213* + PMBN**
NBD-Azm	32	8 + 16	no synergy
NBD-Rox	>64	8 + 32	**--**
***E. coli* MC4100 - various media types**			
	LB+HCO_3	**R10LB**	**CAMHB**
NBD-Azm	4	4	>32
NBD-Rox	64	32	>64
MRSA LAC – NBD-Azm			
LB	**LB+HCO_3**	**R10LB**	**CAMHB**
3.2	0.06	0.05	6.4

2.9 References

1. Aminov, R.I., *A brief history of the antibiotic era: lessons learned and challenges for the future.* Front Microbiol, 2010. **1**: p. 134.

2. Reza, A., Sutton, J.M., and Rahman, K.M., *Effectiveness of Efflux Pump Inhibitors as Biofilm Disruptors and Resistance Breakers in Gram-Negative (ESKAPEE) Bacteria.* Antibiotics (Basel, Switzerland), 2019. **8**(4): p. 229.

3. Santajit, S. and Indrawattana, N., *Mechanisms of Antimicrobial Resistance in ESKAPE Pathogens.* BioMed research international, 2016. **2016**: p. 2475067-2475067.

4. Silhavy, T.J., Kahne, D., and Walker, S., *The bacterial cell envelope.* Cold Spring Harbor perspectives in biology, 2010. **2**(5): p. a000414-a000414.

5. Delcour, A.H., *Outer membrane permeability and antibiotic resistance.* Biochimica et biophysica acta, 2009. **1794**(5): p. 808-816.

6. Nikaido, H., *Molecular basis of bacterial outer membrane permeability revisited.* Microbiology and molecular biology reviews : MMBR, 2003. **67**(4): p. 593-656.

7. Mahmood, H.Y., Jamshidi, S., Sutton, J.M., and Rahman, K.M., *Current Advances in Developing Inhibitors of Bacterial Multidrug Efflux Pumps.* Curr Med Chem, 2016. **23**(10): p. 1062-81.

8. Ball, P.R., Shales, S.W., and Chopra, I., *Plasmid-mediated tetracycline resistance in Escherichia coli involves increased efflux of the antibiotic.* Biochem Biophys Res Commun, 1980. **93**(1): p. 74-81.

9. Li, X.-Z., Plésiat, P., and Nikaido, H., *The challenge of efflux-mediated antibiotic resistance in Gram-negative bacteria.* Clinical microbiology reviews, 2015. **28**(2): p. 337-418.

10. Fernández, L. and Hancock, R.E.W., *Adaptive and mutational resistance: role of porins and efflux pumps in drug resistance.* Clinical microbiology reviews, 2012. **25**(4): p. 661-681.

11. Mahlapuu, M., Håkansson, J., Ringstad, L., and Björn, C., *Antimicrobial Peptides: An Emerging Category of Therapeutic Agents.* Frontiers in cellular and infection microbiology, 2016. **6**: p. 194-194.

12. Bechinger, B. and Gorr, S.U., *Antimicrobial Peptides: Mechanisms of Action and Resistance.* Journal of dental research, 2017. **96**(3): p. 254-260.

13. Vaara, M., *Agents that increase the permeability of the outer membrane.* Microbiological reviews, 1992. **56**(3): p. 395-411.

14. Stansly, P.G. and Schlosser, M.E., *Studies on Polymyxin: Isolation and Identification of Bacillus polymyxa and Differentiation of Polymyxin from Certain Known Antibiotics.* Journal of bacteriology, 1947. **54**(5): p. 549-556.

15. Vaara, M., *Polymyxins and Their Potential Next Generation as Therapeutic Antibiotics.* Frontiers in microbiology, 2019. **10**: p. 1689-1689.

16. Vaara, M. and Viljanen, P., *Binding of polymyxin B nonapeptide to gram-negative bacteria.* Antimicrobial agents and chemotherapy, 1985. **27**(4): p. 548-554.

17. Viljanen, P. and Vaara, M., *Susceptibility of gram-negative bacteria to polymyxin B nonapeptide.* Antimicrobial agents and chemotherapy, 1984. **25**(6): p. 701-705.

18. Rončević, T., Puizina, J., and Tossi, A., *Antimicrobial Peptides as Anti-Infective Agents in Pre-Post-Antibiotic Era?* International journal of molecular sciences, 2019. **20**(22): p. 5713.

19. Durr, U.H., Sudheendra, U.S., and Ramamoorthy, A., *LL-37, the only human member of the cathelicidin family of antimicrobial peptides.* Biochim Biophys Acta, 2006. **1758**(9): p. 1408-25.

20. Lin, M.-F., Tsai, P.-W., Chen, J.-Y., Lin, Y.-Y., and Lan, C.-Y., *OmpA Binding Mediates the Effect of Antimicrobial Peptide LL-37 on Acinetobacter baumannii.* PloS one, 2015. **10**(10): p. e0141107-e0141107.

21. Zaiou, M., Nizet, V., and Gallo, R.L., *Antimicrobial and protease inhibitory functions of the human cathelicidin (hCAP18/LL-37) prosequence.* J Invest Dermatol, 2003. **120**(5): p. 810-6.

22. Lin, L., Nonejuie, P., Munguia, J., Hollands, A., Olson, J., Dam, Q., Kumaraswamy, M., Rivera, H., Jr., Corriden, R., Rohde, M., Hensler, M.E., Burkart, M.D., Pogliano, J., Sakoulas, G., and Nizet, V., *Azithromycin Synergizes with Cationic Antimicrobial Peptides to Exert Bactericidal and Therapeutic Activity Against Highly Multidrug-Resistant Gram-Negative Bacterial Pathogens.* EBioMedicine, 2015. **2**(7): p. 690-8.

23. Ulloa, E.R., Dillon, N., Tsunemoto, H., Pogliano, J., Sakoulas, G., and Nizet, V., *Avibactam Sensitizes Carbapenem-Resistant NDM-1-Producing Klebsiella pneumoniae to Innate Immune Clearance.* J Infect Dis, 2019. **220**(3): p. 484-493.

24. Hutchings, M.I., Truman, A.W., and Wilkinson, B., *Antibiotics: past, present and future.* Curr Opin Microbiol, 2019. **51**: p. 72-80.

25. Hancock, R.E. and Bell, A., *Antibiotic uptake into gram-negative bacteria.* Eur J Clin Microbiol Infect Dis, 1988. **7**(6): p. 713-20.

26. Hancock, R.E. and Woodruff, W.A., *Roles of porin and beta-lactamase in beta-lactam resistance of Pseudomonas aeruginosa.* Rev Infect Dis, 1988. **10**(4): p. 770-5.

27. Bryan, L.E. and Van den Elzen, H.M., *Streptomycin accumulation in susceptible and resistant strains of Escherichia coli and Pseudomonas aeruginosa.* Antimicrob Agents Chemother, 1976. **9**(6): p. 928-38.

28. Capobianco, J.O. and Goldman, R.C., *Erythromycin and azithromycin transport into Haemophilus influenzae ATCC 19418 under conditions of depressed proton motive force (delta mu H).* Antimicrob Agents Chemother, 1990. **34**(9): p. 1787-91.

29. Tsujimoto, H., Gotoh, N., and Nishino, T., *Diffusion of macrolide antibiotics through the outer membrane of Moraxella catarrhalis.* Journal of Infection and Chemotherapy, 1999. **5**(4): p. 196-200.

30. Prochnow, H., Fetz, V., Hotop, S.K., Garcia-Rivera, M.A., Heumann, A., and Bronstrup, M., *Subcellular Quantification of Uptake in Gram-Negative Bacteria.* Anal Chem, 2019. **91**(3): p. 1863-1872.

31. Stone, M.R.L., Butler, M.S., Phetsang, W., Cooper, M.A., and Blaskovich, M.A.T., *Fluorescent Antibiotics: New Research Tools to Fight Antibiotic Resistance.* Trends Biotechnol, 2018. **36**(5): p. 523-536.

32. Stone, M.R.L., Masi, M., Phetsang, W., Pages, J.M., Cooper, M.A., and Blaskovich, M.A.T., *Fluoroquinolone-derived fluorescent probes for studies of bacterial penetration and efflux.* Medchemcomm, 2019. **10**(6): p. 901-906.

33. Stone, M.R.L., Phetsang, W., Cooper, M.A., and Blaskovich, M.A.T., *Visualization of Bacterial Resistance using Fluorescent Antibiotic Probes.* J Vis Exp, 2020(157).

34. Nonejuie, P., Burkart, M., Pogliano, K., and Pogliano, J., *Bacterial cytological profiling rapidly identifies the cellular pathways targeted by antibacterial molecules.* Proc Natl Acad Sci U S A, 2013. **110**(40): p. 16169-74.

35. Lamsa, A., Liu, W.T., Dorrestein, P.C., and Pogliano, K., *The Bacillus subtilis cannibalism toxin SDP collapses the proton motive force and induces autolysis.* Mol Microbiol, 2012. **84**(3): p. 486-500.

36. Quach, D.T., Sakoulas, G., Nizet, V., Pogliano, J., and Pogliano, K., *Bacterial Cytological Profiling (BCP) as a Rapid and Accurate Antimicrobial Susceptibility Testing Method for Staphylococcus aureus.* EBioMedicine, 2016. **4**: p. 95-103.

37. Htoo, H.H., Brumage, L., Chaikeeratisak, V., Tsunemoto, H., Sugie, J., Tribuddharat, C., Pogliano, J., and Nonejuie, P., *Bacterial Cytological Profiling as a Tool To Study Mechanisms of Action of Antibiotics That Are Active against Acinetobacter baumannii.* Antimicrob Agents Chemother, 2019. **63**(4).

38. Buyck, J.M., Plesiat, P., Traore, H., Vanderbist, F., Tulkens, P.M., and Van Bambeke, F., *Increased susceptibility of Pseudomonas aeruginosa to macrolides and ketolides in eukaryotic cell culture media and biological fluids due to decreased expression of oprM and increased outer-membrane permeability.* Clin Infect Dis, 2012. **55**(4): p. 534-42.

39. Kumaraswamy, M., Lin, L., Olson, J., Sun, C.F., Nonejuie, P., Corriden, R., Dohrmann, S., Ali, S.R., Amaro, D., Rohde, M., Pogliano, J., Sakoulas, G., and Nizet, V., *Standard susceptibility testing overlooks potent azithromycin activity and cationic peptide synergy against MDR Stenotrophomonas maltophilia.* J Antimicrob Chemother, 2016. **71**(5): p. 1264-9.

40. Ersoy, S.C., Heithoff, D.M., Barnes, L.t., Tripp, G.K., House, J.K., Marth, J.D., Smith, J.W., and Mahan, M.J., *Correcting a Fundamental Flaw in the Paradigm for Antimicrobial Susceptibility Testing.* EBioMedicine, 2017. **20**: p. 173-181.

41. Dorschner, R.A., Lopez-Garcia, B., Peschel, A., Kraus, D., Morikawa, K., Nizet, V., and Gallo, R.L., *The mammalian ionic environment dictates microbial susceptibility to antimicrobial defense peptides.* FASEB J, 2006. **20**(1): p. 35-42.

42. Farha, M.A., French, S., Stokes, J.M., and Brown, E.D., *Bicarbonate Alters Bacterial Susceptibility to Antibiotics by Targeting the Proton Motive Force.* ACS Infectious Diseases, 2018. **4**(3): p. 382-390.

43. Vaara, M., *Outer membrane permeability barrier to azithromycin, clarithromycin, and roxithromycin in gram-negative enteric bacteria.* Antimicrobial agents and chemotherapy, 1993. **37**(2): p. 354-356.

44. Schindelin, J., Arganda-Carreras, I., Frise, E., Kaynig, V., Longair, M., Pietzsch, T., Preibisch, S., Rueden, C., Saalfeld, S., Schmid, B., Tinevez, J.-Y., White, D.J., Hartenstein, V., Eliceiri, K., Tomancak, P., and Cardona, A., *Fiji: an open-source platform for biological-image analysis.* Nature Methods, 2012. **9**(7): p. 676-682.

45. Vaara, M. and Vaara, T., *Polycations as outer membrane-disorganizing agents.* Antimicrobial agents and chemotherapy, 1983. **24**(1): p. 114-122.

46. Ersoy, S.C., Abdelhady, W., Li, L., Chambers, H.F., Xiong, Y.Q., and Bayer, A.S., *Bicarbonate Resensitization of Methicillin-Resistant Staphylococcus aureus to β-Lactam Antibiotics.* Antimicrobial agents and chemotherapy, 2019. **63**(7): p. e00496-19.

47. Vázquez-Laslop, N. and Mankin, A.S., *How Macrolide Antibiotics Work.* Trends in biochemical sciences, 2018. **43**(9): p. 668-684.

48. Müller, O., *An open comparative study of azithromycin and roxithromycin in the treatment of acute upper respiratory tract infections.* Journal of Antimicrobial Chemotherapy, 1996. **37**(suppl_C): p. 83-92.

49. Schönwald, S., Baršlc, B., Klinar, I., and Gunjac˘a, M., *Three-day Azithromycin Compared with Ten-day Roxithromycin Treatment of Atypical Pneumonia.* Scandinavian Journal of Infectious Diseases, 1994. **26**(6): p. 706-710.

50. Kobayashi, N., Nishino, K., and Yamaguchi, A., *Novel macrolide-specific ABC-type efflux transporter in Escherichia coli.* Journal of bacteriology, 2001. **183**(19): p. 5639-5644.

51. Phetsang, W., Pelingon, R., Butler, M.S., Kc, S., Pitt, M.E., Kaeslin, G., Cooper, M.A., and Blaskovich, M.A., *Fluorescent Trimethoprim Conjugate Probes To Assess Drug Accumulation in Wild Type and Mutant Escherichia coli.* ACS Infect Dis, 2016. **2**(10): p. 688-701.

CHAPTER 3:

Using bacterial cytological profiling to uncover interplay between *Pseudomonas aeruginosa* jumbo phages and antibiotic treatment

3.1 Abstract

Due to the rise of resistance to almost all available antibiotics, phage therapy has been touted as a promising alternative to antibiotic treatment of infection by the ESKAPEE pathogens. In this chapter, we investigated the interplay between antibiotic treatment against *Pseudomonas aeruginosa* and the ability of jumbo phage φKZ to establish an infection, replicate DNA, and position the phage nucleus at midcell- three key events of this phage's life cycle. With the fluorescence microscopy technique Bacterial Cytological Profiling, we observed mechanism of action specific differences between antibiotics and φKZ replication. Antibiotics that block translation dramatically inhibit phage DNA replication, while cell wall active antibiotics (mecillinam) either had no effect on the establishment of infection or appeared to slightly but significantly increase phage infection rates (ceftazidime). Treatment with antibiotics that increase host cell length (ceftazidime, piperacillin) prevented the PhuZ spindle from properly centering the phage nucleus at midcell. We developed a computational model that explains how the dynamic properties of the PhuZ spindle lead to phage nucleus centering and why some antibiotics affect nucleus positions while others do not. These findings provide a cornerstone in understanding the molecular mechanisms underlying the synergy between antibiotics and phage therapy that can influence a clinician's choice of antibiotic treatment in cases where phage therapy may become required.

3.2 Introduction

Pseudomonas aeruginosa has the largest genome of the ESKAPEE group of pathogens and its genetic complexity is thought to contribute to its phenotypic plasticity in diverse environments, which allows it to thrive in soil as well as in humans [1, 2]. According to the Centers for Disease Control and Prevention, *P. aeruginosa* is the causative agent of approximately 33,000 healthcare-

associated infections in the United States alone [3]. In addition to its' intrinsic resistance mechanisms, *P. aeruginosa* can form biofilms, especially in the lungs of patients with cystic fibrosis or on surgical implants, which can complicate successful antibiotic treatment. These factors make potential phage therapy for *P. aeruginosa* infections in lieu of antimicrobials particularly appealing.

The beginnings of phage therapy can be tracked to Felix D'Herelle in the early 1920s using phage to clear chickens of the pathogen *Salmonella gallinarum* and then humans of infections caused by *Shigella dysenteriae* [4]. Not much was known about bacteriophage biology at the time, and despite widespread usage by the former Soviet Union during World War II, phage therapy was quickly forgotten due to the world's excitement for the newly discovered antibiotics [4, 5]. Modern phage therapy is still in its nascent stages, despite the large push towards using bacteriophages as alternatives to the dwindling supply of antibiotics. In the last few years, there has been more reported successful uses of phage therapy against multi-drug resistant infections caused *Acinetobacter baumannii* and *Mycobacterium abscessus* [6-8].

Because phage therapy is more often considered a treatment of last resort, patients are most likely already receiving one or more antibiotics despite their lack of efficacy in clearing the infection. This highlights the necessity for understanding how antibiotics and phages interact with each other. The term phage-antibiotic synergy (PAS) was first used by Comeau et al. in 2007 where they observed increased phage plaque sizes during co-treatment and infection of *Escherichia coli* with β-lactam antibiotics and lytic phage ΦMFP [9]. Since then, PAS has been demonstrated in a variety of species, including *P. aeruginosa* and other members of the ESKAPE pathogens [10-16]. Synergistic interactions are not observed for each combination of antibiotic treatment and phage, however, and the underlying mechanisms behind PAS are still unclear.

In the age of rampant multi-drug resistance, choosing what antibiotic to use to treat any infection, especially one caused by *P. aeruginosa*, requires several considerations. This includes, but is not limited to, location of infection, the likelihood of acquired resistance to an antimicrobial agent, and monotherapy versus combination therapy of two or more drugs. For example, β-lactam-containing antibiotics, like piperacillin and ceftazidime, are commonly used to treat *P. aeruginosa* infections, often in combination with either β-lactamase inhibitors or aminoglycosides such as gentamicin [17]. The fluoroquinolone ciprofloxacin, which inhibits DNA replication, is another drug of choice to treat infections causes by *Pseudomonas* species [18], although use of DNA damaging compounds, including ciprofloxacin, has been associated with increased rates of resistant mutations [19]. Analogous considerations are required when selecting candidate viruses for phage therapy, such as confirming their host range, lack of toxin-producing genes, obligate lytic lifecycle, and determining the number of phage to use during treatment [20].

Jumbo phages are classified as tailed phages containing genomes larger than 200 kbp [21], which dwarves the well-studied *Escherichia coli* Lambda phage which has a genome of around 50 kbp [22]. Several jumbo phages that infect *P. aeruginosa* have been isolated, including the bacteriophage φKZ whose genome was first described by Mesyanzhinov et al. in 2002 [23]. Our lab has studied φKZ and related phages and discovered a novel replication strategy that involves the formation of a proteinaceous shell around replication phage DNA, "phage nucleus", that is centered in the *P. aeruginosa* host cell by the phage-encoded tubulin PhuZ. Immediately after DNA injection, PhuZ assembles polymers at each end of the cell to establish a bipolar spindle. Filaments of the spindle use the force generated by polymerization to push the phage nucleus towards midcell. Later during the infection cycle, PhuZ filaments deliver capsids to the phage nucleus, where they dock to initiate DNA packaging. The PhuZ spindle is rotated within the cell,

which allows capsids to be evenly distributed over its surface. [24-27]. After DNA packaging, capsids assemble with tails and the cell lyses to release progeny phage.

Jumbo phages can be utilized for phage therapy, as shown for phage OMKO1 against a *P. aeruginosa* infection in an aortic graft [28]. It is interesting to note that OMKO1 utilizes the outer membrane protein M, a subunit of the MexAB and MexXY efflux pump systems, as its receptor for infection. As the bacteria evolves resistance to OMKO1, it experiences an evolutionary trade-off and becomes more susceptible to antibiotics [29].

In this study, we used bacterial cytological profiling to look at interactions between the jumbo phage ΦKZ and commonly used antibiotics for treatment of *P. aeruginosa* infections. . We study phage-antibiotic interactions using Bacterial Cytological Profiling (BCP), a fluorescence microscopy tool that classifies the mechanism of action (MOA) of an antibiotic based on cytological changes of the bacterial cell, such as cell wall or DNA morphology, during treatment [30-35]. The benefit of BCP over previous methods to study PAS is the ability to observe phenotypic changes in both phage infection and cytological shifts due to antibiotics at the single cell level.

3.3 Materials and Methods

Bacterial strains, growth, bacteriophage preparation, and antibiotics

Pseudomonas aeruginosa strains PAO1 and K2733 (PAO1ΔmexB, ΔmexX, ΔmexCD-oprJ, ΔmexEF-oprN) was used in this study. The bacteria were grown in LB, with gentamicin for selection when necessary, at 37^{o}C for all experiments. Preparations of antibiotics were performed according to the manufacturer's recommendations. Jumbo phage φKZ lysate was prepared by adding 5 mL phage lysate and 100 mL fresh LB to 50 mL saturated ON culture of *P. aeruginosa* PAO1 and incubating at 37^{o}C for at least 5 hours, or until visible clearance of culture. Cultures

were centrifuged at 4000 rpm for 15 min and the supernatant filtered to remove bacterial cell debris. Titers were performed and the phage lysate was stored at 4°C until use.

Minimal inhibitory concentration (MICs) Assays

MICs for all antibiotics, shown in **Table 3.1**, were determined using the broth microdilution method (16). In brief, overnight cultures of *P. aeruginosa* K2733 were diluted 1:100 in fresh LB and allowed to grow at 37°C with rolling until they reached an optical density at 600 (OD_{600}) of ~0.2, or early exponential phase. The bacterial culture was diluted to OD_{600} ~ 0.05, and then diluted 1:100 into the appropriate wells of a 96-well plate containing serially diluted antibiotics. MICs were determined by OD_{600} readings after incubation at 37°C with shaking for 18-4 hours.

Fluorescence microscopy

Overnight cultures of *P. aeruginosa* K2733 were diluted 1:100 into fresh LB, with appropriate arabinose concentrations when required, and allowed to grow at 37°C with rolling until they reached an OD_{600} ~0.12 – 0.15. 400 uL culture was then added to cultures tubes containing 1X, 2X, or 5X MIC of each antibiotic and incubated at 37°C with rolling for one hour, for antibiotic only controls, or 30 minutes, for subsequent phage infection. Lysate of the jumbo phage was then added to cultures, at a multiplicity of infection (MOI) of 5, before incubation at 37°C with rolling for an additional 30 minutes. Uninfected and untreated controls were done each experimental day. After infection, 4 uL culture was added to 4 uL dye mix containing 100 ug/mL FM4-64 and spotted onto pad slides containing 1.2% agarose in 20% LB with 0.2 ug/mL DAPI for microscopy. Microscopy was performed as previously described [30], with slight modifications. Excitation and emission settings were kept consistent for all replicate experiments.

Quantitation and statistical analysis of phage infection

φKZ infection, defined as a distinct phage nucleus or the presence of a distinct phage DNA puncta upon injection within the host cell, was quantified manually using FIJI (ImageJ 1.51w). All microscopy experiments were performed in biological triplicate. Statistical analysis was conducted in GraphPad Prism 8.4.3. One-way ANOVA followed by Dunnett's multiple comparisons test was used to determine significance differences between the untreated infected control and the treatment conditions. Statistical significance was defined as a p value of < 0.05. In quantitation graphs, p values indicated as follows: * ≤ 0.050, – 0.0100, ** ≤ 0.0100 – 0.0010, *** ≤ .0010 – 0.0001, **** < 0.0001.

Stochastic modeling of PhuZ filaments

A 1D model of PhuZ filament movement was created by considering the net movement of a filament's position to be a balance between polymerization, depolymerization and catastrophe. A simple equation to describe this movement in the positive direction is given as:

$$\frac{dx}{dt} = v_{polymerization} - v_{depolymerization} - v_{catastrophe}$$

The speed of polymerization, depolymerization and catastrophic depolymerization can both be sampled from a Gaussian distribution determined by the mean and standard deviation of parameters based on previous measurements and publications [25] as well as parameter optimizations to measured data.

The model consists of two filaments with initial positions at x = 0, L_c, where L_c is the cell length and was run with a timestep of 0.01 seconds. All parameters related to movement of filaments get sampled from a Gaussian distribution and positions are updated if the random time sampling associated with their movement has passed. Catastrophe occurs after a given time, which is again sampled from a Gaussian distribution, after which time the speed of catastrophic

depolymerization becomes non-zero. Simultaneous to the occurance of catastrophe, a recovery time is generated which determines when catastrophic depolymerization again becomes zero. The position of the nucleus is initially set at 90% of the cell length and moves either by random diffusion for a sphere with a Stokes radius of 1 μm or by collisions with growing filaments. If a filament would move beyond the boundary of the phage nucleus in a given timestep, the nucleus position is pushed by an equal amount to prevent clipping. However, if the filament from the opposite pole is pushed to the boundary of the phage nucleus when this would occur, no movement from either nucleus or filaments takes place. In this condition, movement can only occur after catastrophe induces rapid depolymerization of a filament away from the nucleus.

Certain parameter means and standard deviations such as polymerization rate were obtained from previous measurements and publications [25]. Other parameters were estimated through an optimization scheme that minimized the root mean squared distance (RMSD) between the measured probability distribution of phage nuclei positioning in untreated, infected cells and the modeled. Initially, parameters were randomly mutated and RMSD was calculated. Using these initial points, the partial derivatives of RMSD with respect to each parameter are estimated and the next randomizations of each parameter are calculated until RMSD is minimized.

Surface plots were generated by linear interpolation between 200 points for any two parameters in order to visualize the RMSD parameter space (**Supplemental Figure 3.1**). The surface plot of polymerization rate vs depolymerization rate illustrates several interesting points about the model. Because RMSD is a measure of nuclei positions at the endpoints, it does not include any kinetic data from the model. This can be seen in the line of low RMSD (blue) which implies that any combination of polymerization rate and depolymerization rate that matches a

certain net growth would produce similar results. This problem is avoided by having measured data for several parameters which helps constrain the parameter space.

3.4 Results

Treatment of *P. aeruginosa* with various antibiotics leads to MOA-dependent morphological changes

BCP can be used identify MOA at the biosynthetic pathway level [30]. In preparation for using BCP to observe antibiotic-phage combinations in *P. aeruginosa,* we first collected a set of control profiles for antibiotics commonly used to treat *P. aeruginosa* infections. *P. aeruginosa* K2733 was grown in 1X, 2X, or 5X MIC of the antibiotics of interested for one hour prior to visualization using fluorescence microscopy. We found that treatment of *P. aeruginosa* with antibiotics targeting different pathways led to distinct cytological changes as expected. For example, treatment with 5X the MIC of the DNA synthesis inhibitors ciprofloxacin (CIP), daunorubicin (DAUN), or mitomycin C (MITO C), we observe aberrant DNA morphology compared to untreated controls, including improper chromosome segregation during cell division (**Figure 3.1A**). Treatment with the RNA synthesis inhibitor rifampicin (RIF) in *E. coli* leads to diffuse DNA within the cell [30], however *P. aeruginosa* typically has diffuse DNA in the absence of antibiotic treatment so this distinguishable cytological feature is unclear (**Figure 3.1A**).

Treatment with the protein synthesis inhibitors chloramphenicol (CAM), gentamicin (GENT), or tetracycline (TET) lead to increased cell death and condensation of the DNA compared to untreated controls (**Figure 3.1B**). Inhibition of cell wall synthesis by ceftazidime (CEFT) or piperacillin (PIP) lead to elongation of the cell, whereas treatment with meropenem (MERO) increased cell length and caused bulge formation at mid-cell (**Figure 3.1C**). Treatment with mecillinam (MEC) causes a rod-to-football morphology change at any concentration (**Figure**

3.1C). This work confirms that *P. aeruginosa* also undergoes specific and differential cytological changes dependent on an antibiotic's MOA.

Treatment with DNA or RNA synthesis inhibitors leads to differential interactions with ϕKZ related to their specific MOA

To understand the effect of antibiotic treatment on φKZ replication, we began by testing the DNA synthesis inhibitors and the transcription inhibitor RIF. We treated K2733 with increasing concentrations of these antibiotics for 30 minutes, and the infected with φKZ at a MOI of ~ 5 for an additional 30 minutes before imaging. Treatment with CIP, which targets DNA-topoisomerases thus preventing proper chromosome maintenance [36] or the antineoplastic antibiotic MITO C, which alkylates and cross-links complementary strands of DNA [37], had no significant effect on phage infection (**Figure 3.2A**). For both antibiotics, the percentage of infected cells were approximately comparable to the untreated controls (**Figure 3.2A)**. The RNA synthesis inhibitor RIF also had no significant effect on phage replication. Note that the slight decrease of phage infection at 5X MIC was not statistically significant (**Figure 3.2A**). The absence of a strong effect with RIF is expected, since replication of φKZ encodes its own rifampicin resistant RNA polymerases and its replication has been shown to be independent of host RNA polymerase [23, 38]. In comparison, treatment with the antineoplastic antibiotic DAUN, which is capable of intercalating into DNA, significantly lowers φKZ infection at all concentrations (**Figure 3.2A**). The strong effect of DAUN is consistent with work by Kronheim et al. showing that DNA intercalation agents are potent anti-phage compounds [39].

Treatment with protein synthesis-targeting antibiotics causes a dose-dependent decrease in φKZ infection

We next examined the effect of protein synthesis inhibitors on phage replication using the same experimental scheme of antibiotic treatment for 30 minutes followed by phage infection for an additional 30 minutes. The protein synthesis inhibitor CAM binds to the 50S subunit of the bacterial ribosome and blocks the elongation of the growing peptide chain while TET blocks tRNA binding to the ribosome. Both CAM and TET treatment led to a dose-dependent decrease in φKZ infection compared to untreated controls (**Figure 3.3A**). Additionally, the phage nucleus during treatment with 2X MIC CAM or 2X MIC TET was noticeably smaller than untreated infected controls. Treatment with the aminoglycoside GENT and TET also prevented phage infection in a dose-dependent manner, with no effect at 1X MIC, a two-fold reduction at 2X MIC, and strong inhibition at 5X MIC (**Figure 3.3A**). One observation in GENT treated cells at 2X MIC is that the phage nucleus had mispositioned nuclei compared to untreated infected controls (**Figure 3.3B**). Thus, all protein synthesis inhibitors appear to strongly inhibit phage replication, likely by preventing the expression of early proteins need for DNA replication and phage nucleus formation.

To determine if we could partially rescue phage replication, we expressed two early phage proteins (gp54 – which makes up the nuclear shell, **Figure 3.9B**, and the PhuZ tubulin, **Figure 3.9C** [26, 27]) via arabinose induction prior to CAM 5X treatment. However, we found that expressing these two proteins before infection did not rescue of infection (**Figure 3.9B, C**, white arrows). Additionally, we tested if the CAM-mediated stall of φKZ infection was reversible. Cells were preteated with CAM 5X for 30 minutes, and then infected with phage. After one additional hour, all phage infections were arrested at the earliest step of DNA injection. We then removed

CAM by washing out the antibiotic using fresh LB (**Figure 3.9D**) and found that phage replication resumed normally.

Treatment with cell wall synthesis inhibitors lead to increase in φKZ infection

It has been previously shown that the β-lactam antibiotics CEFT and PIP have synergistic effects with KPP22 phage infection against *P. aeruginosa* [15]. We also observed synergy with the jumbo phage φKZ in the presence of the cell wall synthesis inhibitors CEFT, MERO, and PIP (**Figure 3.3A**). For all concentrations with the cell wall synthesis inhibitors CEFT, PIP, or MERO, the percentage of infected cells were 1.5 – 2X higher than the untreated controls (**Figure 3.4A**). All three antibiotics prevent cell division by inhibiting the penicillin-binding proteins that catalyze peptidoglycan cross-linking [18], which phenotypically presents as elongated cells (**Figure 3.4B**). In comparison, MEC specifically binds to PBP2 [40] causing transition of *P. aeruginosa* from rods to oval-shaped cells (**Figure 3.1C, 3.4B**) and had comparable levels of φKZ infection at all concentrations relative to untreated infected control (**Figure 3.4A**).

Injection of φKZ DNA during early infection of *P. aeruginosa* occurs primarily at the poles of the host cell

Since treatment with CEFT, PIP, or MERO lead to both elongated cells and increased infection rates (**Figure 3.1C**, **3.3B**), we hypothesized that increased infection is correlated with increased host cell length due to the increased likelihood of cell-phage interactions in the culture. In order to test this, we visualized CEFT, MEC, or CIP treated cells after incubation with φKZ for only 5 minutes, in order to more accurately quantitate the initial rate of infection. For all concentrations of MEC or CIP, the percentage of early infected cells were slightly lower than or comparable to the untreated controls (**Figure 3.5B**). In comparison, treatment with CEFT at 2X

and 5X MIC showed increased percentage of early infected cells, about 1.5X that of the untreated controls (**Figure 3.5B**).

This data suggests that increased cell length is correlated with increased phage infection. We imagine two models by which CEFT treatment could lead to increased infections. In the first model, increased cell length alone may contribute to increased phage binding by providing additional surface area for initial contact. However, it is important to note that the phage DNA is injected preferentially at the poles of *P. aeruginosa* host cell (**Figure 3.5C, D**). Therefore, for this model to make sense, we would need to postulate that phage make initial weak contact with *Pseudomonas* along the sides of the cells, and then diffuse along it until they reach a high affinity receptor located at the cell pole that allows for the injection of DNA. This model is similar to one previously proposed for phage lambda, where it is thought to initially form weak interaction with the cell surface, diffusing along the surface of the cell until engaging its receptor LamB and injecting DNA [41, 42].

Alternatively, it's possible that the CEFT and other cell wall antibiotics that promote infection alter the cell surface by interfering with peptidoglycan synthesis in a way that leads to increased exposure of phage receptors, which would promote increased phage binding. One experiment that may be performed in the future to potentially distinguish between these two possibilities will be to create cells that are elongated without using an antibiotic to inhibit cell wall synthesis and then measure phage infection rates. For example, we can create elongated *P. aeurginsoa* cells by expressing SulA, an inhibitor of FtsZ formation, from a plasmid. If elongated cells formed by directly inhibiting FtsZ also show increased infection rates, that suggests cell length alone is likely sufficient for increased infectivity.

Phage-encoded tubulin PhuZ exhibits altered dynamics during co-treatment with ceftazidime and φKZ infection

A key function of the PhuZ spindle encoded by φKZ and related jumbo phages is to position the phage nucleus at the center of the cell [25-27, 43]. Without antibiotic treatment, the phage nucleus was positioned closely to the center of the host cell (**Figure 3.6A**). However, during treatment with the cell wall synthesis inhibitors such as CEFT or PIP, the position of the phage nucleus becomes increasingly off-centered compared to untreated controls as the length of the cell increased (**Figure 3.4C**). In cases where the host cell was elongated due to antibiotic treatment, there were greater instances of mispositioning of the phage nucleus away from mid-cell (**Figure 3.6B, C**).

To determine if treatment with these antibiotics prevented spindle assembly, we treated *P. aeruginosa* expressing a low level GFP-fused PhuZ protein [26] with increasing concentrations of CEFT, MEC, or CIP prior to infection with φKZ (**Figure 3.7**). In the untreated infected condition, the PhuZ spindle forms at both poles of the cells, attaching to the phage nucleus to position the nucleus at approximately mid cell (**Figure 3.7A**). During treatment with CEFT and CIP, filaments formed in the elongated cells, with one PhuZ filament extending from the far pole of the cell and the other maintaining similar length to the untreated condition (**Figure 3.7B, C**). In comparison, for all concentrations of MEC, no mispositioning of the nucleus or asymmetrical PhuZ filaments occur (**Figure 3.7C**). In both the properly positioned and mispositioned nuclei, PhuZ filaments appeared to be assemble. Therefore, nucleus mispositioning was not due to the inability of the spindle to form.

Stochastic modeling of PhuZ filaments

Why, then, is the nucleus mispositioned? To address this question we developed a computational to understand how PhuZ filaments are able to center the nucleus in a wild type cell and how perturbing cell length might influence centering. Previous work in our lab demonstrated that DNA objects can be centered in anisotropic cells when the rates of filament polymerization and depolymerization matched to a specific range of cell lengths [24, 43]. Therefore a 1D stochastic model of PhuZ filaments was created to see if cell length changes could explain the various changes to phage nucleus positioning observed across different antibiotic treatments. Visualizations of filament and nucleus positions can be seen (**Figure 3.8A, B**) as modeled over 30 minutes. Sampling cell length from a Gaussian distribution given by the mean and standard deviations of various treatment conditions shows a good fit to measured nuclei position distributions indicating that cell length could be the determining factor in nucleus mispositioning (**Figure 3.8C**). To illustrate this further, a comparison of measured nuclei positions against cell length (**Figure 3.8D**) with modeled distributions in which cell lengths were maintained constant (**Figure 3.8E**) was performed. The degree of agreement between measured and modeled data indicates the major role that cell length plays in phage nucleus positioning. These results suggest that the phage co-evolved with the host cell to optimize the rates of PhuZ polymerization and depolymerization in such a way as to properly center the phage nucleus. During treatments that lead to aberrant cell length, the spindle properties do not adapt, leading to mispositioning of the phage nucleus.

3.5 Discussion

Using BCP we can visualize interactions between phages and antibiotics during infection which allows us to generate potential mechanistic explanations for the observed differences in the

infection rates. In this chapter, we highlighted the observation that cell wall active antibiotics that lead to longer cells, such as CEFT, MERO, and PIP, had higher percentages of infected cells compared to treatment with MEC and CIP, and to the untreated controls (**Figure 3.2, 3.4**). We found that the increase in cell length was correlated to increased phage infection due to higher levels of initial phage binding and injection of DNA, which seems to preferentially occur at the poles of the host cell (**Figure 3.5**).

Based on computational modeling, we determined that the elongation of *P. aeruginosa* cells is likely the main factor that contributes to the observed mislocalization of the phage nucleus away from mid-cell (**Figure 3.6, 3.7, 3.8**). The ability to find the cell midpoint is a critical feature that is essential among diverse biological systems. Many rod-shaped bacteria, for example, divide precisely in the middle of the cell, after the cell has reached twice its length. In *E.coli* and many other bacteria, the Min system is responsible for positioning the FtsZ ring at the cell center [44], although despite three decades of study, the mechanisms by which it does so is still not fully understood. Here we have described a phage encoded tubulin-based system that can position replicating phage DNA within a protein shell, in this case the phage nucleus. Our computation model correctly predicts DNA centering under normal conditions and when cell length is strongly affected by the antibiotics, suggesting that we understand the molecular basis for PhuZ spindle centering in bacteria.

It is important to note that the synergistic effects between phage infection and antibiotic treatment with cell wall targeting compounds in these experiments were observed for only a single round of infections. In other research studies, such as Uchiyama et al., the phage was allowed to infect over multiple generations and the presence of PAS was determined by increase in the size of the phage plaque compared to untreated controls [15]. It is difficult to use plaque size as a

quantification method for jumbo phage infection due to the reduced ability of these larger phage to diffuse through top agar. In this study, we observed that in cases where the length of the host cell is greatly increased, such as during treatment with CEFT and PIP (**Figure 3.4**), the size of the phage nucleus is also increased (**Figure 3.9**), which suggest the possibility of a greater number of progeny. We hypothesize that the size of the phage nucleus is usually constrained by the host cell width and that the destabilization of the cell wall caused by CEFT or PIP treatment allow for larger phage nuclei. Therefore, if we allowed φKZ to infect over multiple generations, we would expect to see enhanced synergy due to both the increased likelihood of phage attachment due to host cell length (**Figure 3.5**), and increased phage progeny due to larger phage nuclei (**Figure 3.9**).

Beyond the mechanisms underlying cell wall antibiotic synergy with φKZ, this study brought to light other interesting phenomena relating to PAS. For example, φKZ and its related phages form a proteinaceous shell around their DNA during replication [27] and compartmentalize their biosynthetic functions in which DNA and RNA synthesis occur within the phage nucleus whereas protein synthesis occurs in the host cytoplasm [26, 27]. The observed differences in phage infection during treatment with ciprofloxacin (CIP) compared to daunorubicin (DAUN) (**Figure 3.2A**) could be due to inability of CIP to pass through the shell, while the intercalation of the host DNA is upstream of phage infection essentially preventing any infection at all.

Treatment of *P. aeruginosa* with RIF showed very little effect on φKZ infection relative to the untreated infected controls, with a slight but statistically insignificant decrease in infection levels at 5X MIC (**Figure 3.2A**). Ceyessens et al. have previously shown that these jumbo phages do not require the use of host RNA polymerases and that the φKZ genome encodes two RNA polymerases that lend resistance against the antibacterial activity of RIF [38]. Another observation we made is that treatment with the protein synthesis inhibitor CAM at 5X MIC reversibly stalls

the process of infection after the phage DNA is injected into the cell (**Figure 3.10A**, white arrows). These experiments demonstrate that we CAM may be a useful tool to study early infection in future studies.

In conclusion, BCP provides an excellent platform in which to observe the interplay of antibiotic treatment and phage infection at the single-cell level. This work highlights how specific differences in MOA can have varying impacts on the progression of phage infection, such as the impact on nucleus centering by the phage spindle during treatment with cell wall antibiotics and the interruption of proper phage infection during treatment with protein synthesis inhibitors. Additionally, this study raises some interesting follow up questions related to understanding how jumbo phages infect their hosts and how antibiotics can be used to alter specific phenotypes associated with phage infection.

3.6 Acknowledgements

The authors would like to thank the current and former members of the Phage Team of the J.Pogliano Lab for their help and insights into the *Pseudomonas* jumbo phage φKZ, and especially Katrina Nguyen for her guidance in generating the φKZ lysates used throughout all experiments.

Chapter 3, in part, is being formulated into a manuscript in preparation for the publication of the material. Hannah Tsunemoto, Joseph Sugie, Joe Pogliano, 2020. The dissertation author was the primary investigator and author of this material.

This work was supported by the National Institutes of Health (NIH) National Institute of Allergy and Infectious Disease (NIAID) grant 1-U01-AI124316.

3.7 Figures

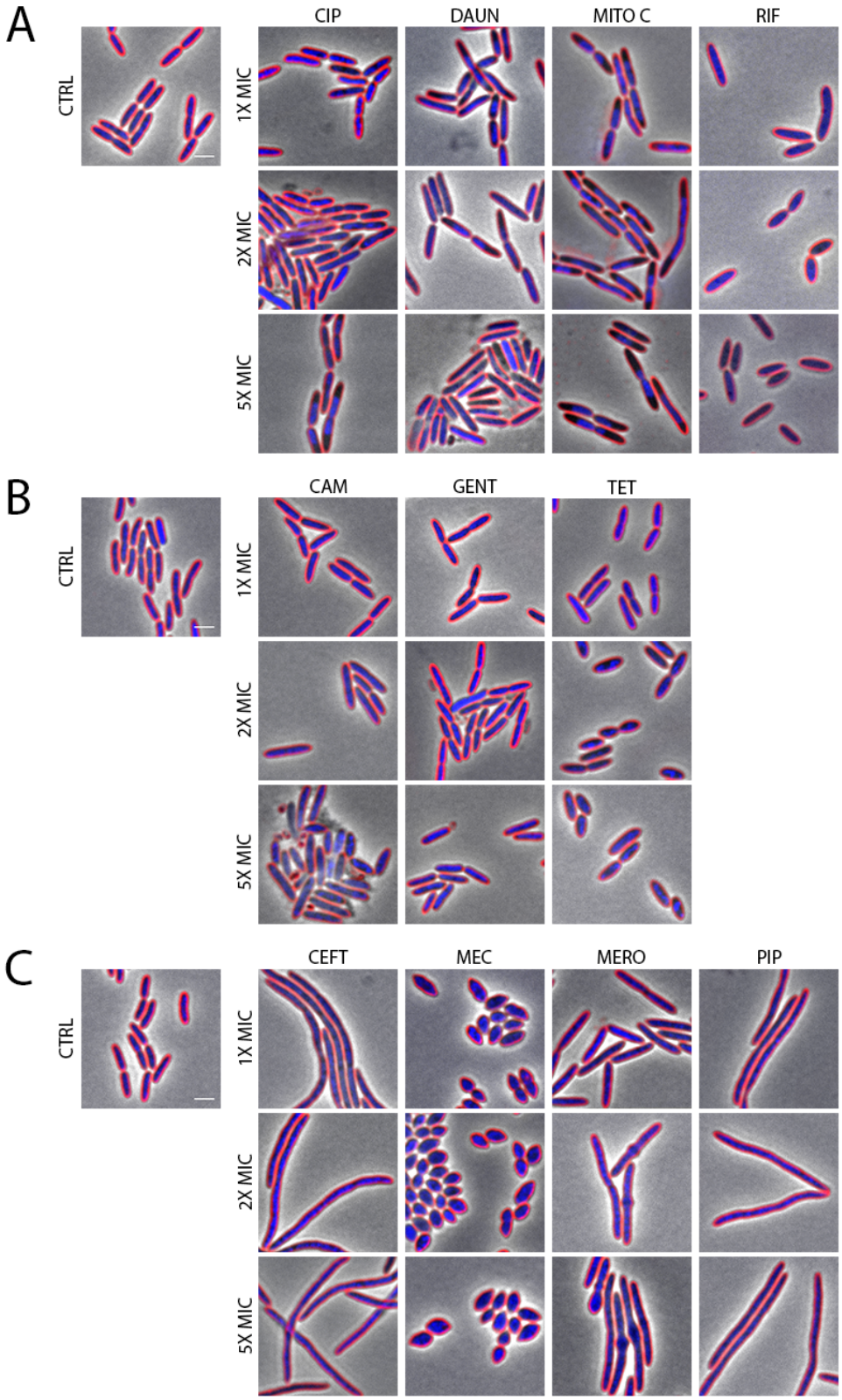
A
CIP
DAUN
MITO C
RIF
CTRL
1X MIC
2X MIC
5X MIC
B
CAM
GENT
TET
CTRL
1X MIC
2X MIC
5X MIC
C
CEFT
MEC
MERO
PIP
CTRL
1X MIC
2X MIC
5X MIC

Figure 3.1 Treatment of *P. aeruginosa* K2733 with various antibiotics leads to differential morphology based on MOA. Cell membrane strained with FM4-64 (red) and DNA stained with DAPI (blue). Scale bar represents 2 μm. Microscopy of treated infected samples DNA synthesis inhibitors, ciprofloxacin (CIP), daunorubicin (DAUN), and mitomycin C (MITO C). RNA synthesis inhibitor, rifampicin (RIF). (B) Microscopy of treated infected samples: Chloramphincol (CAM), gentamicin (GENT), and tetracycline (TET). (C) Microscopy of treated infected samples: Ceftazidime (CEFT), mecillinam (MEC), meropenem (MERO), and piperacillin (PIP).

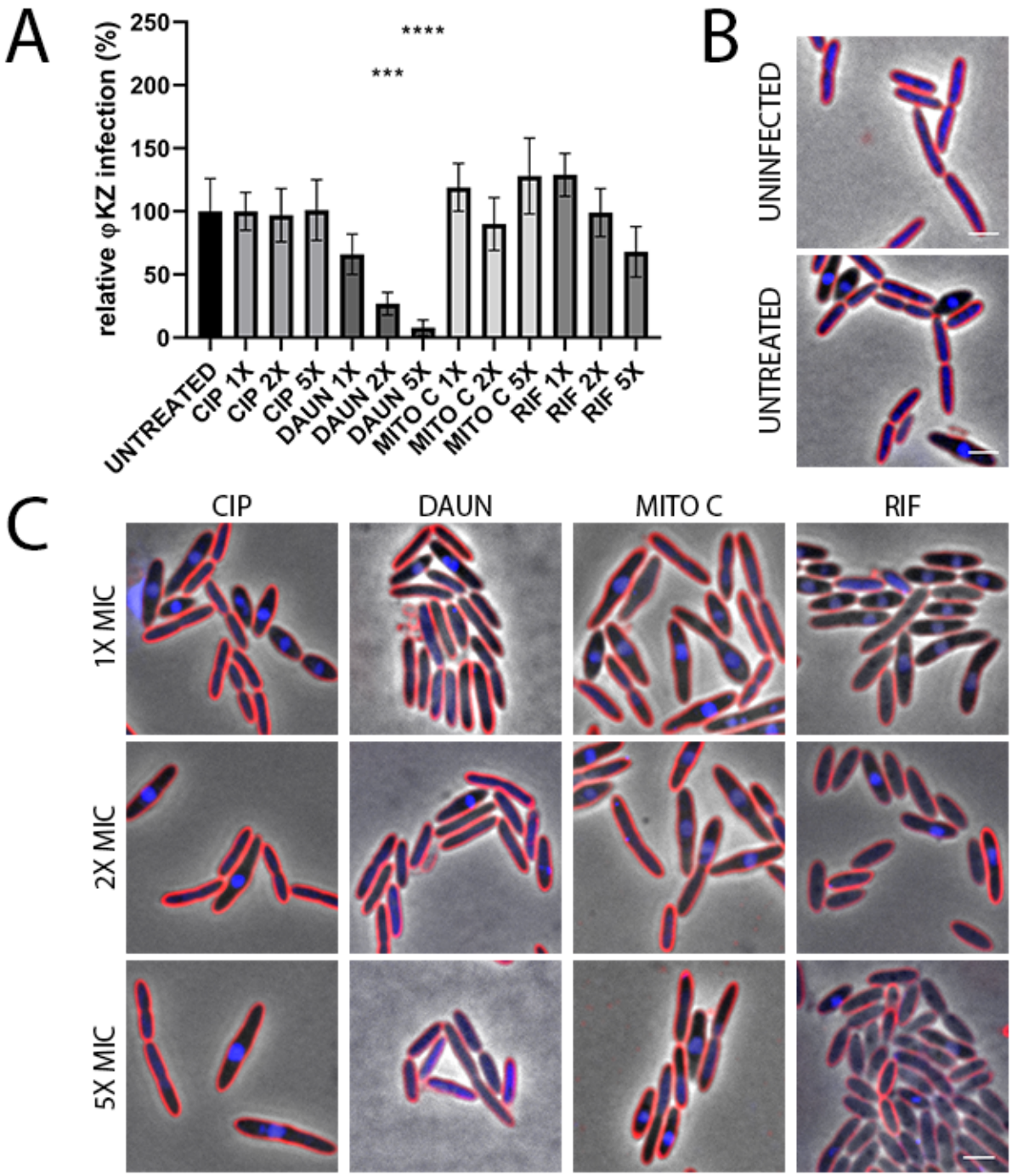

Figure 3.2 Treatment of *P. aeruginosa* K2733 with antibiotics that target either DNA or RNA synthesis followed by infection with φKZ. (A) Quantification of phage infection under treatment conditions, relative to the untreated infected control. Error bars represent standard deviation of biological replicates. (B) Microscopy of uninfected and untreated infected controls, and (C) treated infected samples: DNA synthesis inhibitors, ciprofloxacin (CIP), daunorubicin (DAUN), and mitomycin C (MITO C). RNA synthesis inhibitor, rifampicin (RIF). Cell membrane strained with FM4-64 (red) and DNA stained with DAPI (blue). Scale bar represents 2 μm.

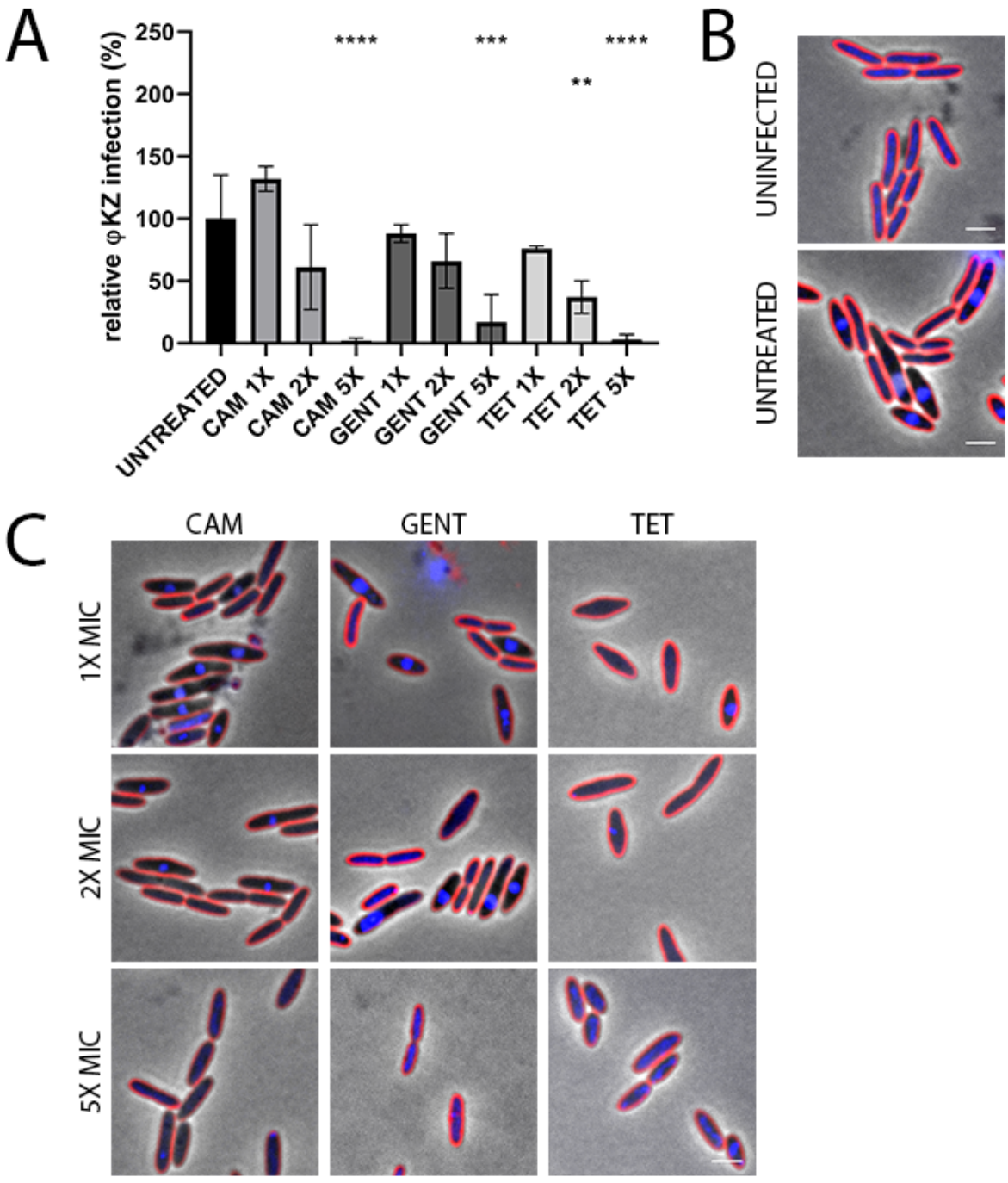

Figure 3.3 Treatment of *P. aeruginosa* K2733 with antibiotics that target protein synthesis followed by infection with φKZ. (A) Quantification of phage infection under treatment conditions, relative to the untreated infected control. Error bars represent standard deviation of biological replicates. (B) Microscopy of uninfected and untreated infected controls, and (C) treated infected samples: Chloramphincol (CAM), gentamicin (GENT), and tetracycline (TET). Cell membrane strained with FM4-64 (red) and DNA stained with DAPI (blue). Scale bar represents 2 μm.

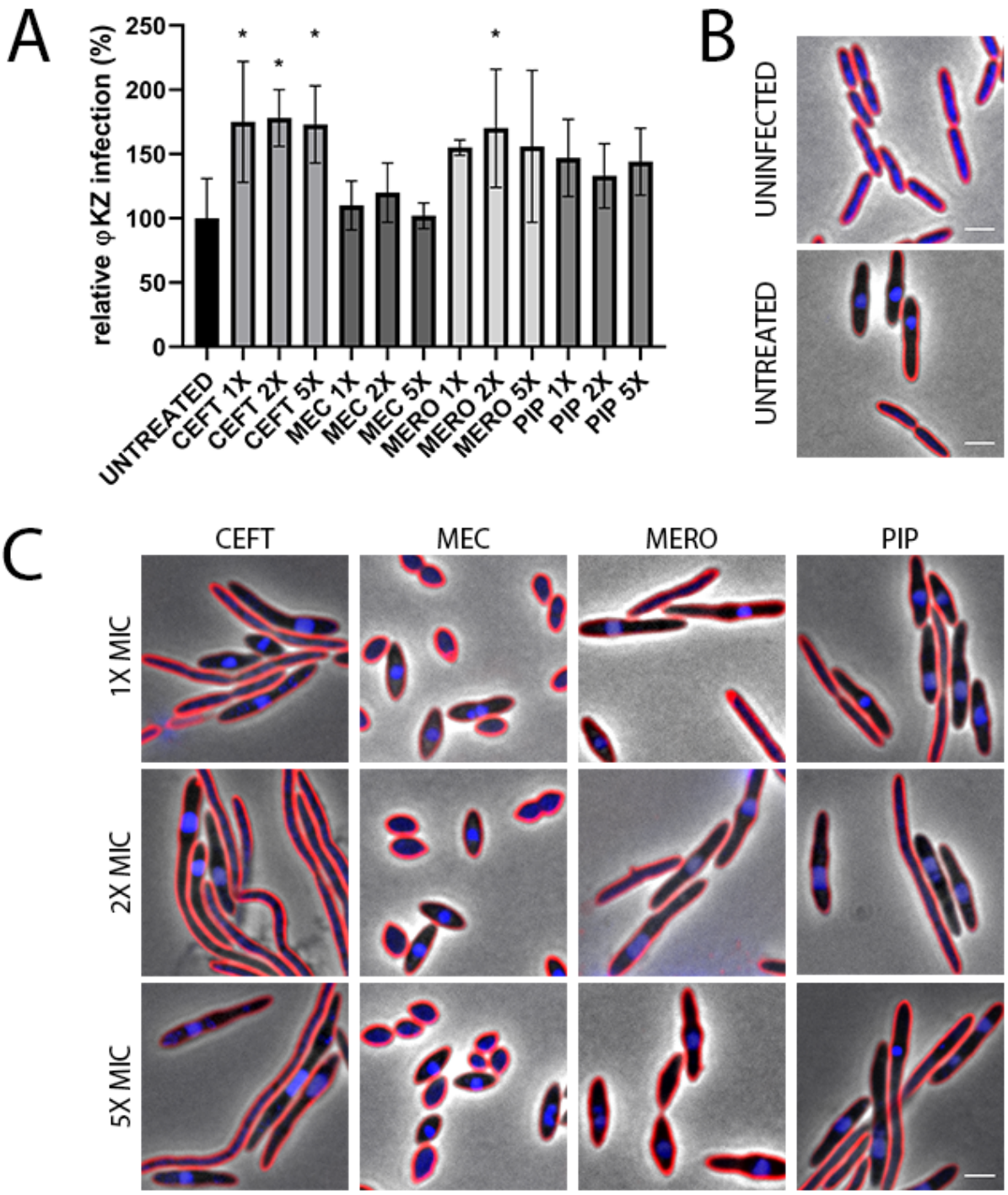

Figure 3.4 Treatment of *P. aeruginosa* K2733 with antibiotics that target cell wall synthesis followed by infection with φKZ. (A) Quantification of phage infection under treatment conditions, relative to the untreated infected control. Error bars represent standard deviation of biological replicates. (B) Microscopy of uninfected and untreated infected controls, and (C) treated infected samples: Ceftazidime (CEFT), mecillinam (MEC), meropenem (MERO), and piperacillin (PIP). Cell membrane strained with FM4-64 (red) and DNA stained with DAPI (blue). Scale bar represents 2 μm.

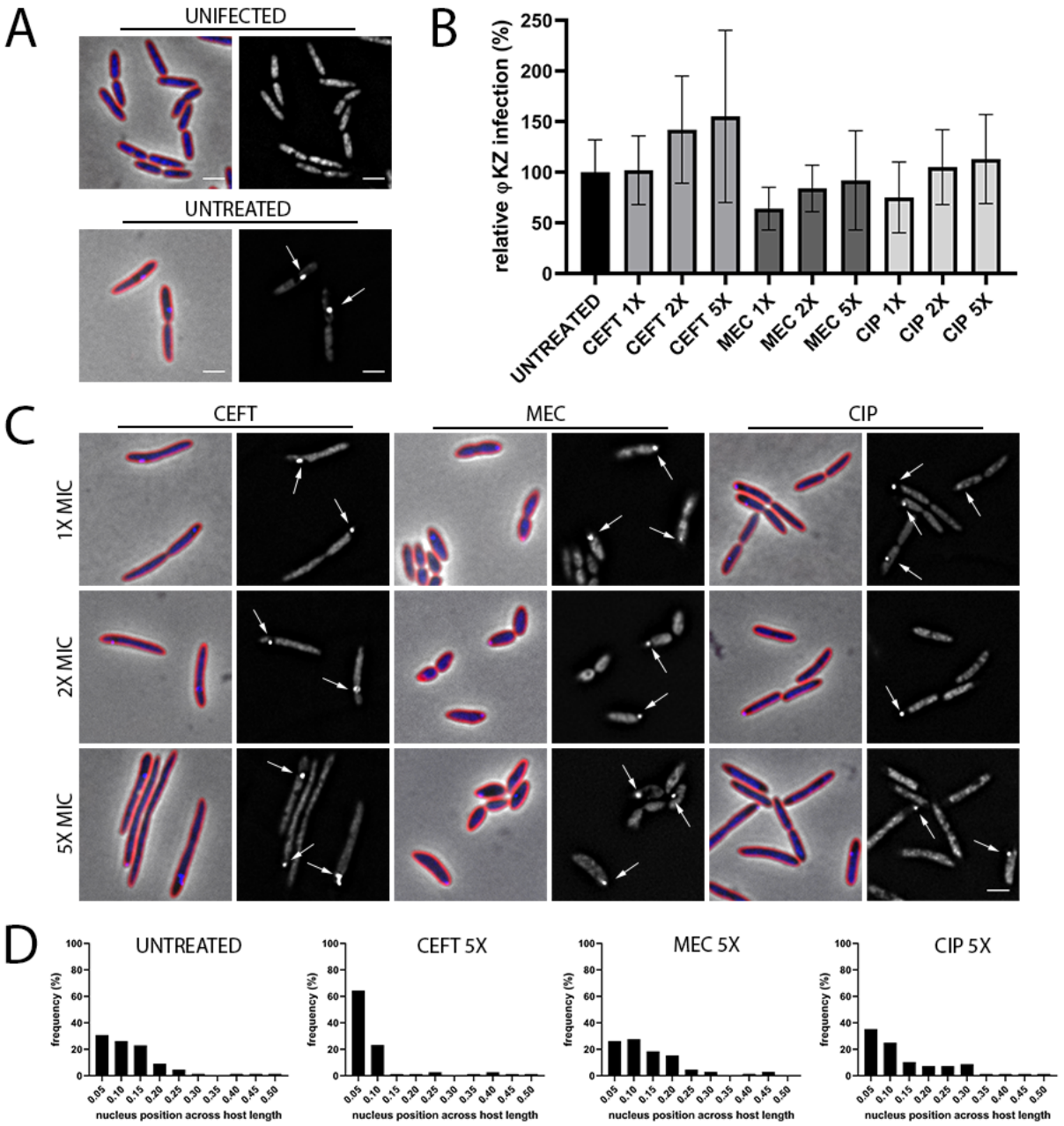

Figure 3.5 Treatment with CEFT increases early φKZ binding and infection. (A) Microscopy of uninfected and untreated infected controls, and (C) treated infected samples after 5 min infection. Cell membrane strained with FM4-64 (red) and DNA stained with DAPI (blue). Scale bar represents 2 μm. White arrows indicate phage DNA at early stages of infection, e.g. right after injection. (B) Quantification of early phage infection post-antibiotic treatment, relative to the untreated infected control. Error bars represent standard deviation of biological triplicates. (D) Histograms of early phage nucleus position across normalized *P. aeruginosa* host cell length. Untreated: n = 65, CEFT 5X: n = 73, MEC 5X: n = 65, CIP 5X: n = 68.

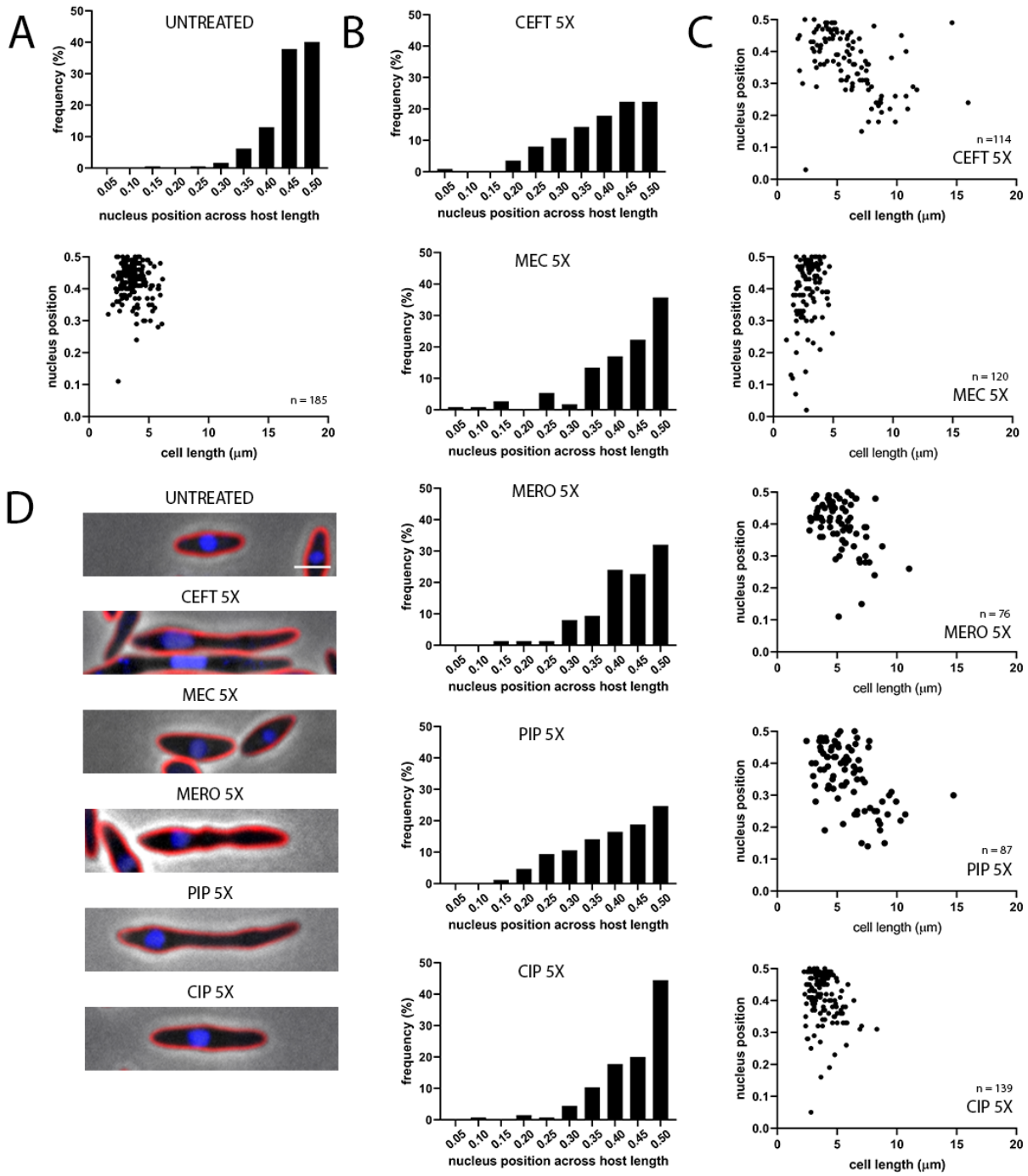

Figure 3.6 Increased cell length is correlated with increased phage nucleus mislocalization away from the center of the host cell. Histogram of nucleus position across normalized *P. aeruginosa* host cell length for (A) untreated infected control and for (B) treated samples at 5X MIC. Scatterplots show nucleus position for across relative *P. aeruginosa* host cell length for (A) untreated infected control and for (C) treated samples at 5X MIC. (D) Representative cell images of untreated infected controls, and treated infected samples. Cell membrane strained with FM4-64 (red) and DNA stained with DAPI (blue). Scale bar represents 2 μm.

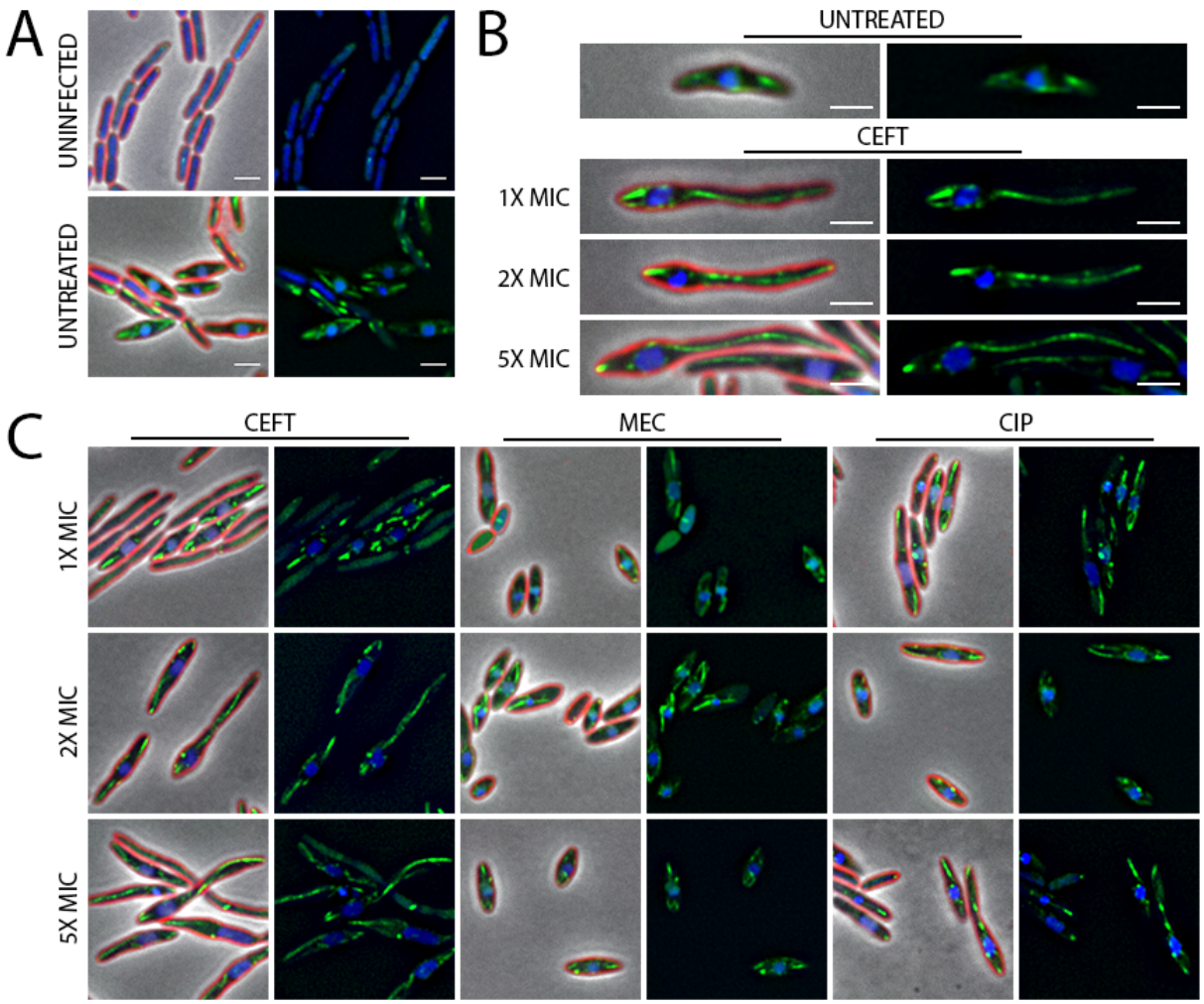

Figure 3.7 Antibiotic treatment leads to aberrant PhuZ filament and spindle dynamics. (A) Microscopy of uninfected and untreated infected controls. (B) Representative cell images of untreated infected controls, and CEFT treated infected samples at all concentrations. (C) Microscopy of treated infected samples. Cell membrane strained with FM4-64 (red) and DNA stained with DAPI (blue). GFP-PhuZ (green) under 0.1% arabinose induction. Scale bar represents 2 μm.

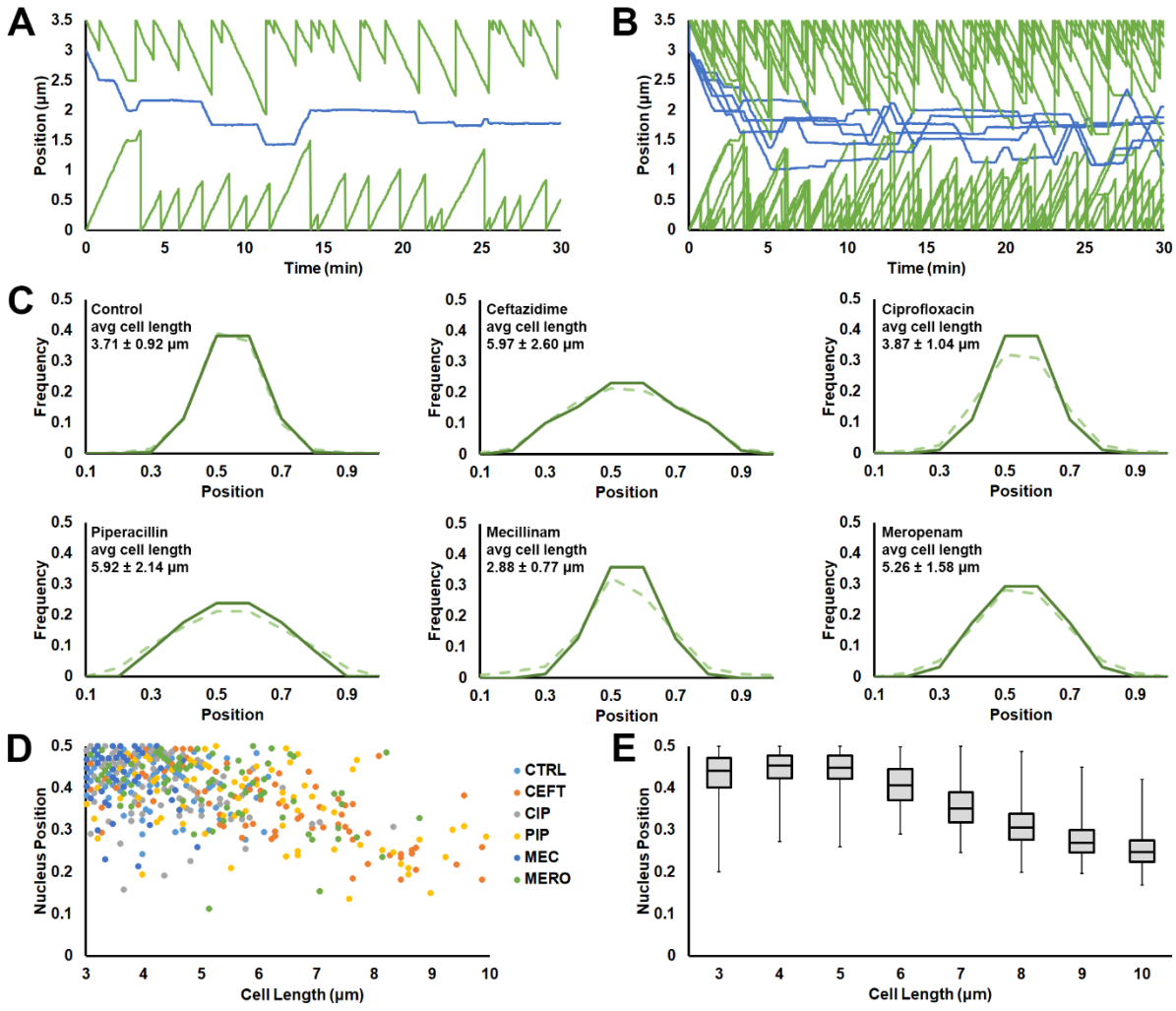

Figure 3.8 Computational modeling of PhuZ dynamics under antibiotic treatment. (A) A single run of the model showing filament end positions in green and the position of the phage nucleus center in blue. The cell length was set at 3.5 μm and the simulation ran for 30 minutes. (B) Five overlapping traces of the model using parameters identical to (A) provide a visualization of the stochastic behavior of the model. (C) Histograms of phage nucleus position after 30 minutes has elapsed for both the model (solid line) and the measured data (dotted line). All model parameters were kept the same with the exception of cell length which was sampled from a normal distribution with mean and standard deviation given by each treatment condition. Measured positions of phage nucleus position plotted against cell length (D) resembles the distribution of phage nuclei positions predicted by modeling (E).

A

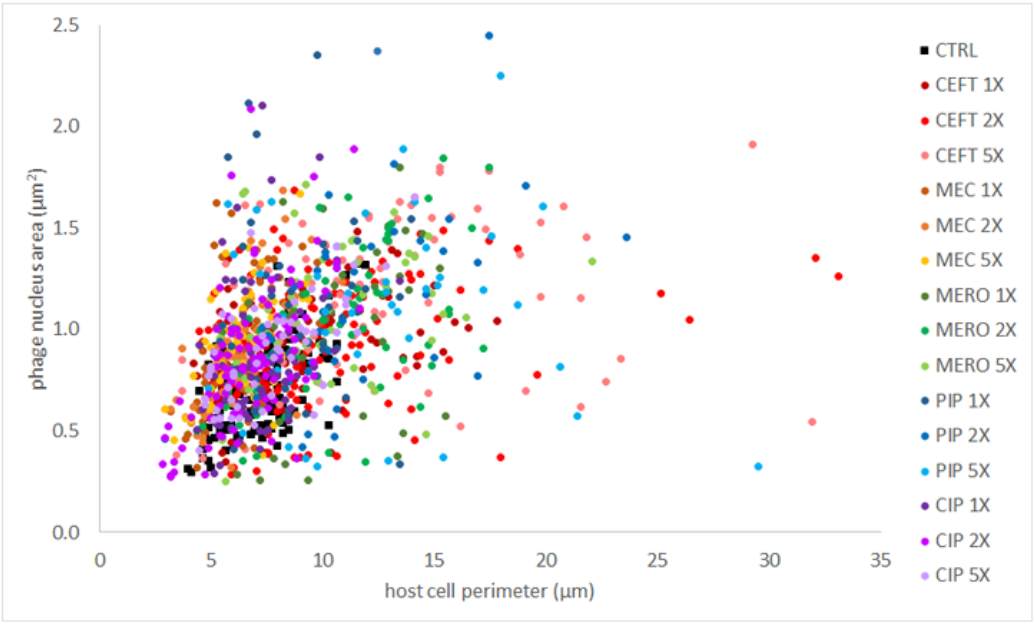
phage nucleus area (µm²)
host cell perimeter (µm)
CTRL
CEFT 1X
CEFT 2X
CEFT 5X
MEC 1X
MEC 2X
MEC 5X
MERO 1X
MERO 2X
MERO 5X
PIP 1X
PIP 2X
PIP 5X
CIP 1X
CIP 2X
CIP 5X

B

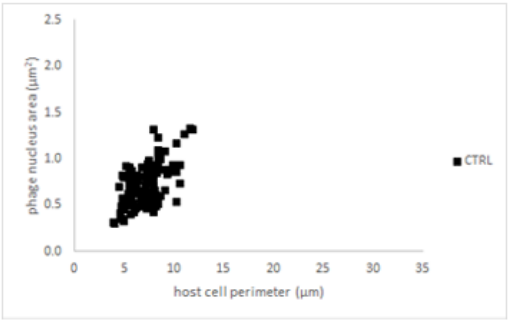
phage nucleus area (µm²)
host cell perimeter (µm)
CTRL

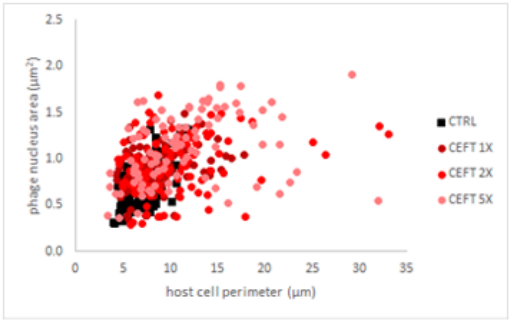
phage nucleus area (µm²)
host cell perimeter (µm)
CTRL
CEFT 1X
CEFT 2X
CEFT 5X

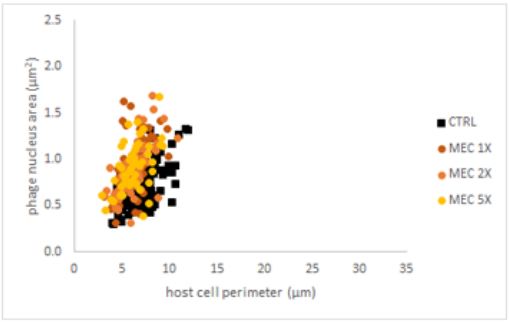
phage nucleus area (µm²)
host cell perimeter (µm)
CTRL
MEC 1X
MEC 2X
MEC 5X

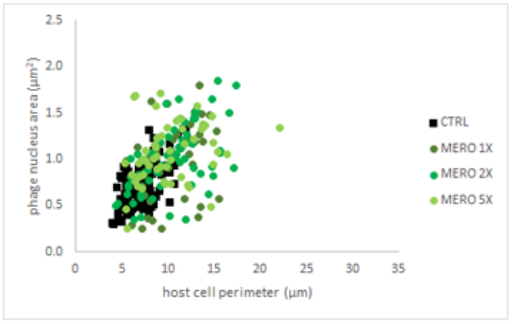
phage nucleus area (µm²)
host cell perimeter (µm)
CTRL
MERO 1X
MERO 2X
MERO 5X

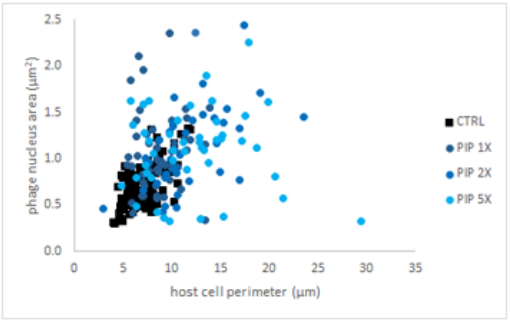
phage nucleus area (µm²)
host cell perimeter (µm)
CTRL
PIP 1X
PIP 2X
PIP 5X

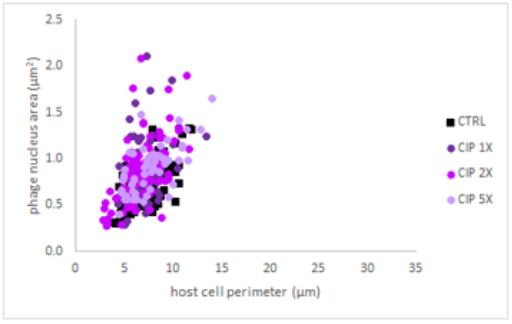
phage nucleus area (µm²)
host cell perimeter (µm)
CTRL
CIP 1X
CIP 2X
CIP 5X

Figure 3.9 Increased cell length is correlated with increased phage nucleus area. (A) Scatterplot overlay of single cell phage nucleus size and host cell perimeter for all conditions of φKZ infection. (B) Scatterplots for each individual antibiotic treatments at all concentrations.

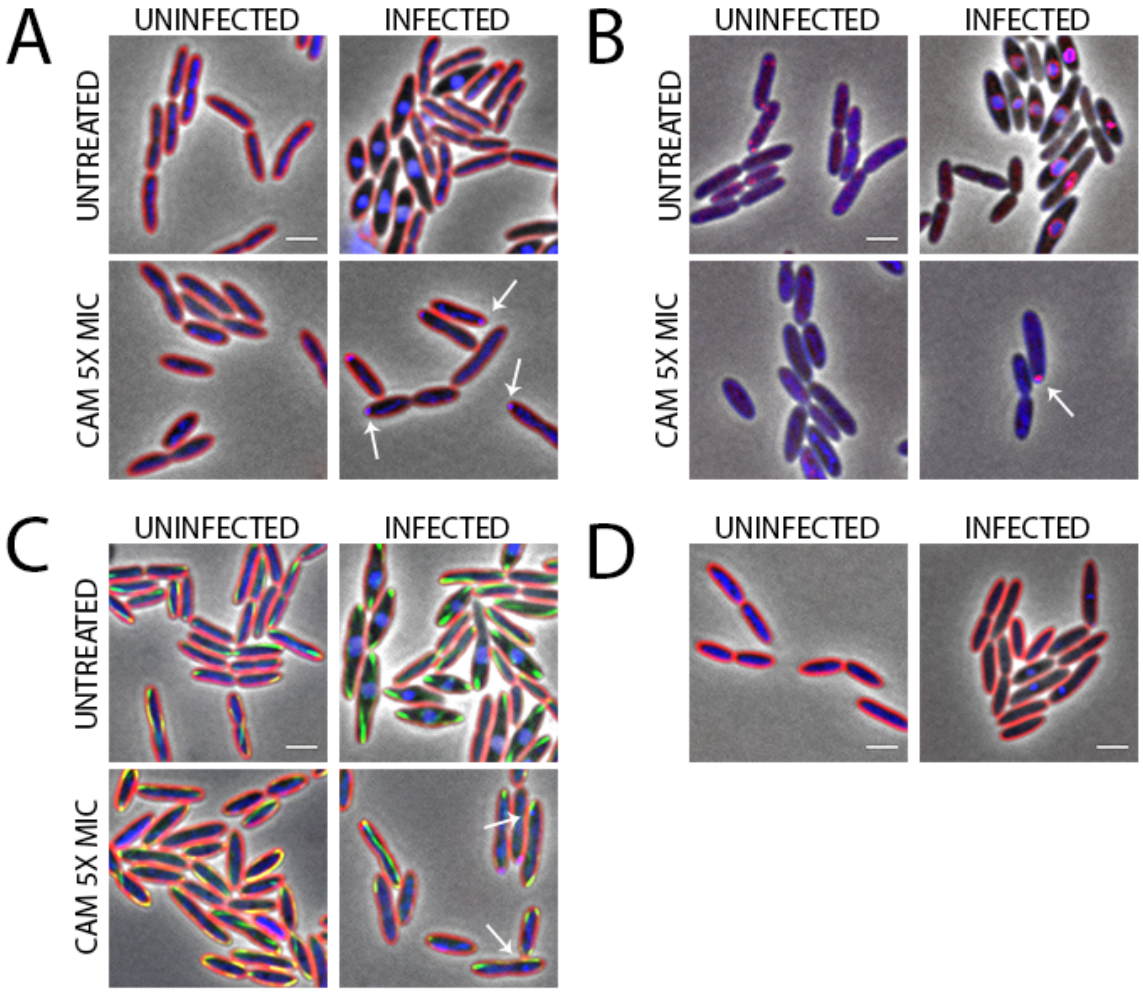

Figure 3.10 Supplemental expression of phage proteins does not rescue chloramphenicol (CAM)-mediated inhibition of φKZ infection. Microscopy of strains untreated or treated with CAM 5X MIC prior to infection with φKZ. (A) *P. aeruginosa* K2733 parental strain, (B) *P. aeruginosa* K2733 expressing mCherry-gp54 (φKZ nuclear shell protein, 0.025% arabinose inducation), (C) *P.aeruginosa* K2733 expressing GFP-PhuZ (φKZ tubulin, 0.5% arabinose induction). (D) Uninfected and infected cells after treatment with CAM 5X MIC and washout. DNA stained with DAPI (blue) and (A, C) Cell membrane strained with FM4-64 (red). Scale bar represents 2 μm. White arrows indicate injected phage DNA that has stalled infecti

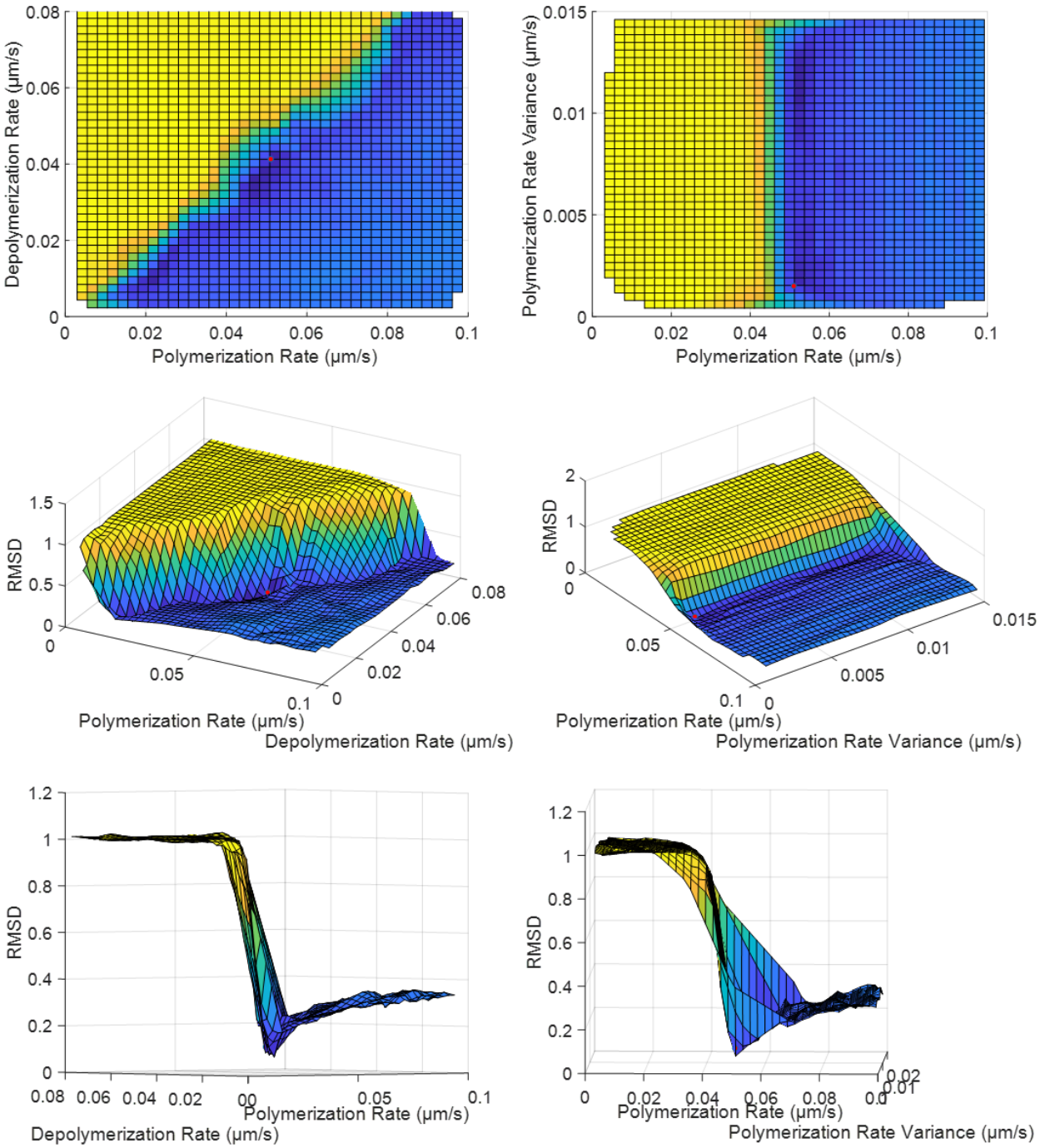

Supplemental Figure 3.1 Surface plots of root mean squared distance (RMSD) parameter spaces. RMSD between measured data and modeled results was used to optimize unknown parameters related to phuZ filament movement. Linear interpolation of 200 randomly sampled points for each parameter space allows for visualization of the relation between parameters. High RMSD (Yellow) is indicative of high deviation from measured data while low RMSD (Blue) indicates a good fit. Red dots indicate the values of parameters used in the final modeling.

3.8 Tables

Table 3.1 Minimum inhibitory concentration (MIC) of antibiotics used in this study against *P. aeruginosa* K2733 (PAO1ΔmexB, ΔmexX, ΔmexCD-oprJ, ΔmexEF-oprN). Concentrations of all compounds shown in μg/mL and represent biological duplicates.

DNA/RNA SYN		PROTEIN SYN		CELL WALL SYN	
CIP	0.013	**CAM**	1.6	**CEFT**	2
DAUN	25.6	**GENT**	0.5	**MEC**	6.4
MITO C	1.6	**TET**	0.4	**MERO**	0.1
RIF	12.8			**PIP**	0.5

3.9 References

1. Stover, C.K., Pham, X.Q., Erwin, A.L., Mizoguchi, S.D., Warrener, P., Hickey, M.J., Brinkman, F.S., Hufnagle, W.O., Kowalik, D.J., Lagrou, M., Garber, R.L., Goltry, L., Tolentino, E., Westbrock-Wadman, S., Yuan, Y., Brody, L.L., Coulter, S.N., Folger, K.R., Kas, A., Larbig, K., Lim, R., Smith, K., Spencer, D., Wong, G.K., Wu, Z., Paulsen, I.T., Reizer, J., Saier, M.H., Hancock, R.E., Lory, S., and Olson, M.V., *Complete genome sequence of Pseudomonas aeruginosa PAO1, an opportunistic pathogen.* Nature, 2000. **406**(6799): p. 959-64.

2. Dotsch, A., Schniederjans, M., Khaledi, A., Hornischer, K., Schulz, S., Bielecka, A., Eckweiler, D., Pohl, S., and Haussler, S., *The Pseudomonas aeruginosa Transcriptional Landscape Is Shaped by Environmental Heterogeneity and Genetic Variation.* mBio, 2015. **6**(4): p. e00749.

3. CDC, *Antibiotic Resistance Threats in the United States*, C. U.S. Department of Health and Human Services, Editor. 2019.

4. Kortright, K.E., Chan, B.K., Koff, J.L., and Turner, P.E., *Phage Therapy: A Renewed Approach to Combat Antibiotic-Resistant Bacteria.* Cell Host Microbe, 2019. **25**(2): p. 219-232.

5. Moelling, K., Broecker, F., and Willy, C., *A Wake-Up Call: We Need Phage Therapy Now.* Viruses, 2018. **10**(12): p. 688.

6. Schooley, R.T., Biswas, B., Gill, J.J., Hernandez-Morales, A., Lancaster, J., Lessor, L., Barr, J.J., Reed, S.L., Rohwer, F., Benler, S., Segall, A.M., Taplitz, R., Smith, D.M., Kerr, K., Kumaraswamy, M., Nizet, V., Lin, L., McCauley, M.D., Strathdee, S.A., Benson, C.A., Pope, R.K., Leroux, B.M., Picel, A.C., Mateczun, A.J., Cilwa, K.E., Regeimbal, J.M., Estrella, L.A., Wolfe, D.M., Henry, M.S., Quinones, J., Salka, S., Bishop-Lilly, K.A., Young, R., and Hamilton, T., *Development and Use of Personalized Bacteriophage-Based Therapeutic Cocktails To Treat a Patient with a Disseminated Resistant Acinetobacter baumannii Infection.* Antimicrob Agents Chemother, 2017. **61**(10).

7. LaVergne, S., Hamilton, T., Biswas, B., Kumaraswamy, M., Schooley, R.T., and Wooten, D., *Phage Therapy for a Multidrug-Resistant Acinetobacter baumannii Craniectomy Site Infection.* Open Forum Infect Dis, 2018. **5**(4): p. ofy064.

8. Dedrick, R.M., Guerrero-Bustamante, C.A., Garlena, R.A., Russell, D.A., Ford, K., Harris, K., Gilmour, K.C., Soothill, J., Jacobs-Sera, D., Schooley, R.T., Hatfull, G.F., and Spencer, H., *Engineered bacteriophages for treatment of a patient with a disseminated drug-resistant Mycobacterium abscessus.* Nature Medicine, 2019. **25**(5): p. 730-733.

9. Comeau, A.M., Tétart, F., Trojet, S.N., Prère, M.-F., and Krisch, H.M., *Phage-Antibiotic Synergy (PAS): beta-lactam and quinolone antibiotics stimulate virulent phage growth.* PloS one, 2007. **2**(8): p. e799-e799.

10. Torres-Barcelo, C., Arias-Sanchez, F.I., Vasse, M., Ramsayer, J., Kaltz, O., and Hochberg, M.E., *A window of opportunity to control the bacterial pathogen Pseudomonas aeruginosa combining antibiotics and phages.* PLoS One, 2014. **9**(9): p. e106628.

11. Chaudhry, W.N., Concepcion-Acevedo, J., Park, T., Andleeb, S., Bull, J.J., and Levin, B.R., *Synergy and Order Effects of Antibiotics and Phages in Killing Pseudomonas aeruginosa Biofilms.* PLoS One, 2017. **12**(1): p. e0168615.

12. Gordillo Altamirano, F.L. and Barr, J.J., *Phage Therapy in the Postantibiotic Era.* Clin Microbiol Rev, 2019. **32**(2).

13. Kamal, F. and Dennis, J.J., *Burkholderia cepacia complex Phage-Antibiotic Synergy (PAS): antibiotics stimulate lytic phage activity.* Applied and environmental microbiology, 2015. **81**(3): p. 1132-1138.

14. Jo, A., Kim, J., Ding, T., and Ahn, J., *Role of phage-antibiotic combination in reducing antibiotic resistance in Staphylococcus aureus.* Food science and biotechnology, 2016. **25**(4): p. 1211-1215.

15. Uchiyama, J., Shigehisa, R., Nasukawa, T., Mizukami, K., Takemura-Uchiyama, I., Ujihara, T., Murakami, H., Imanishi, I., Nishifuji, K., Sakaguchi, M., and Matsuzaki, S., *Piperacillin and ceftazidime produce the strongest synergistic phage–antibiotic effect in Pseudomonas aeruginosa.* Archives of Virology, 2018. **163**(7): p. 1941-1948.

16. Tagliaferri, T.L., Jansen, M., and Horz, H.-P., *Fighting Pathogenic Bacteria on Two Fronts: Phages and Antibiotics as Combined Strategy.* Frontiers in cellular and infection microbiology, 2019. **9**: p. 22-22.

17. Cardozo, C., Rico, V., Agüero, D., and Soriano, A., *Antibiotic selection in the treatment of acute invasive infections by Pseudomonas aeruginosa.* Revista espanola de quimioterapia : publicacion oficial de la Sociedad Espanola de Quimioterapia, 2019. **32 Suppl 2**(Suppl 2): p. 32-34.

18. Burgess, D.S., *Use of pharmacokinetics and pharmacodynamics to optimize antimicrobial treatment of Pseudomonas aeruginosa infections.* Clin Infect Dis, 2005. **40 Suppl 2**: p. S99-104.

19. Oliver, A., Canton, R., Campo, P., Baquero, F., and Blazquez, J., *High frequency of hypermutable Pseudomonas aeruginosa in cystic fibrosis lung infection.* Science, 2000. **288**(5469): p. 1251-4.

20. Hyman, P., *Phages for Phage Therapy: Isolation, Characterization, and Host Range Breadth.* Pharmaceuticals (Basel, Switzerland), 2019. **12**(1): p. 35.

21. Yuan, Y. and Gao, M., *Jumbo Bacteriophages: An Overview.* Front Microbiol, 2017. **8**: p. 403.

22. Casjens, S.R. and Hendrix, R.W., *Bacteriophage lambda: Early pioneer and still relevant.* Virology, 2015. **479-480**: p. 310-30.

23. Mesyanzhinov, V.V., Robben, J., Grymonprez, B., Kostyuchenko, V.A., Bourkaltseva, M.V., Sykilinda, N.N., Krylov, V.N., and Volckaert, G., *The genome of bacteriophage phiKZ of Pseudomonas aeruginosa.* J Mol Biol, 2002. **317**(1): p. 1-19.

24. Erb, M.L., Kraemer, J.A., Coker, J.K., Chaikeeratisak, V., Nonejuie, P., Agard, D.A., and Pogliano, J., *A bacteriophage tubulin harnesses dynamic instability to center DNA in infected cells.* Elife, 2014. **3**.

25. Chaikeeratisak, V., Khanna, K., Nguyen, K.T., Sugie, J., Egan, M.E., Erb, M.L., Vavilina, A., Nonejuie, P., Nieweglowska, E., Pogliano, K., Agard, D.A., Villa, E., and Pogliano, J., *Viral Capsid Trafficking along Treadmilling Tubulin Filaments in Bacteria.* Cell, 2019. **177**(7): p. 1771-1780 e12.

26. Chaikeeratisak, V., Nguyen, K., Egan, M.E., Erb, M.L., Vavilina, A., and Pogliano, J., *The Phage Nucleus and Tubulin Spindle Are Conserved among Large Pseudomonas Phages.* Cell Rep, 2017. **20**(7): p. 1563-1571.

27. Chaikeeratisak, V., Nguyen, K., Khanna, K., Brilot, A.F., Erb, M.L., Coker, J.K., Vavilina, A., Newton, G.L., Buschauer, R., Pogliano, K., Villa, E., Agard, D.A., and Pogliano, J., *Assembly of a nucleus-like structure during viral replication in bacteria.* Science, 2017. **355**(6321): p. 194-197.

28. Chan, B.K., Turner, P.E., Kim, S., Mojibian, H.R., Elefteriades, J.A., and Narayan, D., *Phage treatment of an aortic graft infected with Pseudomonas aeruginosa.* Evolution, medicine, and public health, 2018. **2018**(1): p. 60-66.

29. Chan, B.K., Sistrom, M., Wertz, J.E., Kortright, K.E., Narayan, D., and Turner, P.E., *Phage selection restores antibiotic sensitivity in MDR Pseudomonas aeruginosa.* Sci Rep, 2016. **6**: p. 26717.

30. Nonejuie, P., Burkart, M., Pogliano, K., and Pogliano, J., *Bacterial cytological profiling rapidly identifies the cellular pathways targeted by antibacterial molecules.* Proc Natl Acad Sci U S A, 2013. **110**(40): p. 16169-74.

31. Htoo, H.H., Brumage, L., Chaikeeratisak, V., Tsunemoto, H., Sugie, J., Tribuddharat, C., Pogliano, J., and Nonejuie, P., *Bacterial Cytological Profiling as a Tool To Study Mechanisms of Action of Antibiotics That Are Active against Acinetobacter baumannii.* Antimicrob Agents Chemother, 2019. **63**(4).

32. Lin, L., Nonejuie, P., Munguia, J., Hollands, A., Olson, J., Dam, Q., Kumaraswamy, M., Rivera, H., Jr., Corriden, R., Rohde, M., Hensler, M.E., Burkart, M.D., Pogliano, J., Sakoulas, G., and Nizet, V., *Azithromycin Synergizes with Cationic Antimicrobial Peptides to Exert Bactericidal and Therapeutic Activity Against Highly Multidrug-Resistant Gram-Negative Bacterial Pathogens.* EBioMedicine, 2015. **2**(7): p. 690-8.

33. Quach, D.T., Sakoulas, G., Nizet, V., Pogliano, J., and Pogliano, K., *Bacterial Cytological Profiling (BCP) as a Rapid and Accurate Antimicrobial Susceptibility Testing Method for Staphylococcus aureus.* EBioMedicine, 2016. **4**: p. 95-103.

34. Lamsa, A., Lopez-Garrido, J., Quach, D., Riley, E.P., Pogliano, J., and Pogliano, K., *Rapid Inhibition Profiling in Bacillus subtilis to Identify the Mechanism of Action of New Antimicrobials.* ACS chemical biology, 2016. **11**(8): p. 2222-2231.

35. Peters, C.E., Lamsa, A., Liu, R.B., Quach, D., Sugie, J., Brumage, L., Pogliano, J., Lopez-Garrido, J., and Pogliano, K., *Rapid Inhibition Profiling Identifies a Keystone Target in the Nucleotide Biosynthesis Pathway.* ACS Chem Biol, 2018. **13**(12): p. 3251-3258.

36. Kohanski, M.A., Dwyer, D.J., and Collins, J.J., *How antibiotics kill bacteria: from targets to networks.* Nat Rev Microbiol, 2010. **8**(6): p. 423-35.

37. Tomasz, M., Chawla, A.K., and Lipman, R., *Mechanism of monofunctional and bifunctional alkylation of DNA by mitomycin C.* Biochemistry, 1988. **27**(9): p. 3182-3187.

38. Ceyssens, P.J., Minakhin, L., Van den Bossche, A., Yakunina, M., Klimuk, E., Blasdel, B., De Smet, J., Noben, J.P., Blasi, U., Severinov, K., and Lavigne, R., *Development of giant bacteriophage varphiKZ is independent of the host transcription apparatus.* J Virol, 2014. **88**(18): p. 10501-10.

39. Kronheim, S., Daniel-Ivad, M., Duan, Z., Hwang, S., Wong, A.I., Mantel, I., Nodwell, J.R., and Maxwell, K.L., *A chemical defence against phage infection.* Nature, 2018. **564**(7735): p. 283-286.

40. Lai, G.C., Cho, H., and Bernhardt, T.G., *The mecillinam resistome reveals a role for peptidoglycan endopeptidases in stimulating cell wall synthesis in Escherichia coli.* PLoS Genet, 2017. **13**(7): p. e1006934.

41. Berkane, E., Orlik, F., Stegmeier, J.F., Charbit, A., Winterhalter, M., and Benz, R., *Interaction of bacteriophage lambda with its cell surface receptor: an in vitro study of binding of the viral tail protein gpJ to LamB (Maltoporin).* Biochemistry, 2006. **45**(8): p. 2708-20.

42. Chatterjee, S. and Rothenberg, E., *Interaction of bacteriophage l with its E. coli receptor, LamB.* Viruses, 2012. **4**(11): p. 3162-78.

43. Drew, K.R. and Pogliano, J., *Dynamic instability-driven centering/segregating mechanism in bacteria.* Proc Natl Acad Sci U S A, 2011. **108**(27): p. 11075-80.

44. Rowlett, V.W. and Margolin, W., *The bacterial Min system.* Current Biology, 2013. **23**(13): p. R553-R556.

CHAPTER 4:

Application of bacterial cytological profiling to study drug combinations against multi-drug resistant bacteria

4.1 Abstract

There has been an ongoing war between humans and pathogens since the first introduction of antibiotics into clinical use. Over the last century, there was been an increase in the number of multi-drug resistant (MDR) and extensively-drug resistant (XDR) bacteria, pressuring healthcare providers to turn to last-line therapies that are can be toxic to the patient. Combination therapy has been proven empirically to clear MDR and XDR infections although the underlying mechanisms behinds these successful treatments is often unknown. Bacterial cytological profiling (BCP) , a fluorescence microscopy tool, can help illuminate the physiological responses of bacteria to antibiotics in combination. This chapter describes two published examples of using BCP to support studies investigating antimicrobial synergy against MDR bacteria *Klebsiella pneumoniae* and *Acinetobacter baumannii*.

4.2 Introduction

Understanding clinical efficacy is important for antimicrobial stewardship and mitigating unnecessary antibiotic usage. Recent research has suggested that the standard medium for susceptibility testing, cation-adjusted Mueller-Hinton broth (CA-MHB), may mask an antibiotic's true potency when used in an infected patient. Additionally, during infection, a pathogen interacts with the host's immune system, including cellular (ie. macrophages) and humoral (ie. antimicrobial peptide) responses [1-3]. Therefore, it is necessary to consider the host context when interpreting antibiotic susceptibility.

Due to the rise of multi-drug resistant (MDR) bacteria and the inability to utilize one antibiotic to clear an infection, healthcare providers turn to using drug combinations to increase effectiveness of one or more of the therapeutic constituents [4]. These synergistic relationships are often enhanced in media conditions that mimic the host, such as the eukaryotic cell culture media.

The following sections are two specific examples of the application of the fluorescence microscopy technique, Bacterial Cytological Profiling, to study antimicrobial synergy in MDR pathogens during treatment in RPMI 1640. BCP provides unique insight into mechanistic explanations for observed synergy at the single cell level.

As part of this dissertation, only the materials and methods, results, and discussion relating to BCP will be shown. The following work has been published in the Journal of Infectious Disease and EBioMedicine, respectively.

The first example, published by Ulloa et al. in 2019, looks at the activity of avibactam (AVI) against a New Delhi metallo-β-lactamase (NDM) strain of *Klebsiella pneumoniae*. While AVI does not have direct bactericidal effects, it synergizes with and leads to increase binding of the antimicrobial peptide LL-37. Additionally, a morphological change and increased cell lysis was observed upon treatment of *K. pneumoniae* with non-β-lactam β-lactamase inhibitors (BLIs), such as zidebactam (ZID) or AVI, alone. These changes and cell death were not observed during treatment with the classic BLI tazobactam (TAZ), which contains the standard β-lactam ring [5].

4.3 Avibactam sensitizes carbapenem-resistant NDM-1-producing *Klebsiella pneumoniae* to innate immune clearance [5]

Material and Methods

Single colonies of NDM-1–producing *K. pneumoniae* were picked from LB plates and grown in LB overnight. Overnight cultures were diluted 1:100 in 5% LB–RPMI and grown to an OD600 of 0.20 prior to seeding in a 96-well plate with 100 μL of culture medium per well. The antibiotic was added to exponentially growing bacteria (OD600 of 0.20), placed in shaker at 37°C, and collected after 2 hours. TAMRA-tagged LL-37 was added, and cultures were incubated for an additional 30 minutes. Cultures were subsequently stained with 2 mg/L of Hoechst

(nucleic acid) and 0.5 μM of SYTOX Green (Life Technologies), and 6 μL was transferred onto a 1.2% agarose pad containing 10% LB–20% RPMI, for microscopy. Imaging analyses were performed using FIJI (ImageJ-1.51 w) and CellProfiler 3.0. The microscopist was not blinded.

Results – AVI induces morphologic changes and boosts LL-37-mediated membrane permeability in NDM-1 producing *K. pneumoniae*

To gain insight into the mechanism of AVI and LL-37 synergy, we used fluorescence microscopy to examine cell morphology, LL-37 binding, and cell viability after 3 hours of monotherapy or combination therapy with LL-37 with or without AVI, ZID, or TAZ. In the presence of AVI or ZID, the normally rod-shaped NDM-1–producing *K. pneumoniae* became spherical (100%; n = 262 and n = 315, respectively; **Figure 4.1A**), an effect previously reported in *E. coli* secondary to PBP2 inhibition [6-8]. While TAZ (20 mg/L) binds PBP2 at high concentrations [9, 10], no morphologic change was observed in the presence of this BLI (**Figure 4.1A**), which is expected to be hydrolyzed by NDM because of its underlying β-lactam structure. Despite a strong effect on cell shape, only 2.4% of cells (n = 262) treated with AVI alone and 0.5% (n = 315) treated with ZID alone became nonviable, similar to the percentage of nonviable cells (3.6%; n = 352) for LL-37 treatment alone (**Figure 4.1B**). In contrast, 19.3% of cells (n = 167) treated with AVI plus LL-37 were nonviable (**Figure 4.1B**). Similarly, 15% (n = 266) treated with ZID plus LL-37 were nonviable (**Figure 4.1B**). This synergistic increase in killing correlated with a proportional increase in LL-37 binding (**Figure 4.1C**); that is, AVI (4 mg/L) or ZID (4 mg/L) pretreatment of NDM-1–producing *K. pneumoniae* enhanced binding of TAMRA-tagged LL-37 to the bacterial outer membrane by approximately 4-fold (**Figure 4.1C**), a phenotype not observed with TAZ (20 mg/L) pretreatment. Among cells that stained positive for LL-37, SYTOX Green permeability increased 2-fold with AVI or ZID cotreatment as compared to LL-37 alone or TAZ

plus LL-37 (**Figure 4.1D**). Overall, these studies suggest that BLIs that confer a rod-to-sphere morphologic change render NDM-1– producing *K. pneumoniae* more susceptible to LL-37 binding, which subsequently increases the frequency of cell death.

Discussion

While the precise molecular mechanism of this synergistic interaction remains to be discovered, subinhibitory concentrations of AVI appear to influence bacterial cell wall mechanics. AVI is a non–β-lactam BLI with no activity against NDMs. However, AVI binds selectively to PBP2 [11], an enzyme critical for maintaining the cellular morphology in gram-negative bacteria [6-8]. Microscopy demonstrated a *K. pneumoniae* morphologic transition from rod to sphere in the presence of AVI, reminiscent of morphologic changes in *E. coli* in the presence of mecillinam, a β-lactam that specifically inactivates PBP2 [6-8].Similar findings were seen in the presence of ZID, a non–β-lactam BLI with high-affinity binding to PBP2. High but pharmacologically attainable doses of TAZ, a β-lactam BLI known to bind PBP2 [9], did not result in *K. pneumoniae* rod-to-sphere transition, presumably because of its inability to withstand hydrolysis by *K. pneumoniae* BLIs. Unlike TAZ-treated cells, AVI- or ZID-treated cells demonstrated increased LL-37 binding, leading to widespread bacterial cell death, detected via a SYTOX Green viability assay. These findings parallel our timekill assay results, in which combination therapy with LL-37 and AVI or ZID (but not TAZ) reduced bacterial growth to below the assay's detection limit within 6 hours (data not shown in dissertation). Overall, our findings underscore a heretofore undescribed synergistic relationship between the innate immune system and diazabicyclooctane BLIs with high-affinity binding to PBP2, such as AVI and ZID.

4.4 Surprising synergy of dual translation inhibition vs. *Acinetobacter baumannii* and other multi-drug resistant bacterial pathogens [12]

The second example of applying BCP to study antimicrobial synergy in MDR pathogens was published by Dillon et. al. in 2019 and examines the media-dependent synergistic activity of the protein synthesis inhibitors azithromycin (AZM) and minocycline (MIN) against *A. baumannii*. In CAMHB, MIN had a lower MIC than AZM. In contrast, during treatment of *A. baumannii* in RPMI 1640 supplemented with 10%LB, AZM had the lower MIC of the two. In either media, treatment of the cells with a combination of drugs lead to observation of toroidal DNA [12], characteristic of protein synthesis inhibition [13], which was absent during single treatment. These experiments with single cells confirmed population studies based using CFU/ml data (not shown in this dissertation) and demonstrate that the presence of the two compounds results in synergistic inhibition of protein synthesis [12].

Material and Methods

Fluorescence microscopy was performed as previously described [13] with modifications. In brief, AB5075 was grown in CA-MHB or RPMI+ at 37 °C to a starting OD600 ~0.13 and then treated with appropriate concentrations of MIN, AZM, or combination of both antibiotics for 2 h at 37 °C. After treatment, cells were stained with 10 μg/ml FM4-64, 4 μg/ml DAPI, and 0.5 μM SYTOX-Green. Samples were transferred to a glass slide containing an agarose pad (1.2% agarose in 20% CA-MHB or RPMI+) for microscopy. Image analysis was done using FIJI (ImageJ 1.51w).

Results - Bacterial cytological profiling (BCP) demonstrates augmented translation inhibition in MDR *A. baumannii* upon AZM plus MIN cotreatment

To further explore the synergistic interaction between AZM and MIN, we employed BCP, a powerful technique that uses quantitative fluorescence microscopy to identify disrupted bacterial

cellular pathways on a single cell level [13]. A characteristic signature of translation inhibition evident in BCP is formation of DNA toroids that arise due to changes in chromosome compaction when ribosome activity is disrupted[7]. In both CA-MHB and RPMI+, we identified drug concentrations in which neither AZM nor MIN inhibited MDR *A. baumannii* translation on their own, as confirmed by minimal toroid formation (**Figure 4.2A, C**). Extensive toroid formation was observed, however, when the two drugs were co-administered at these same concentrations (**Figure 4.2A, C**). In CA-MHB, visible toroids were seen in 2.2% of untreated *A. baumannii* cells, 2.8% of cells treatment with 0.15 μg/ml MIN, 4.2% of cells treated with 96 μg/ml AZM, and 34.0% of cells treated with 0.15 μg/ml MIN + 96 μg/ml AZM (**Figure 4.2B**). In RPMI+, visible toroids were seen in 0.3% of untreated *A. baumannii* cells, 4.5% of cells treatment with 50 μg/ml MIN, 2.5% of cells treated with 0.25 μg/ml AZM, and 27.2% of cells treated with 50 μg/ml MIN + 0.25 μg/ml AZM (**Figure 4.2D**).

Discussion

Under ideal circumstances, antimicrobial therapy would sufficiently reduce bacterial burden at the end of therapy to reduce the likelihood of relapse and the emergence of drug resistance. Therapies with conditionally independent activity profiles are desirable because efficient bacterial killing in vivo typically requires eliminating the pathogen from multiple host microenvironments. On their own, both AZM and MIN displayed media-dependent conditional activity, a potential limiting trait for their use in monotherapy. However, AZM + MIN combination therapy complemented the intrinsic inhibition profile seen with either drug alone, yielding a conditionally-independent synergistic therapy with efficacy against MDR *A. baumannii* in laboratory culture and a murine pneumonia model. The synergistic drug combination promoted

enhanced translation inhibition kinetics, melding the fast-acting activity of MIN with the sustained inhibition of AZM to create a potent, long lasting, and efficacious antibiotic profile.

The AZM+MIN drug-drug interaction appears to represent a parallel pathway interaction, when the two drugs, often each having suboptimal activity against the same primary target, combine their activities to more effectively inhibit a bacterial system or biochemical pathway [4, 14, 15], in this case protein translation at the ribosome. Both drugs have associated deficiencies as monotherapy. AZM activity is notably delayed due to its slow release from tissues [16] and a low rate of association with ribosomes [17]. Compared to AZM, the therapeutic window for MIN is shorter (half-life ~ 12–16 h in humans) [18] and its bactericidal capacity has been brought into question [19, 20]. In combination, however, expedited MIN activity buys time for the slower acting, yet longer lasting, AZM-associated inhibition to occur. Furthermore, the media-dependent activity of each drug was complemented by the other, so that their synergistic activity was independent of media composition. And while we established parallel pathway synergy for MIN + AZM in translation inhibition kinetics, an important caveat of our study is that we cannot exclude the possibility of additional mechanisms of synergy such as compounding downstream effects on a tertiary target, or one drug acting to improve the bioavailability of the other [4, 14, 15].

This study also highlights the benefit of investigating antibiotic activity in more than one medium condition to infer potential clinical efficacy and opportunities for synergistic therapy. Limitations of testing only the standard bacteriological medium (CA-MHB) have previously been illustrated [3, 21], testing in a more physiologic tissue culture-based medium was also not fully predicative of in vivo efficacy as MIN is active in the murine pneumonia model despite little to no activity in RPMI+. One important compositional difference between the two media we have highlighted is the presence of the physiological buffer bicarbonate anion (HCO3-) in RPMI.

HCO3- is an essential component of multiple biological processes in humans and its presence stimulates both transcriptional and translational changes in bacteria [22], impacting antibiotic activity against numerous species when added to CA-MHB [21]. Recent work has linked HCO3-mediated effects on antibiotic activity to reductions in bacterial proton motive force [23]. While AZM activity is known to improve in response to a loss of protonmotive force, indicating that AZM is not actively imported [24], the entry of tetracyclines into the bacterial cell is an energy dependent process requiring active transport [25]. Enhanced macrolide activity against both *Escherichia coli* and *Staphylococcus aureus* have been reported in the presence of HCO3- due to the dissipation of the pH gradient required for a functioning proton motive force [21]. The loss of active transport renders the bacteria unable to export AZM leading to its intracellular accumulation, an effect which has previously been associated with enhanced AZM activity [3].

In summary, the therapeutic potential of AZM and MIN combination therapy warrants clinical study as the two drugs were found to interact synergistically against MDR *A. baumannii* in all conditions and models examined in this study. This benefit may extend to other MDR pathogens, in particular MDR *K. pneumoniae* and MRSA. A limitation of our study at present is that future work is required to explore if MIN synergy is also found with other macrolides. Nevertheless, as both AZM and MIN are already FDA approved, readily available for use, and familiar to clinicians, the potential for clinical trials to determine the efficacy of the combinatorial therapy *for A. baumannii* is immediately at hand.

4.5 Acknowledgements

The work published as Ulloa et al. was supported by the Eunice Kennedy Shriver National Institute of Child Health and Human Development, National Institutes of Health (NIH; Pediatric Scientist Development Program Fellowship K12-HD000850 to E. R. U. and grant U54-HD090259

to V. N. and G. S.), and the National Institute of Allergy and Infectious Diseases, NIH (grant U01-AI124316 to V. N., G. S., and J. P.) [5].

The work published as Dillon et al. was funded by the National Institutes of Health U01 AI124326 (JP, GS, VN) and U54 HD090259 (GS, VN). IC was supported by the UCSD Research Training Program for Veterinarians T32 OD017863 [12].

Chapter 4, in part, is a reprint of the material as it appears in Ulloa, ER., Dillon, N., Tsunemoto, H., Pogliano, J., Sakoulas, G., & Nizet, V., 2019, Avibactam sensitizes carbapenem-resistant NDM-1-producing *Klebsiella pneumoniae* to innate immune clearance in The Journal of Infectious Disease, and in Dillon, N., Holland, M., Tsunemoto, H., Hancock, B., Cornax, I., Pogliano, J., Sakoulas, G., & Nizet, V., 2019, Surprising synergy of dual translation inhibition vs *Acinetobacter baumannii* and other multidrug-resistant bacterial pathogens in EBioMedicine. The dissertation author was a co-author of these papers.

4.6 Figures

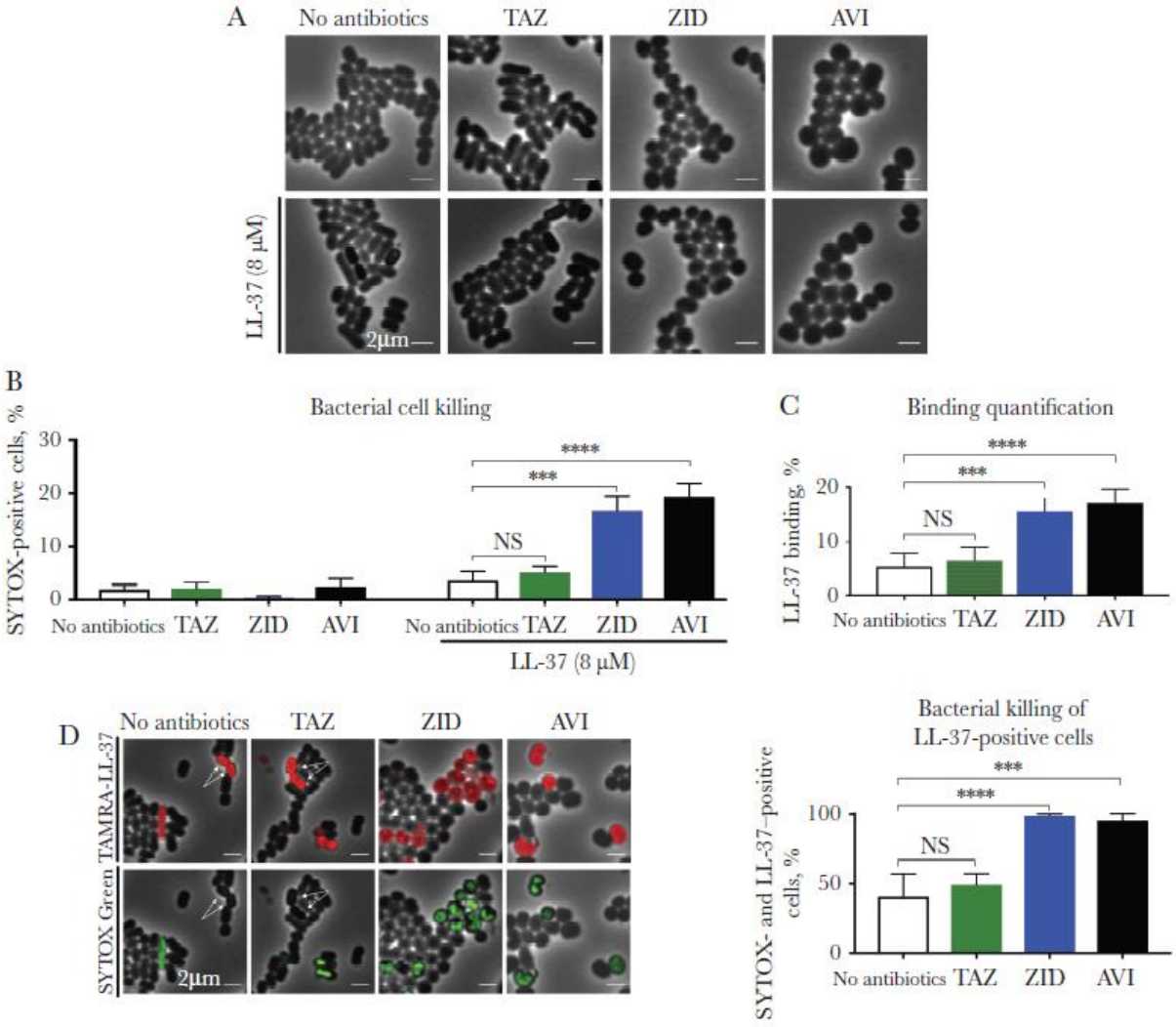

Figure 4.1 Treatment of New Delhi metallo-β-lactamase (NDM)-1–producing *Klebsiella pneumoniae* (KP) with sub–minimum inhibitory concentrations (MICs) of avibactam (AVI) or zidebactam (ZID) results in a rod-to-sphere morphologic change that increases the frequency of cell death only in the presence of LL-37. *A–C,* AVI (4 mg/L) or ZID (4 mg/L) induce a rod-to-coccus shape change (*A*) that, while nonlethal to the organism (*B*), results in increased binding of fluorescence-labeled LL-37 (8 μM) to the NDM-1–producing KP cell wall (*C*). *D*, Upon AVI (4 mg/L) or ZID (4 mg/L) treatment, nearly 100% of cells bound by fluorescence-labeled LL-37 (8 μM) were also SYTOX Green positive, a proxy for compromised membranes characteristic of dead cells, yet only approximately 50% of cells in the control conditions had concomitant staining. Arrows denote LL-37–positive cells that were SYTOX Green negative. NS, not significant.***$P < .001$ and ****$P < .0001$, by Kruskal-Wallis 1-way analysis of variance.[5]

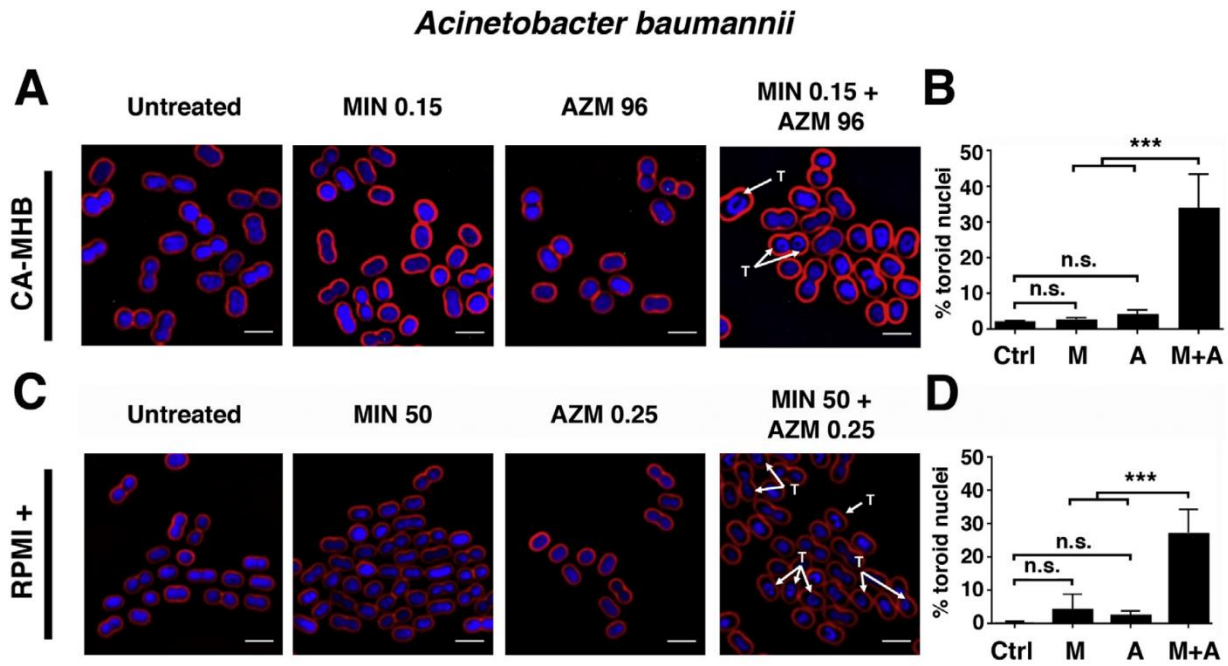

Figure 4.2 Bacterial cytological profiling (BCP) demonstrates augmented translation inhibition in MDR A. baumannii upon AZM + MIN cotreatment. A. baumannii strain AB5075 cells were grown in CA-MHB to a starting OD600 of 0.13 and treated for 2 h with MIN, AZM, or both drugs combined. Cells were strained for fluorescence microscopy with FM4–64 (red cell membrane dye), DAPI (blue DNA dye), and SYTOX-Green (green membrane-impermeable DNA dye, used as proxy for cell lysis). "T" denotes observed toroidal nuclei. (A) BCP was carried out for AZM and MIN both alone and in combination in CA-MHB. (B) The percentage of total cells counted, between 100 and 200 in at least 3 frames, with toroid nuclei for untreated and treated cultures in CA-MHB. (C) BCP was carried out for AZM and MIN both alone and in combination in RPMI+. (D) The percentage of total cells counted, between 100 and 200 in at least 3 frames, with toroid nuclei for untreated and treated cultures in RPMI+. BCP images are representative of 3 independent experiments. Percent total toroid containing cells is combined data from 3 independent experiments for each media type. Scale bar = 2 μm. For panels (B) and (D), statistical significance was calculated using a two-way ANOVA with ** ≤0.01 and *** ≤0.001.[6]

4.7 References

1. Buyck, J.M., Plesiat, P., Traore, H., Vanderbist, F., Tulkens, P.M., and Van Bambeke, F., *Increased susceptibility of Pseudomonas aeruginosa to macrolides and ketolides in eukaryotic cell culture media and biological fluids due to decreased expression of oprM and increased outer-membrane permeability.* Clin Infect Dis, 2012. **55**(4): p. 534-42.

2. Kumaraswamy, M., Lin, L., Olson, J., Sun, C.F., Nonejuie, P., Corriden, R., Dohrmann, S., Ali, S.R., Amaro, D., Rohde, M., Pogliano, J., Sakoulas, G., and Nizet, V., *Standard susceptibility testing overlooks potent azithromycin activity and cationic peptide synergy against MDR Stenotrophomonas maltophilia.* J Antimicrob Chemother, 2016. **71**(5): p. 1264-9.

3. Lin, L., Nonejuie, P., Munguia, J., Hollands, A., Olson, J., Dam, Q., Kumaraswamy, M., Rivera, H., Jr., Corriden, R., Rohde, M., Hensler, M.E., Burkart, M.D., Pogliano, J., Sakoulas, G., and Nizet, V., *Azithromycin Synergizes with Cationic Antimicrobial Peptides to Exert Bactericidal and Therapeutic Activity Against Highly Multidrug-Resistant Gram-Negative Bacterial Pathogens.* EBioMedicine, 2015. **2**(7): p. 690-8.

4. Wambaugh, M.A., Shakya, V.P.S., Lewis, A.J., Mulvey, M.A., and Brown, J.C.S., *High-throughput identification and rational design of synergistic small-molecule pairs for combating and bypassing antibiotic resistance.* PLoS Biol, 2017. **15**(6): p. e2001644.

5. Ulloa, E.R., Dillon, N., Tsunemoto, H., Pogliano, J., Sakoulas, G., and Nizet, V., *Avibactam Sensitizes Carbapenem-Resistant NDM-1-Producing Klebsiella pneumoniae to Innate Immune Clearance.* J Infect Dis, 2019. **220**(3): p. 484-493.

6. Vinella, D., Joseleau-Petit, D., Thevenet, D., Bouloc, P., and D'Ari, R., *Penicillin-binding protein 2 inactivation in Escherichia coli results in cell division inhibition, which is relieved by FtsZ overexpression.* J Bacteriol, 1993. **175**(20): p. 6704-10.

7. Spratt, B.G. and Pardee, A.B., *Penicillin-binding proteins and cell shape in E. coli.* Nature, 1975. **254**(5500): p. 516-7.

8. Legaree, B.A., Daniels, K., Weadge, J.T., Cockburn, D., and Clarke, A.J., *Function of penicillin-binding protein 2 in viability and morphology of Pseudomonas aeruginosa.* J Antimicrob Chemother, 2007. **59**(3): p. 411-24.

9. Urban, C., . Go, E., Mariano, N., & Rahal, J.J, *Interaction of sulbactam, clavulanic acid and tazobactam with penicillin-binding proteins of imipenem-resistant and -susceptible Acinetobacter baumannii.* FEMS Microbiology Letters, 1995(125): p. 193-197.

10. Sakoulas, G., Rose, W., Berti, A., Olson, J., Munguia, J., Nonejuie, P., Sakoulas, E., Rybak, M.J., Pogliano, J., and Nizet, V., *Classical beta-Lactamase Inhibitors Potentiate the Activity of Daptomycin against Methicillin-Resistant Staphylococcus aureus and Colistin against Acinetobacter baumannii.* Antimicrob Agents Chemother, 2017. **61**(2).

11. Sutaria, D.S., Moya, B., Green, K.B., Kim, T.H., Tao, X., Jiao, Y., Louie, A., Drusano, G.L., and Bulitta, J.B., *First Penicillin-Binding Protein Occupancy Patterns of beta-Lactams and beta-Lactamase Inhibitors in Klebsiella pneumoniae.* Antimicrob Agents Chemother, 2018. **62**(6).

12. Dillon, N., Holland, M., Tsunemoto, H., Hancock, B., Cornax, I., Pogliano, J., Sakoulas, G., and Nizet, V., *Surprising synergy of dual translation inhibition vs. Acinetobacter baumannii and other multidrug-resistant bacterial pathogens.* EBioMedicine, 2019. **46**: p. 193-201.

13. Nonejuie, P., Burkart, M., Pogliano, K., and Pogliano, J., *Bacterial cytological profiling rapidly identifies the cellular pathways targeted by antibacterial molecules.* Proc Natl Acad Sci U S A, 2013. **110**(40): p. 16169-74.

14. Zimmermann, G.R., Lehar, J., and Keith, C.T., *Multi-target therapeutics: when the whole is greater than the sum of the parts.* Drug Discov Today, 2007. **12**(1-2): p. 34-42.

15. Yeh, P.J., Hegreness, M.J., Aiden, A.P., and Kishony, R., *Drug interactions and the evolution of antibiotic resistance.* Nat Rev Microbiol, 2009. **7**(6): p. 460-6.

16. Lode, H., *The pharmacokinetics of azithromycin and their clinical significance.* Eur J Clin Microbiol Infect Dis, 1991. **10**(10): p. 807-12.

17. Dinos, G.P., Michelinaki, M., and Kalpaxis, D.L., *Insights into the mechanism of azithromycin interaction with an Escherichia coli functional ribosomal complex.* Mol Pharmacol, 2001. **59**(6): p. 1441-5.

18. Shankar, C., Nabarro, L.E.B., Anandan, S., and Veeraraghavan, B., *Minocycline and Tigecycline: What Is Their Role in the Treatment of Carbapenem-Resistant Gram-Negative Organisms?* Microb Drug Resist, 2017. **23**(4): p. 437-446.

19. Tang, H.J., Chen, C.C., Ko, W.C., Yu, W.L., Chiang, S.R., and Chuang, Y.C., *In vitro efficacy of antimicrobial agents against high-inoculum or biofilm-embedded meticillin-resistant Staphylococcus aureus with vancomycin minimal inhibitory concentrations equal to 2 mug/mL (VA2-MRSA).* Int J Antimicrob Agents, 2011. **38**(1): p. 46-51.

20. Yang, Y.S., Lee, Y., Tseng, K.C., Huang, W.C., Chuang, M.F., Kuo, S.C., Lauderdale, T.L., and Chen, T.L., *In Vivo and In Vitro Efficacy of Minocycline-Based Combination Therapy for Minocycline-Resistant Acinetobacter baumannii.* Antimicrob Agents Chemother, 2016. **60**(7): p. 4047-54.

21. Ersoy, S.C., Heithoff, D.M., Barnes, L.t., Tripp, G.K., House, J.K., Marth, J.D., Smith, J.W., and Mahan, M.J., *Correcting a Fundamental Flaw in the Paradigm for Antimicrobial Susceptibility Testing.* EBioMedicine, 2017. **20**: p. 173-181.

22. Dorschner, R.A., Lopez-Garcia, B., Peschel, A., Kraus, D., Morikawa, K., Nizet, V., and Gallo, R.L., *The mammalian ionic environment dictates microbial susceptibility to antimicrobial defense peptides.* FASEB J, 2006. **20**(1): p. 35-42.

23. Farha, M.A., French, S., Stokes, J.M., and Brown, E.D., *Bicarbonate Alters Bacterial Susceptibility to Antibiotics by Targeting the Proton Motive Force.* ACS Infect Dis, 2018. **4**(3): p. 382-390.

24. Capobianco, J.O. and Goldman, R.C., *Erythromycin and azithromycin transport into Haemophilus influenzae ATCC 19418 under conditions of depressed proton motive force (delta mu H).* Antimicrob Agents Chemother, 1990. **34**(9): p. 1787-91.

25. Yamaguchi, A., Shiina, Y., Fujihira, E., Sawai, T., Noguchi, N., and Sasatsu, M., *The tetracycline efflux protein encoded by the tet(K) gene from Staphylococcus aureus is a metal-tetracycline/H+ antiporter*. FEBS Lett, 1995. **365**(2-3): p. 193-7.

CHAPTER 5:

Concluding remarks and future directions

The work of this dissertation details the application of fluorescence microscopy, specifically the technique bacterial cytological profiling (BCP), to study antibiotics and their interactions with their targeted bacteria, bacteriophage infection, and other antimicrobial compounds.

Chapter 2 describes the integration of microfluidics and fluorescence microscopy to observe uptake of fluorescently labeled antibiotics in *E. coli* under various conditions, including altered genetic backgrounds and media. Combining these two tools allowed us to identify the individual contributions of the outer membrane and efflux pumps, as well as the impact of bicarbonate, on the accumulation of macrolides. In the future, it would be interesting to test other fluorescent antibiotics that have cytoplasmic targets, such as trimethoprim or ciprofloxacin, and antibiotics that have targets within the periplasmic space, such as penicillin and vancomycin.

The limitations of the microfluidics uptake technique mainly lie in the intensity of the fluorescence signal. Because macrolides and many other protein synthesis inhibitors bind the ribosome, the signal tends to be relatively robust due to the sheer number of ribosomes within any given bacterial cell that can concentrate the antibiotic to higher intracellular levels. For trimethoprim, which inhibits dihydrofolate reductase, and ciprofloxacin, which binds to DNA gyrase, their protein partners exist at much lower densities within the host cell, and so the subsequent fluorescent signal may not be boosted above background in these cases.

For penicillin and vancomycin, these antibiotics already have a difficult time traversing the Gram-negative outer membrane, even in the absence of the bulky fluorophore. Thus, for cases in which there exists an intact outer membrane, it would be difficult to obtain meaningful data of their accumulation, if any. However, similar studies could be done with clinically relevant Gram-positive bacteria, such as *S. aureus*, for which these cell-wall active drugs are potent. Data

published in Poudel et al. [1, 2] and Rajput et al. [2] showed that different MRSA strains have varying responses to nafcillin treatment dependent on the growth media, specifically the swelling of MRSA USA300, but not USA100, in the standard bacteriologic media CAMHB, but lysing in the eukaryotic cell culture media RPMI 1640. Using microfluidics and fluorescence microscopy, these differential reactions could be observed temporally in conjunction with fluorescent antibiotic localization.

Chapter 3 describes the visualization of jumbo phage φKZ infection of *P. aeruginosa* during treatment with antibiotics of varying mechanisms of action. Using BCP, we confirmed that treatment with the antibiotics alone lead to distinct cytological changes in the *P. aeruginosa* host cell. Inhibition of specific biosynthetic pathways influenced the initiation and progression of φKZ infection either negatively, such as in the case of the protein synthesis inhibitors and the DNA intercalator daunorubicin, or positively, such as in the case of the cell wall synthesis inhibitors. We observed differences in the phage-encoded tubulin PhuZ during treatment with antibiotics that increased the host cell length that lead to mislocalization of the phage nucleus away from mid-cell.

Our data highlighted some cytological changes during co-treatment and infection that would interesting to investigate further in the future. This includes the observed stall of phage infection during treatment with antibiotics that block protein synthesis inhibitors, and we demonstrated that removing the chloramphenicol allows for progression of phage infection. This provides a potential tool to allow for genetic editing of these phages before they produce their protective proteinaceous nuclear shell. Another question that may be answered in the future is the processes underlying the widening of the host cell during infection and the constraints placed on the phage nucleus during antibiotic treatment that causes aberrant bulge formation or movement of the phage nucleus away from these bulges.

The application of BCP to study phage-antibiotic interactions is not limited by the lifestyle of the phage of interest. This work relied on observable changes in the phage nucleus and other phage-specific cytological features, such as the nuclear shell or tubulin. In cases where the phage of interest does not make these obvious cellular structures, it will be interesting determine which cytological observations can be informative. For example, degradation of the host chromosome, replication of phage DNA, and assembly of viral particles using GFP fusions is open to discovery and for observing phage-antibiotic interactions using the methods detailed in this chapter. It is also possible, however, that non-nucleus forming phages impact the morphology of the host cell in unknown alternative ways that may be of interest to study using this technique.

Finally, Chapter 4, in part, summarizes two published works, by Ulloa et al. [3] and Dillon et al. [4], that used BCP to investigate antimicrobial synergy. This chapter highlights the flexibility of BCP through is application to study a variety of bacterial species, including those that are multi-drug resistant.

5.1 References

1. Poudel, S., Tsunemoto, H., Meehan, M., Szubin, R., Olson, C.A., Lamsa, A., Seif, Y., Dillon, N., Vrbanac, A., Sugie, J., Dahesh, S., Monk, J.M., Dorrestein, P.C., Pogliano, J., Knight, R., Nizet, V., Palsson, B.O., and Feist, A.M., *Characterization of CA-MRSA TCH1516 exposed to nafcillin in bacteriological and physiological media.* Scientific data, 2019. **6**(1): p. 43-43.

2. Rajput, A., Poudel, S., Tsunemoto, H., Meehan, M., Szubin, R., Olson, C.A., Lamsa, A., Seif, Y., Dillon, N., Vrbanac, A., Sugie, J., Dahesh, S., Monk, J.M., Dorrestein, P.C., Knight, R., Nizet, V., Palsson, B.O., Feist, A.M., and Pogliano, J., *Profiling the effect of nafcillin on HA-MRSA D712 using bacteriological and physiological media.* Scientific data, 2019. **6**(1): p. 322-322.

3. Ulloa, E.R., Dillon, N., Tsunemoto, H., Pogliano, J., Sakoulas, G., and Nizet, V., *Avibactam Sensitizes Carbapenem-Resistant NDM-1-Producing Klebsiella pneumoniae to Innate Immune Clearance.* J Infect Dis, 2019. **220**(3): p. 484-493.

4. Dillon, N., Holland, M., Tsunemoto, H., Hancock, B., Cornax, I., Pogliano, J., Sakoulas, G., and Nizet, V., *Surprising synergy of dual translation inhibition vs. Acinetobacter baumannii and other multidrug-resistant bacterial pathogens.* EBioMedicine, 2019. **46**: p. 193-201.